Enhanced Oil Recovery by CO_2 and CO_2-foam Injection in Fractured Limestone Rocks

Master Thesis in Reservoir Physics

by

Stig André Winter Langlo

Department of Physics and Technology
University of Bergen

June 2013

Summary

This thesis is part of an ongoing study of integrated enhanced oil recovery methods in Reservoir Physics group at the Department of Physics and Technology at the University of Bergen. This experimental thesis investigates through laboratory tests the miscible, liquid CO_2 injection for enhanced oil recovery in an outcrop limestone rock, analogue to carbonate reservoirs.

A total of 18 CO_2 injection experiments have been performed to study the influence on CO_2 EOR from parameters such as presence of fractures, presence of initial water as irreducible water saturation, wettability preference of the matrix, injection of foam for mobility control, and comparing secondary to tertiary recovery. Core plugs were artificially fractured by cutting the cores along the length of the core. A spacer was placed in the fracture to maintain a constant aperture and identical fracture permeability between tests. As a part of the thesis, experimental setups were designed and built to be able to inject CO_2 at elevated pressures over 90bars to develop miscibility between CO2 and the oil phase (n-Decane).

Results from laboratory tests show that CO_2 has a significant recovery potential in whole and fractured limestone core plugs, with total recoveries ranging from 92-100 % OOIP for fully oil saturated cores, and 75-92 % OOIP for cores with irreducible water saturation.

The presence of fractures dramatically reduced the rate of oil recovery, where oil recovery was mainly driven by diffusion, with negligible viscous displacement. The presence of water, either as initial irreducible water saturation, or after a waterflood reduces the total oil recovery and reduced the rate of oil recovery.

In fractured core plugs, the injection of CO_2-foam accelerated oil recovery compared to pure CO_2 injection by adding a viscous displacement in addition to diffusion. The oil recovery rate was also increased during a Huff 'n' Puff scenario compared to continuous CO_2 injection.

Moderately oil-wet cores demonstrate a higher total oil recovery than water-wet cores for both pure CO_2 and CO_2-foam injection. During CO_2-foam injection, differential pressure is higher near the end of production, indicating that oil has a detrimental effect on foam.

Numerical simulations have been performed with CMG GEM simulator to study liquid CO_2-injection in a fractured system, and the simulations were able to satisfactory reproduce the experimental data. The validated numerical model should be used further for increased understanding, for better depth of analysis, and to reduce time usage compared to advanced, time-consuming experimental work.

The results from this thesis show the potential for CCUS in fractured carbonate reservoirs. Even though the oil recovery rate is reduced with fractures, the total oil recovery is still high and diffusion can be an effective recovery mechanism. It is important to note that oil recovery on a reservoir scale will be reduced compared to oil recovery on core plugs.

Contents

Acknowledgements

First of all I would like to thank my supervisors, Dr. Martin A. Fernø and Professor Arne Graue at the Department of Physics and Technology at the University of Bergen for their guidance, interesting discussions and for giving me the opportunity to travel during my study.

I would also like to thank the employees of the group, and specially Dr. Geir Ersland and MSc Øyvind Eide for help with experiments, simulations and good discussions.

Thanks to Dr. David Schecter at Texas A&M, College station, Texas for interesting discussions and help during my stay. I would also like to thank Francisco Tovar for his never-ending willingness to help in the lab, and to show us the Texan way of life.

I would also like to thank all my fellow master students for interesting conversations (sometimes scientific), "god stemning" and good times at room 522. A special thank you to my lab partner Tom Ydstebø for good cooperation in the lab and for a great time during our stay at College Station, Texas.

I would like to thank my family, especially my parents Peder Langlo and Reidun D. Winter for their support and motivation during my study.

I would like to express my thanks to Karina R. Nesheim for her patience, motivation, uplifting mood and support these five years.

Finally, I would like to express my thanks to friends for the fun times and of course support and motivation throughout my whole study. I would not be able to do it without you!

Thank you!

Bergen, May 2013

Stig Andre Winter Langlo

Introduction

After conventional primary and secondary oil recovery, there is usually a great amount of oil remaining in the reservoir. This unrecovered oil is a target for enhanced oil recovery in order to meet the energy demand in the future. The interest for enhanced oil recovery has increased due to increasing oil prices, and because most of the easily recovered oil has been or is being produced. Enhanced oil recovery techniques can be thermal exposure, gas injection, WAG, polymers, surfactant and foam.

It is estimated that more than 60% of the world's oil reserves are held in carbonate reservoirs, and a significant part of these reservoirs are naturally fractured (Roehl, 1985). The oil recovery from these fractured carbonate reservoirs are typically low because approximately 80% are mixed-wet or oil-wet, leading to an ineffective water injection (Hirasaki and Zhang, 2004, Roehl, 1985). This make carbonates good candidates for CO_2 enhanced oil recovery (EOR), because CO_2 can achieve miscibility with oil at pressures of only 100-300 bars (Skjæveland and Kleppe, 1992).

Over the last year there has been a realization that CCS (Carbon Capture and Sequestration) will not be commercial in the next decade or more due to weak or non-existent climate policy. This has increased the interest of CCUS (Carbon Capture Utilization and Storage), where utilization typically refer to EOR (Hite et al., 2012). CO_2 injection for enhanced oil recovery can be an effective way to recover more oil, and to storing large quantities of CO_2 underground (Malik, 2000). Storing CO_2 in oil reservoirs has an excellent potential since oil reservoirs have stored oil and gas for millions of years (Gozalpour et al., 2005). Better understanding for CO_2 EOR is important to mitigate risks and improve the attractiveness of injecting CO_2, for the sake of the environment and to increase oil recovery (Hite et al., 2012).

CO_2 has been used commercially for over 40 years as an enhanced oil recovery technique (Enick et al., 2012). The first patent for CO_2 EOR was granted in 1952 in Whorton, USA (Sweatman et al., 2011). In the United States, CO_2 EOR contributes 280 000 barrels of oil per day, just over 5 % of the total U.S. oil production. CO_2 injection has become more and more attractive due to better technology in areas such as reservoir characterization and mobility control, as well as due to "high" oil prices. If the U.S. Department of Energy's "next generation" EOR target of 67 billion barrels is to be realized, new technologies and solutions are required. Such solutions include CO_2 foams which have been one of the focuses in this master thesis (Enick et al., 2012). CO_2 can actually recover 15 to 25% of the OOIP, and prolong the life time of a field by 15 to 20 years (Dong et al., 1999). According to other literature, CO_2 injection into a waterflooded field increases the oil recovery by 4-12% (Gozalpour et al., 2005). A lot of oil fields are fast approaching their economic limit of production making EOR measures such as CO_2 even more significant.

On a microscopic scale the CO_2 can in theory displace all the oil. There are however problems with CO_2; the high cost of capturing CO_2, and the fact that CO_2 is very mobile and has a low density which causes fingering, gravity segregation, and early breakthrough. This gives poor macroscopic sweep efficiency. Mobility control with the use of foam can give a more favorable mobility ratio, and can thereby improve oil recovery. Foam can be relatively cost effective considering the liquid only needs a surfactant concentration in the order of one weight percent. The implementation of foam as an enhanced oil recovery technique has been hindered because of a lack understanding of foam behavior in a reservoir because of the complex nature of foam and contradictions in foam studies. In naturally fractured reservoirs foam can be used to create a viscous pressure drop in the fracture, which forces the CO_2 into the oil bearing matrix, thus accelerating oil production (Farajzadeh et al., 2010, Kovscek et al., 1993, Alvarez et al., 1999, Skjæveland and Kleppe, 1992)

The aim of this thesis has been to study CO_2 injection in fractured limestone cores, which is a carbonate rock type. The research that has laid the groundwork for this thesis has been performed by Msc Malin Haugen on CO_2-injection in chalk, by Msc Sondre Svenningsen on tertiary CO_2-injection in Edwards Limestone, by Msc Stuart Baird on CT-images of CO_2-injection in chalk, Anders Christophersen and Ane Skibenes on CO_2-foam in fractured Edwards Limestone (Haugen, 2012, Skibenes, 2012, Christophersen, 2012, Svenningsen, 2011, Baird, 2013).

The results from this thesis show the potential for CCUS in fractured carbonate reservoirs. Even though the oil recovery rate is reduced with fractures, the total oil recovery is still high and diffusion can be an effective recovery mechanism.

This thesis consists of 8 chapters. Chapter 1 gives an introduction to basic theory. Chapter 2 focuses on CO_2 and foam. Chapter 3 gives an overview of the experimental setups and procedures. Chapter 4 presents the experimental results performed, and includes published results from the Reservoir Physics group between 2011- 2013. Chapter 5 discusses the work and compares the experimental results. Chapter 6 gives the general conclusions from the discussions. Chapter 7 and 8 include nomenclature and references respectively.

1. Basic Theory

1.1 Porosity

Sedimentary rock types consist of grains that are packed and cemented together. Between these grains we have cavities often referred to as pores. The size of pores is in the region of 10 – 100 μm and contains either a gas or a liquid or a combination of the two. The sedimentary rock grains makes up what is called the matrix volume, and the pores make up what is called the pore volume. The sum of the matrix volume and pore volume is called the bulk volume, the total volume of the sedimentary rock.

Porosity is a dimensionless unit that is defined as

$$\phi = \frac{V_p}{V_b} \cdot 100\% = \frac{V_b - V_m}{V_b} \cdot 100\% \tag{1.1}$$

$V_p = Porevolume$
$V_b = Bulkvolume$

$V_m = Matrix\ volume$

We can divide porosity into two categories effective porosity and residual porosity. Effective porosity is defined as the pores that are connected to each other in a pore network. The residual porosity is defined as pores that are not interconnected. The effective porosity is the interconnected pores, and fluid flow would not be possible without effective porosity. The sum of effective porosity and residual porosity is called total porosity. Porosity is highly dependent on grain size, shape and distribution (Zolotukhin, 2000).

$$\phi_{tot} = \phi_{eff} + \phi_{res} \tag{1.2}$$

1.2 Absolute Permeability

Absolute permeability is defined as the capacity for a fluid to flow through a porous medium, and is measured in Darcy. For example a porous medium with low permeability will have a high resistance (low capacity) to flow and vice versa. Permeability depends on the effective porosity, on the aspect ratio between pore throats and pore bodies, on pore size distribution and on tortuosity.

Absolute permeability can be defined from the Darcy equation

$$Q = \frac{kA\Delta P}{\mu L} \tag{1.3}$$

Q = volume rate, k = Absolute permeability, ΔP = Pressure difference, μ = Viscosity, L = length.

Absolute permeability is a property of the porous medium, and it is independent of the fluid in place.

The criteria for the Darcy law expressed as the equation above are (Zolotukhin, 2000):

I. 100% saturated with one fluid
II. Stationary flow
III. Laminar flow
IV. Horizontal flow
V. Incompressible fluid
VI. No chemical reaction between the fluid and the porous medium

1.2.1 The Klinkenberg Effect

It has been noted, in laboratory experiments that, at low mean pressure, the measurements of gas permeability often yield a higher absolute permeability than that from liquid. Gas behaves at low pressure as if it has negligible friction towards the pore walls. This causes the gas to have a higher velocity compared to that of a liquid or a high-pressure gas. This phenomenon is known as the Klinkenberg effect or slippage-at-the-wall effect. The Darcy law relies on the fluid to have typical Newtonian fluid behavior, and the klinkenberg effect requires a correction to be made (Klinkenberg, 1941).

1.3 Fluid Saturation

Total pore volume can be written as:

$$V_p = V_o + V_g + V_w \tag{1.4}$$

From V_o, V_g and V_w we can define saturation as a fraction of the pore volume from a particular fluid:

$$S_i = \frac{V_i}{V_p}, \qquad i = 1, \ldots, n \tag{1.5}$$

"n" tells us the total number of fluids in place. For example if we have oil, water and gas present, n equals three. This leads to the following equation:

$$\sum_{i=1}^{n} S_i = 1 \tag{1.6}$$

The fluid saturations can vary from 0 - 1. The endpoint saturations are of a specific interest, in the reservoir there will always be some oil left behind after production seizes. The oil left behind after a displacement process is commonly referred to as residual oil saturation (Sor), which we preferably want to be as low as possible. The remaining water after oil displacement is known as the irreducible water saturation (S_{wi}).

1.4 Miscibility and Wettability

1.4.1 Miscibility

Miscibility is a very important parameter in reservoir physics for the reason that miscibility increases the displacement efficiency and ultimate recovery (Adepoju et al., 2013). A miscible fluid can in theory displace all the oil on a microscopic scale(Skjæveland and Kleppe, 1992). Miscible displacement can leave a substantial amount of residual oil behind the displacing front, this is mainly caused by two factors: instabilities caused by local heterogeneities (viscous fingering) or water shielding(Mûller and Lake, 1991). Water shielding will be explained in more detail in chapter 2.1.2. Molecules in a mixture can either be attracted to molecules of its own kind, or attracted to molecules of different kinds. Their preference towards each other depends on cohesion also known as Van der Waals forces. If for example the two fluids in place have a greater attraction towards their own kind, the fluids will be immiscible and vice versa, if the fluids have a greater attraction towards the other fluid in place, they will mix with each other and are called miscible (Zolotukhin, 2000). From experience we know that water and oil are immiscible fluids, while water and alcohol are miscible.

There are three different miscibility categories, depending on the composition of the fluids; First contact miscibility, vaporizing gas drive, and condensing gas drive.

First contact miscibility

Figure 1-1 shows a first contact miscibility process in a ternary diagram. We have two different compositions of a crude oil and a gas respectively in each corner. If the dilution path does not intersect the two-phase region (the shaded area), the displacement will consist of a single hydrocarbon phase with a gas-oil mixing zone, and is therefore what is called first contact miscible. (Lake, 1989)

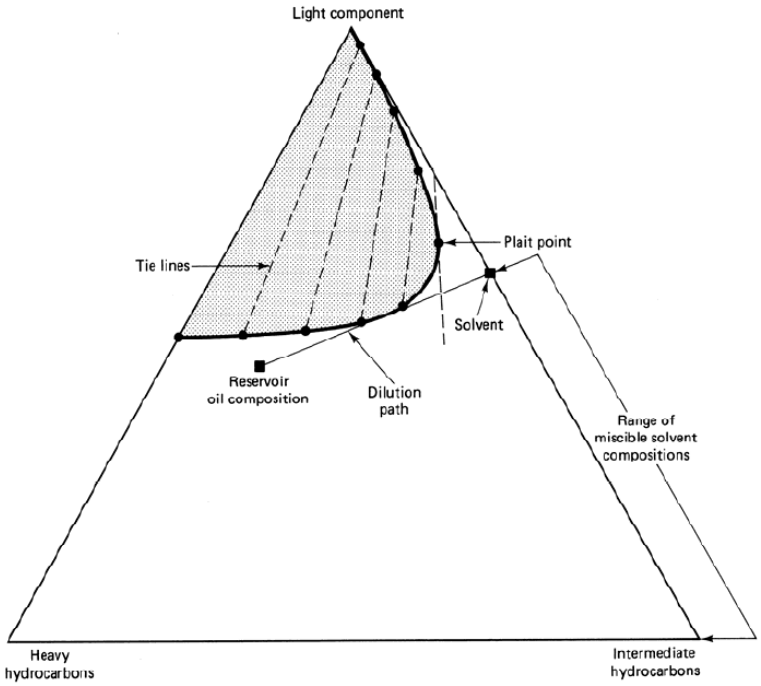

Figure 1-1 - First contact miscibility (Lake, 1989)

Vaporizing gas drive

Suppose there are two compositions of gas and oil as shown in the Figure 1-2. In this case the dilution path intersects the two-phase region, which means it is not first-contact miscible. The displacing gas consists entirely of methane (C_1), and displaces the oil. Consider a series of cells in a one-dimensional displacement. The first cell initially contains oil, where gas then is added. The new composition is now given as M_1. The mixture then splits into two phases, G_1 for the gas and L_1 for the liquid. The gas is now more mobile than the liquid and starts mixing with more oil in the next cell. The composition in the second cell will now be M_2, which in turn splits into two phases G_2 and L_2. The gas is again more mobile than the liquid, and starts mixing with the oil in the next cell. This continues until the gas is so enriched with intermediate components that it becomes first-contact miscible with the given oil. This occurs at the plait point also known as the point of tangency. Miscibility in this case is developed at the front of the displacement. Miscibility will develop or occur as long as the two compositions are on opposite sides of the critical tie line. (Lake, 1989)

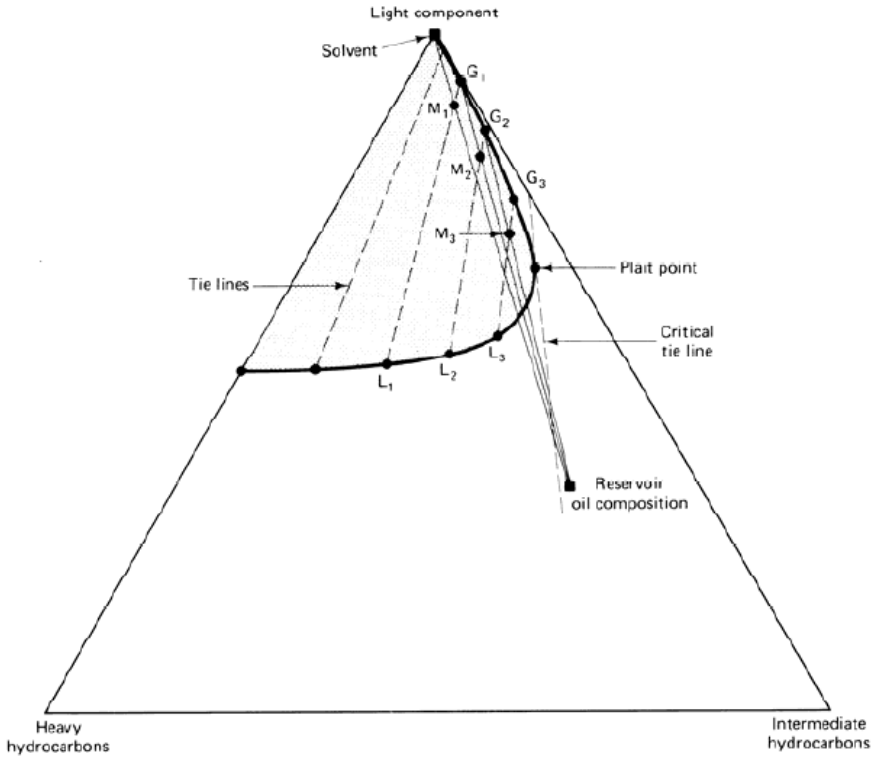

Figure 1-2 - Vaporizing gas drive (Lake, 1989)

Condensing gas drive

Given the two compositions as shown in Figure 1-3, miscibility will develop since the compositions of gas and oil are on different sides of the critical tie line. Gas is injected and mixed with the oil in the first cell. The new composition M1 splits into two phases, G1 for the gas and L1 for the liquid. The gas is more mobile and moves on to the next mixing cell. The liquid that stays behind mixes with fresh gas, which is made into composition M2. This continues until the composition at the rear develops miscibility. The liquid face becomes more and more enriched with intermediate components, which is why it is called condensing gas drive, because the gas releases the intermediate components. The front of the mixing zone is an immiscible displacement, since the gas phase at the front is not miscible with the oil.(Lake, 1989)

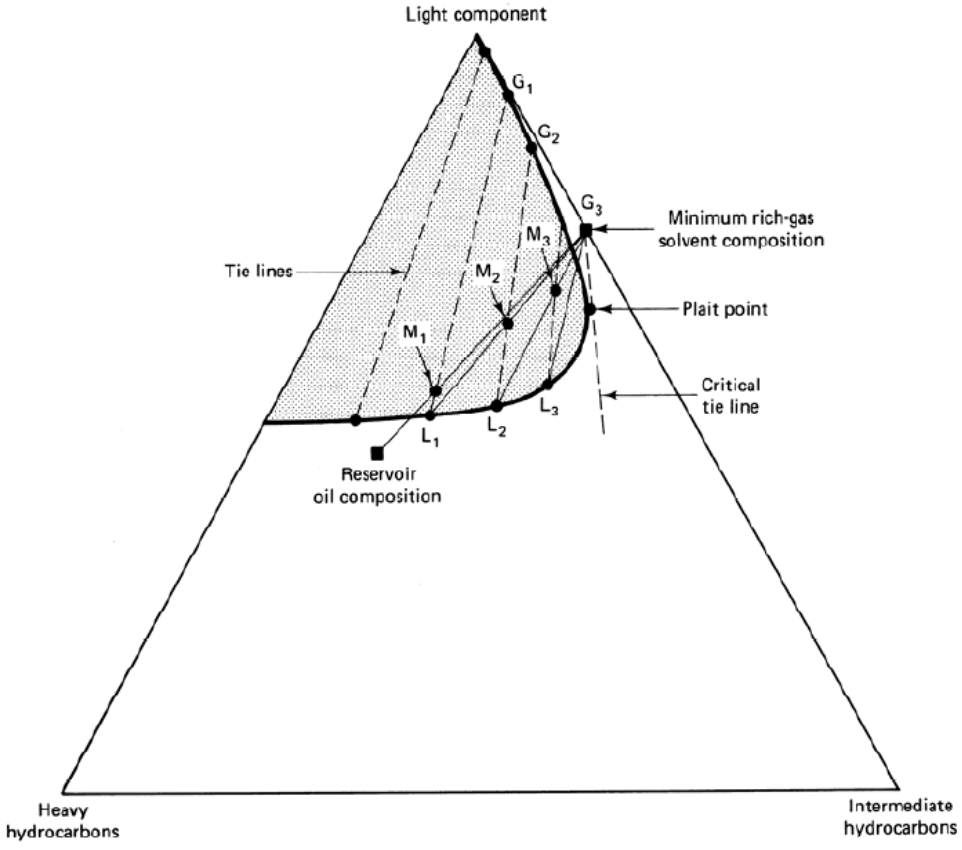

Figure 1-3 - condensing gas drive (Lake, 1989)

Minimum Miscibility Pressure (MMP).

Two phases that are immiscible may become miscible at a higher pressure. The two-phase area in the ternary diagram in Figure 1-3 increases in size with decreasing pressure. The particular composition shown in the ternary diagram would become immiscible if pressure was decreased. Vice versa if the given two-phase area becomes smaller with higher pressure it can cause two phases that are immiscible at a certain pressure, to become miscible at a higher pressure (at constant temperature). The pressure needed to develop miscibility (at a constant temperature and composition) is called *minimum miscibility pressure* and is schematically shown in Figure 1-4.

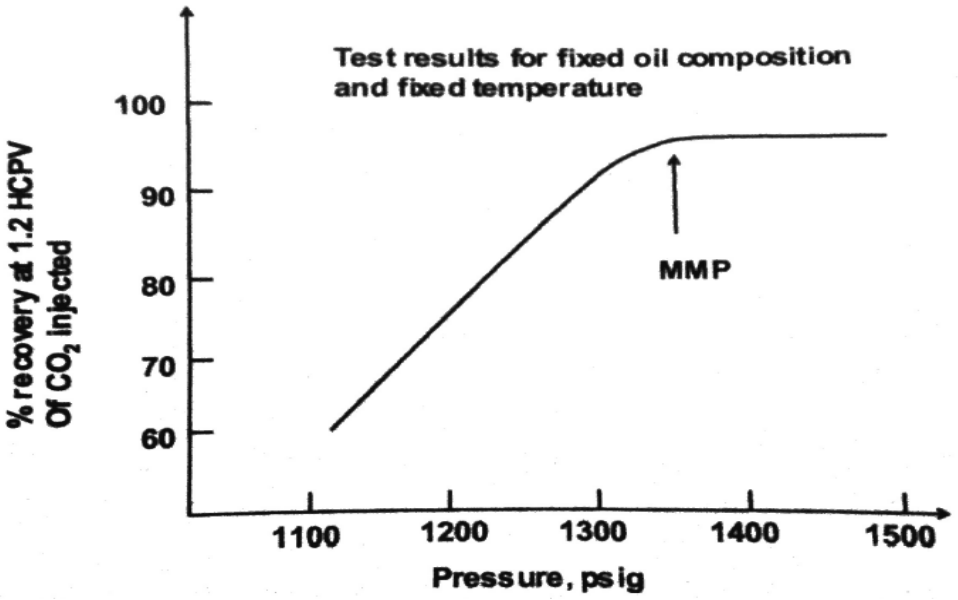

Figure 1-4 – Schematic illustration showing minimum miscibility pressure for CO_2 for a fixed oil composition (Skarrestad and Skauge, 2011)

1.4.2 **Wettability**

"*Wettability can be defined as the tendency of one fluid to spread on or adhere to a solid surface in the presence of other immiscible fluids*" (Zolotukhin, 2000). The interactions between the water, oil, gas and rock mineral decide which fluid is placed where in the porous medium, and effects properties such as flow, and saturation.

Adhesive forces are the forces between the fluids and a solid surface. If there is more than one fluid present the fluid with the most adhesive attraction with the pore wall is called the wetting fluid(Zolotukhin, 2000).

Wettability may range from strongly water-wet to intermediate-wet to strongly oil-wet. If a porous media does not have any preference of any of the liquids the porous media is neutrally wet. Figure 1-5 shows the effect of wettability in a porous rock.

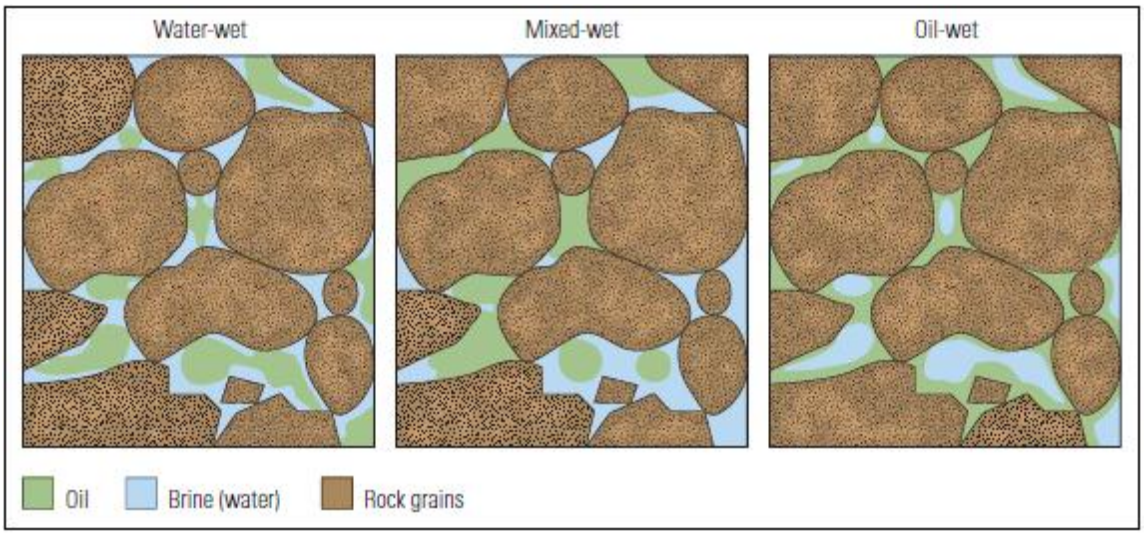

Figure 1-5 – Illustration showing effect of wettability in a porous medium modified from (Abdallah et al., 2007)

Reservoirs are water-wet before becoming in contact with oil, but polar components in the oil such as resins and asphaltenes interact with the surface of the pore walls. This can cause wettability to become more oil-wet. The pores only become oil wet in the pores/pore walls that the oil are in contact with, which in turn depends on pore geometry and mineralogy, which makes classifying a porous medium difficult.

Three classes of wettability have been proposed (Skarrestad and Skauge, 2011):

- Fractionally-wet (FW) where the oil-wet pores are uncorrelated to size
- Mixed-wet small pores (MWS) where the smallest pores are oil-wet
- Mixed wet large pores (MWL) where the largest pores are oil-wet

Measuring wettability

To measure wettability there are two main tests that are performed. One of the methods is called the USBM (US Bureau of Mines) test which is based on the capillary pressure curve shown in Figure 1-6 the area (A1) between the forced oil injection curve and the saturation axis and the area (A2) between the forced water injection curve and the saturation axes as shown in Figure 1-6. The USBM test values goes from -∞ (strongly oil-wet) to +∞ (strongly water-wet), this can be shown from the equation (1.7).

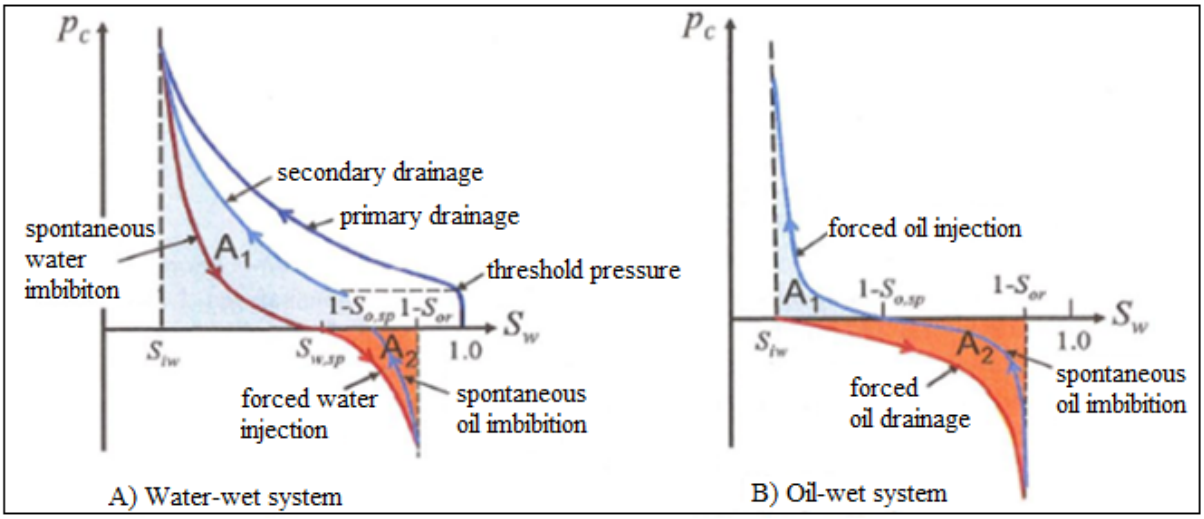

Figure 1-6 – Schematic illustration showing the capillary pressure curve for a water-wet system A) and an oil-wet system B), and the corresponding areas(A1 and A2) used in the USBM equation for determining the systems wettability. The figure also shows amott-Harvey wettability values (saturations) used for wettability measurements. (Lien, 2006)

$$I_{USBM} = \log\frac{A_1}{A_2} \tag{1.7}$$

The Amott-Harvey method combines imbibition and forced displacement to measure the average wettability of a core (Anderson, 1986). The Amott-Harvey method is the test used in this thesis. This method is based on the fact that a porous medium saturated with a non-wetting fluid may spontaneously imbibe if placed in contact with the wetting fluid until equilibrium is reached. The Amott-Harvey index is the difference between the "displaced-by-water ratio" and the "displaced-by-oil ratio". As shown from equation.

$$I_{A-H} = I_W - I_o = \frac{V_{w,sp}}{V_{w,t}} - \frac{V_{o,sp}}{V_{o,t}} = \frac{S_{w,sp} - S_{iw}}{1 - S_{iw} - S_{or}} - \frac{(1 - S_{o,sp}) - S_{iw}}{1 - S_{iw} - S_{or}} \tag{1.8}$$

$V_{w,sp}$ is the volume of oil spontaneously displaced by water, $V_{w,t}$ is the total volume of oil displaced(forced and spontaneous) by water, $V_{o,sp}$ is the total volume of water spontaneously displaced by oil, and $V_{o,t}$ is the total volume of water displaced(forced and spontaneous) by oil. How these liquid volumes are measured will be explained in the experimental part of this thesis.

1.4.3 **Interfacial Tension**

The interface between two immiscible fluids can be considered as a membrane-like surface separating phases with relatively strong intermolecular cohesion. The strength of the interfacial tension is related to the work, or energy, required keeping the two fluids apart. (Zolotukhin, 2000). This means that if for example we have a positive interfacial tension (σ) the fluids have a higher attraction for its own kind, and the fluids are immiscible. If the interfacial tension is close to zero they will after a given time (with diffusion) become mixed and are truly miscible. Negative interfacial tension means dissolution and can cause a chemical reaction between the two fluids, making a new fluid.

1.4.4 **Wetting Angle**

The wetting angle between two immiscible fluids and a solid surface can be used to describe the wettability preference of the system if for example if a drop of water is placed on a solid surface with surrounding oil see Figure 1-7. The interaction between the cohesive forces (electrostatic forces between the fluids) and adhesive forces (electrostatic forces between the different fluids and the solid surface) will decide what shape and thus what angle the water droplet will have. If the water has the highest attraction towards the surface, then the water will be the wetting phase and will disperse over the solid. The wetting angle will then be zero. In the opposite case if oil has a much higher attraction to the solid, then the water will form as a droplet so that as little of the water touches the solid as possible.

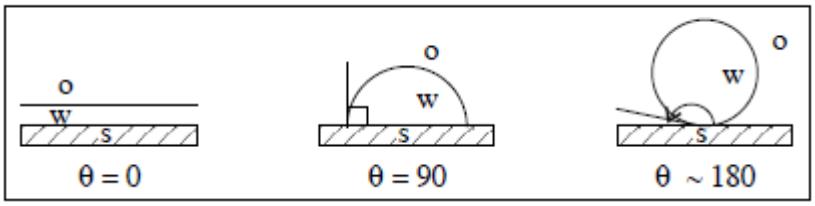

Figure 1-7 – Schematic illustration showing wetting preference between different solids by water and oil system. (Zolotukhin, 2000)

Contact angle values	Wettability preference
0 – 30	Strongly water wet
30 – 90	Preferentially water wet
90	Neutral wettability
90 – 150	Preferentially oil wet
150 – 180	Strongly oil wet

Table 1-1 – Contact Angle Values (Craig, 1971)

Table 1-1 shows for which values we have a given wettability preference, ranging for strongly water-wet at 0 degrees, and strongly oil-wet at 180 degrees.

1.5 Capillary Pressure

When two immiscible fluids inhabit a narrow (capillary) tube, or a pore, adhesive forces causes the wetting fluid to curve along the wall. The meniscus between the two fluids creates an angle with the pore wall. This angle is called the wetting angle. Capillary pressure can be defined as the molecular pressure difference across the interface of the two fluids. Capillary pressure can also be defined as the pressure difference between the wetting phase and the non-wetting phase.

$$P_c = p_w - p_{nw} \tag{1.9}$$

Where P_C is the capillary pressure, p_W is the pressure of the wetting phase, p_{nw} is the non-wetting phase. The pressure difference is caused by interaction between the adhesive force and the cohesive force. If the tube or pore is placed vertical the wetting fluid will displace the non-wetting fluid until the capillary pressure reaches equilibrium with the fluid gravity. Capillary pressure can be defined as:

$$P_c = \Delta\rho g h \tag{1.10}$$

Where P_C is the capillary pressure, $\Delta\rho$ is the density difference, g is the gravity constant, h is the height. This equation can tell us for example where we will find our oil water contact in an oil reservoir. When oil migrates up from the source rock to a reservoir with a trap, it is because of the lighter density of oil that oil migrates upwards. Before it can get into the reservoir it needs to overcome the capillary pressure. The capillary pressure that needs to be overcome in order to migrate into the reservoir is called the threshold pressure. It is at the threshold pressure the depth of the oil water contact is given.

Capillary pressure can also be defined as:

$$P_c = \frac{2\sigma_{nw,w} cos\theta}{r} \tag{1.11}$$

Where P_C is the capillary pressure, $\sigma_{nw,w}$ is the interfacial tension between the non-wetting and the wetting fluid, θ is the wetting angle, and r is the radius of the capillary. This equation tells us that the capillary pressure is highest in the smallest pores, so for example in a water wet porous medium the smallest pores will have the most water, while the oil will be in the bigger pores with water along the pore walls.(Zolotukhin, 2000)

1.5.1 **Drainage and imbibition**

Injecting a non-wetting fluid into a porous medium and displacing the wetting fluid is a process called drainage. The opposite phenomenon is called imbibition. These processes displace the fluids differently. In a drainage process the non-wetting fluid will displace the middle of the pores, while in an imbibition process the wetting fluid will displace from along the pore walls which will cause the non-wetting fluid to "snap-off" and this effect is called capillary trapping.

1.5.2 **Capillary pressure curve**

The capillary pressure curve shows how the capillary pressure changes with the different saturations. Where a positive capillary pressure means that if the porous medium comes in contact with the wetting fluid, the wetting fluid will imbibe to restore equilibrium ($P_c = 0$) of the porous medium. Figure 1-8 shows a capillary pressure curve for a water-wet rock type.

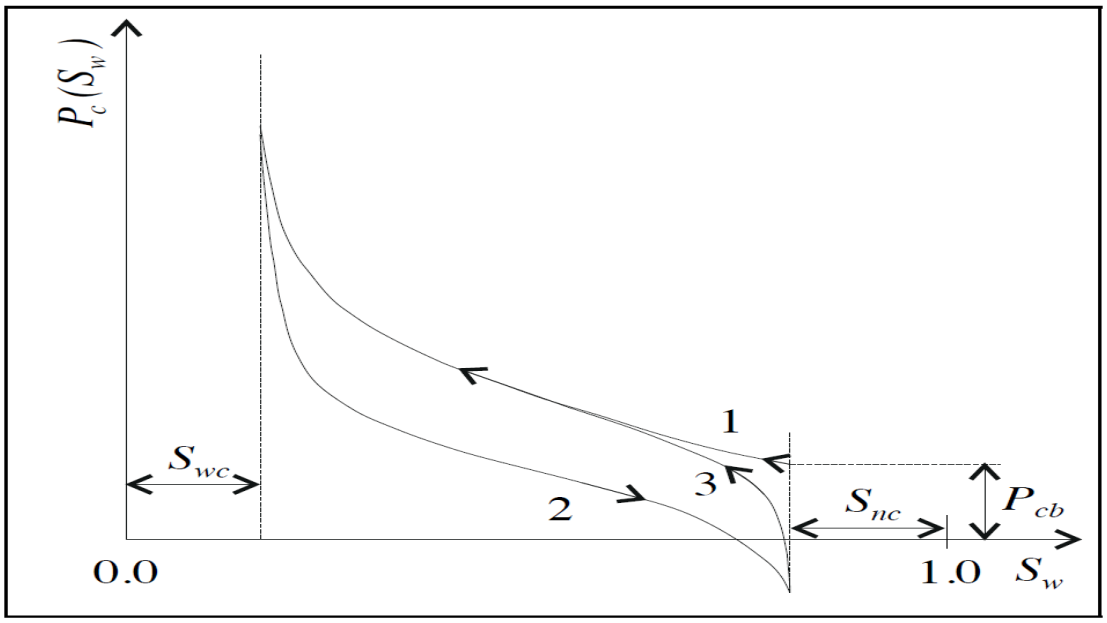

Figure 1-8 - Capillary pressure curve for two phase flow in the conditions of drainage (1), imbibition (2) and secondary drainage (3). P_{cb} is the threshold capilary pressure of the fluid displacement. S_{wc} and S_{nc} denote the "connate" (irreducible) saturations of the wetting and the non-wetting phases, respectively. (Zolotukhin, 2000)

The capillary pressure curve can give a lot of information. For example the pore size distribution. If for instance the drainage curve after the threshold pressure went straight to Swc, this would indicate that we had a very homogeneous porous medium, with only one typical pore throat size. If the drainage curve went from the threshold pressure towards Swc with a very oblique angle then this would indicate a heterogeneous porous medium with different pore throat sizes. The imbibition curve can tell us something about the wettability of the medium from which point the imbibition curve intersects the saturation line (P_c=0). The further to the right the intersection occurs, the more water wet the porous medium is. The curves for drainage and imbibition are not the same; the shape of the two curves together resembles a loop. This effect is called capillary hysteresis. (Zolotukhin, 2000)

1.6 Relative permeability

Relative permeability is a parameter used to describe the permeability when we have more than one fluid present in the pores. When only one fluid is present we talk about the absolute permeability. Absolute permeability is independent of the fluid type (as long as the Klinkenberg effect is not taking place). When more than one immiscible fluid is occupying a porous medium the two fluids will affect each other. They affect each other by where they are flowing, for instance in a water-wet system the water will prefer to flow along the pore walls, while the oil will occupy the middle of the pores. This will give oil an easier flow path, than the water, which in turn will cause the oil generally to have a higher relative permeability at the same saturation as water. Although oil in this case will generally have a higher permeability relative permeability is highly dependent on saturation. For instance, there is little oil in the pores, the oil will not flow as freely and thus have lower relative permeability for the given saturation.

Relative permeability is related to the effective and the absolute permeability of a particular fluid in the system.

Effective permeability can be defined as:

$$k_e = \frac{q\ \mu\ \Delta x}{A\ \Delta p} \tag{1.12}$$

Where k_e is the effective permeability. k_e will be equal to the absolute permeability for 100% saturation.

In a multiphase flow Darcy law can be generalized as:

$$k_{je} = \frac{q_j \mu_j \Delta x}{A\ \Delta p_j} \tag{1.13}$$

j denotes a fluid phase *j*, and k_{je} is the effective (phase) permeability.

The sum of effective permeability is less than the total or absolute permeability of a given porous medium:

$$\sum_{j=1}^{n} k_{je} < k \tag{1.14}$$

Effective permeability is a function of the fluid saturation, as well as rock property, absolute permeability, fluid property, and reservoir conditions (pressure, temperature) (Zolotukhin, 2000)

Relative permeability can be defined as:

$$k_{rj} = \frac{k_{ej}}{k} \tag{1.15}$$

In a two phase system effective permeability and thus relative permeability can be expressed as a function of saturation. The relationship between k_{rj} and S_j is affected by rock properties and wettability, see Figure 1-9. (Zolotukhin, 2000)

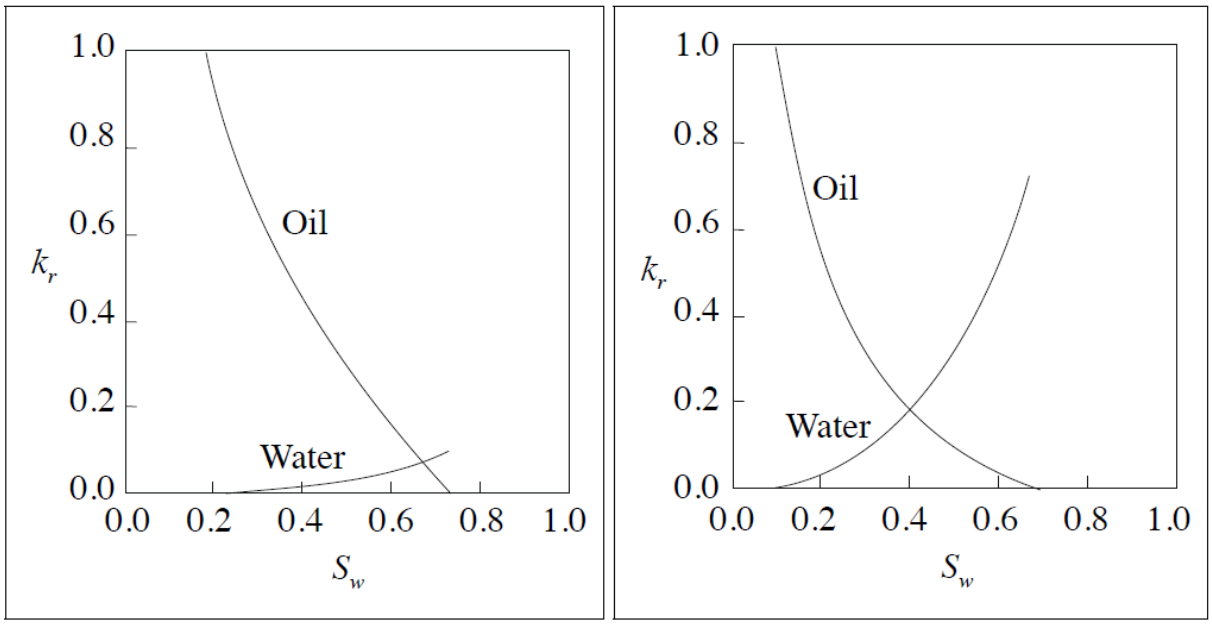

Figure 1-9 - Characteristics of typical relative permeability for a two-phase flow. (left figure is a water-wet formation and the right figure is an oil-wet formation) (Zolotukhin, 2000)

1.7 Capillary number

In a porous medium where one immiscible fluid is displacing another we have three forces involved. The viscous force (VF), the gravitational force (GF), and the capillary force (CF) (Skarrestad and Skauge, 2011). The capillary force is what captures the residual oil in the pores, and makes it more difficult to recover. The viscous force is what displaces the oil (related to the velocity and viscosity). The gravitational force can both stabilize a front, and cause segregation. From these forces we have a dimensionless number called the capillary number that expresses the ratio between the viscous force and capillary force, and can be defined as:

$$N_{vc} = \frac{VF}{CF} = \frac{u_w \cdot \mu_w}{\sigma_{o/w}} \tag{1.16}$$

Where N_{vc} is the capillary number, u_W is the velocity, μ_W is the viscosity and $\sigma_{O/W}$ is the interfacial tension between oil and water.

This capillary number can be related to residual oil saturation, S_{or}, in the porous medium. From laboratory experiments there has been created a curve called the capillary desaturation curve (CDC) which shows the relation between the capillary number and residual oil.

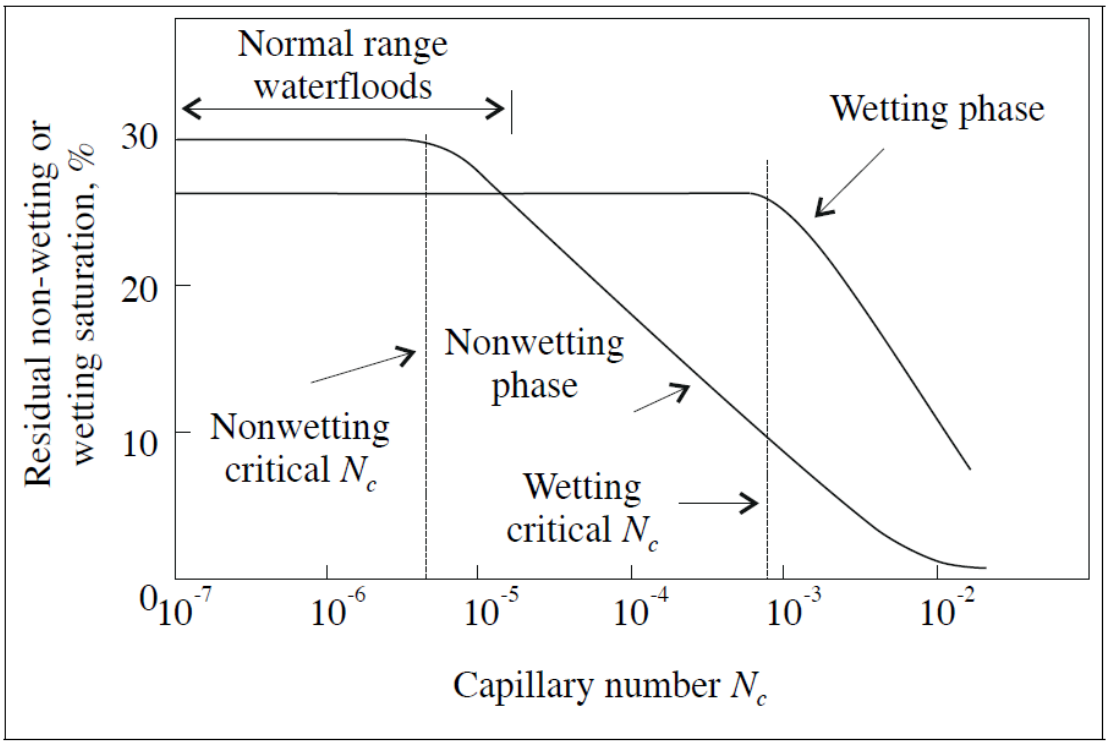

Figure 1-10 - Schematic capillary desaturation curve (CDC) (Skarrestad and Skauge, 2011)

This schematic shows that after we reach a certain critical capillary number the residual saturation decreases which gives a higher microscopic recovery. We can increase the capillary number by either increasing the velocity or viscosity (viscous force) or by reducing the interfacial tension (capillary force).

1.8 Dispersion in porous media

Dispersion can be defined as the mixing between two miscible fluids, caused by diffusion and convection (also called mechanical dispersion) (Lake, 1989). If two miscible fluids are in contact with each other the sharp boundary between the two fluids will slowly start to diffuse into one another. This boundary will diffuse and become a mixed zone where the concentration will change throughout the zone, as shown in Figure 1-11. The extent of dispersion increases with increasing heterogeneity (Adepoju et al., 2013). The diffusion is caused by random motion of molecules (Perkins, 1963).

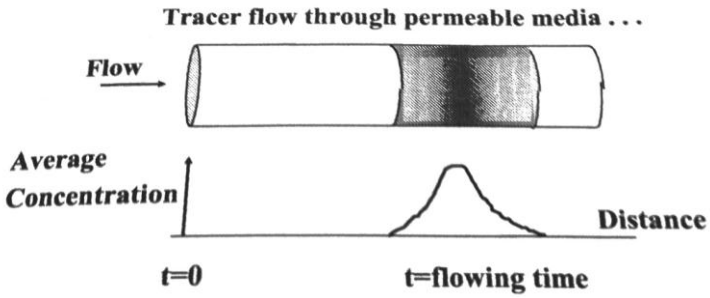

Figure 1-11- Schematic illustration of the phenomenon of dispersion (Skarrestad and Skauge, 2011)

1.8.1 Diffusion

Molecular diffusion can be defined as the movement of ions or molecules from regions of high concentration to low concentration within an isotropic media (Darvish, 2007). The movement is caused by the system trying to regain equilibrium in the concentration distribution.

Fick's second law describes diffusion between to miscible fluids in one dimension:

$$\frac{\partial C}{\partial t} = D_O \frac{\partial^2 C}{\partial^2 x} \tag{1.17}$$

Where C is the concentration of one fluid, t is the time, D_O is the diffusion coefficient in the absence of a porous medium and x is the traveled distance.

The equation can be correlated to work for a porous medium. The diffusion coefficient must then be correlated, to the apparent diffusion coefficient, D. The porous media will reduce the diffusion coefficient for the reason that the porous media acts as a barrier causing molecules to travel a longer distance, twisting and winding inside the porous media. The reduction in diffusivity is related to the formation factor F and porosity φ, which gives the relationship $1/F\varphi = D/D_O$ (Bijeljic and Blunt, 2006). This causes lower permeable formations like limestone to have lower rates of diffusion. According to Fick's second law of diffusion, if the boundary condition with a constant concentration at the boundary, then the depth of penetration is proportional to the square root of time. This means that the further from a concentration source (for example a fracture) CO_2 diffuses, the slower diffusion occurs. This relationship makes saturation (concentration) related to the square root of time, if diffusion is the only mixing mechanism (Cussler, 1997), as shown in Figure 1-12.

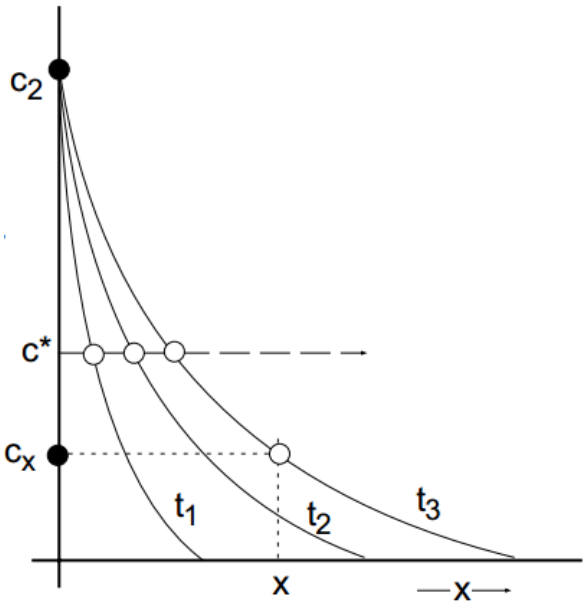

Figure 1-12 – Shows advance of the concentration front (c*) as a function of distance at different times. C_2 is a constant concentration. Modified from (Bird et al., 1960)

1.8.2 **Convection**

Convection is mechanical mixing resulting from velocity variations in longitudinal and transverse directions within the porous medium (Adepoju et al., 2013). Macroscopic behavior of dispersion in porous media can be explained with the help of the peclet number.

$$Pe = \frac{u\,L}{D_m} \tag{1.18}$$

Where *Pe* is the Peclet number, *u* is the average flow speed, *L* is the length (inter-pore distance), and D_m is the molecular diffusion coefficient.

Figure 1-13 shows three different flow regimes, presenting whether the dispersion is diffusion dominated or convection (mechanical dispersion) dominated. The x-axis shows the Peclet number in a logarithmic scale. For longitudinal dispersion in absence of convection, a low Peclet number regime, molecular diffusion is the only mechanism for fluid mixing (Bijeljic and Blunt, 2006). Figure 1-13 shows that convection becomes more dominating at higher flow rates.

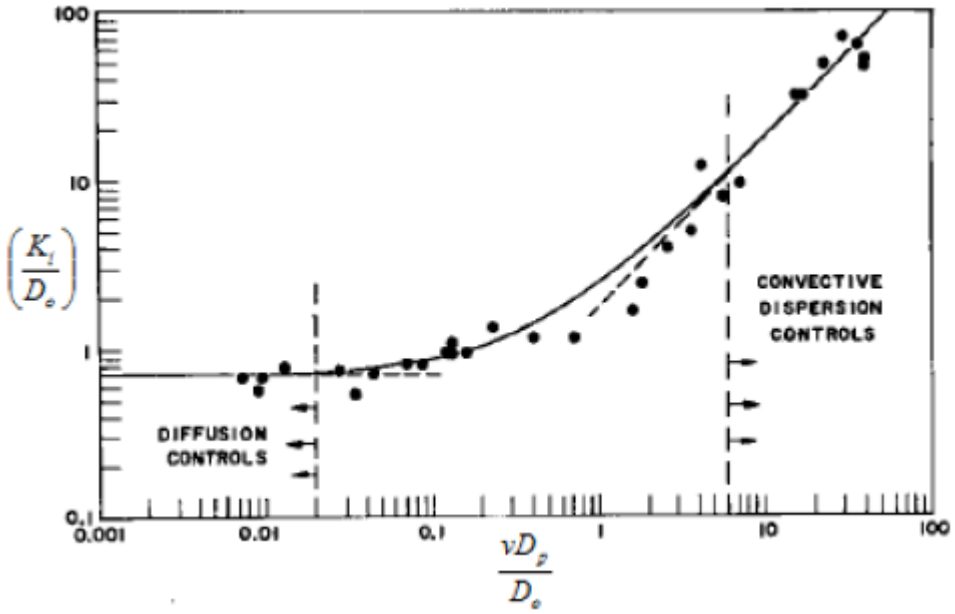

Figure 1-13 – Schematic illustration showing three dispersion flow regimes, the x-axis giving the Peclet number. K_l is the longitudinal dispersion coefficient [cm^2/sec], Do is the molecular diffusion coefficient [cm^2/sec], v is the average interstitial velocity [cm/sec] and Dp is the average diameter of the particles [cm]. modified from (Perkins, 1963)

Figure 1-14 shows the random hopping along streamlines (a) , mixing at intersections(b), and mixing at low velocity regions (c). The points (a) and (b) in the figure is where the mechanical mixing (Convection) becomes more dominant. For low Peclet numbers the mixing is only diffusion dominated. From around 0,1 (numbers observed in Berea sandstone) convection is observed, and gradually becomes more dominating with higher Peclet numbers. Along the edges the velocity is lower, and diffusion can still dominate the mixing. In dead and pores as illustrated at (c) in Figure 1-14 even at very high Peclet numbers diffusion can be the leading mixing method (Bijeljic and Blunt, 2006).

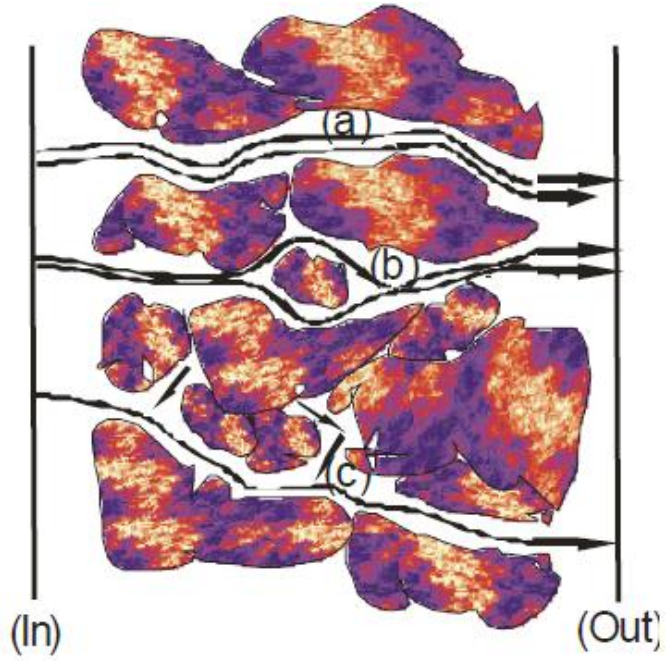

Figure 1-14 –Schematic illustration showing the mechanisms of dispersion in a porous medium. (a) Random hoping along the streamlines, (b) mixing at pore intersections and (c) mixing at low velocity regions. (Bijeljic and Blunt, 2006)

2. CO_2 and Foam

2.1 CO_2

Carbon dioxide i.e. CO_2, is a greenhouse gas and is at the head of the global warming debate. The increasing concentration of CO_2 in the atmosphere causes temperature on Earth to rise. The increasing temperature on Earth occurs because CO_2 has an isolating effect (absorption) on radiation leaving the planet, but the CO_2 does not affect radiation coming in to the atmosphere (radiation coming in to the atmosphere is mainly affected by H_2O and O_3) (Holter et al., 2010). This has to do with the wavelength of the radiation. The effect of CO_2 causes the same amount of energy to be let into the atmosphere, but less energy is released out of the atmosphere. Prior to the industrial revolution, (approximately 1750) the concentration was fairly stable at 280 ppm. Today the levels are approximately 370 ppm (NOAA, 2013). This increase in concentration is due to the rise in anthropogenic activity.

Storing CO_2 in oil reservoirs has an excellent potential since oil reservoirs have stored oil and gas for millions of years. One of the advantages to CO_2 is that it can be used in the petroleum industry as CCUS (Carbon Capture Utilization and Storage). CO_2 can be used to displace oil and at the same time leaving parts of the CO_2 underground in place of the oil (Gozalpour et al., 2005). CO_2 has a relatively low MMP compared to other injection gases such as methane, and range between 100-300 Bars, depending on the temperature and composition of the displaced fluid (Skjæveland and Kleppe, 1992). Meaning that on a microscopic scale the CO_2 can in theory displace all the oil. Figure 2-1 is a basic figure showing how CO_2 mixes and swells the oil, while at the same time mobilizing the trapped oil on a microscopic scale. There are however three problems with CO_2; one is the high cost of capturing CO_2, and the fact that CO_2 is very mobile and has a low density which causes fingering, gravity segregation and early breakthrough. This gives poor macroscopic sweep efficiency. There are several ways to solve the mobility problem. Mobility control with the use of WAG or foam can give a more favorable mobility ratio.(Skjæveland and Kleppe, 1992, Farajzadeh et al., 2010, NETL, 2010, Enick et al., 2012)

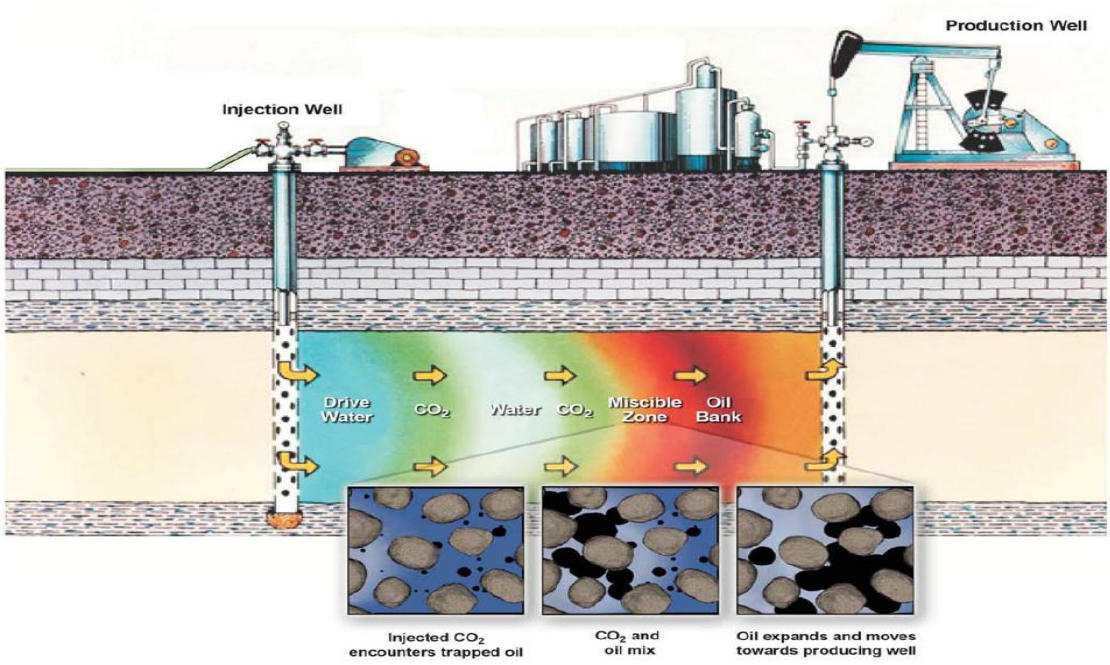

Figure 2-1- Basic figure Showing a miscible CO2 flooding (NETL, 2010)

CO_2 has been used in commercially in over 40 years as an enhanced oil recovery technique (EOR). (Enick et al., 2012). The first patent for CO_2 EOR was granted in 1952 in Whorton, USA (Sweatman et al., 2011). In the United States, CO_2 EOR contributes 280 000 barrels of oil per day, just over 5 % of the total U.S. oil production. CO_2 injection has become more and more attractive due to better technology in areas such as reservoir characterization and mobility control, as well as "high" oil prices. If the U.S. Department of Energy's "next generation" EOR target of 67 billion barrels is to be realized, new technologies and solutions are required. Such solutions include CO_2 foams which have been one of the focuses in this master thesis. About 74.7% of the CO_2 used for EOR in the U.S. is provided from CO_2-rich natural gas from formations (Enick et al., 2012). Injecting CO_2 into oil reservoirs for EOR has been applied in 18 077 active wells worldwide, 17 112 of these in the U.S according to the latest EOR survey (Sweatman et al., 2011).

Without any EOR techniques such as WAG (water alternating gas), gravity stable displacement, huff-and-puff or mobility control, CO_2-flooding has a relatively low recovery in field cases. For a miscible CO_2 flood the CO_2 only recovers around 10-20% of the OOIP (5-10% in immiscible cases) with 0.8 hydrocarbon (oil) pore volume (HCPV) injected (Enick et al., 2012). This low recovery is caused by high mobility which leads to viscous fingering and early CO_2 breakthrough. The unfavorable mobility ratio also causes CO_2 to mainly flood the high permeable layers. Another reason for the low recovery is the low density which can cause gravity override of the CO_2 only recovering the attic oil (oil in the top layers). Therefore to recover a larger amount of oil, EOR techniques such as WAG and foam are needed. Injecting CO_2 can be effective when a light oil field is nearing depletion under waterflood. There are different opinions on how effective CO_2 can be after a waterflood, according some papers , CO_2 can actually recover 15 to 25% of the OOIP and prolong the life time of a field by 15 to 20 years (Dong et al., 1999). According to other literature CO_2 injection into a waterflooded field increases the oil recovery by 4-12% (Gozalpour et al., 2005). A lot of oil fields are fast approaching their economic limit of production making EOR measures such as CO_2 even more significant.

2.1.1 Advantages and disadvantages of using CO_2 as displacing fluid

Advantages of using CO_2 as displacing fluid

As mentioned earlier in this thesis, CO_2 has a relatively low MMP compared to other injection gases. Meaning that on a microscopic scale the CO_2 can in theory displace all the oil. The problem is that the high mobility of CO_2, compared to, for example water, makes it harder for the carbon dioxide to contact the whole reservoir (can be inefficient on a macroscopic scale).

Carbon dioxide has a higher density than other gases, with increasing pressure it can actually reach a density similar to oil. This is positive in a horizontal displacement process as it minimizes the chances of segregation. In a gravity stable process it is favorable to have a large density difference between the fluids. CO_2 has a higher viscosity than other injected gases; this gives CO_2 a more favorable mobility ratio than for example methane. (Skjæveland and Kleppe, 1992)

CO_2 can extract components up to C30. Extracting components from immobile oil into the CO_2 phase can increase oil recovery. Extracting components also reduces interfacial tension, which in turn can cause a development of miscibility. Extraction of components causes relatively low interfacial tension (zero, if miscible develops) between the oil and carbon dioxide, this gives a lower residual oil on a microscopic scale. Molecular diffusion for the CO_2 makes it possible for the CO_2 to diffuse into low permeability zones of one meter in times of three to thirty years (Skjæveland and Kleppe, 1992).

Because CO_2 is soluble with water it can more easily reach water shielded oil, water shielding detailed in chapter 2.1.2. Carbon dioxide mixed with water gives the water lower interfacial tension, which can give a lower residual oil when water displaces the oil in a CO_2 WAG (Water Alternating Gas) process. CO_2 increases the oil density, thus reducing the density difference between oil and water which is positive to avoid segregation. CO_2 causes oil swelling, which may cause immobile oil to become mobile. When CO_2 swells the oil it decreases the oils viscosity giving a more favorable mobility ratio (Skjæveland and Kleppe, 1992). Oil may swell to as much as twice the original volume (Do and Pinczewski, 1991). Given enough time oil swelling can cause water shielded oil, immobile oil, to break through the water barrier and become mobile (Grogan, 1987).

- Relatively low MMP
- High microscopic displacement
- Higher density than other gases
- Higher viscosity than other gases
- Can extract components up to C30
- Low interfacial tension between CO_2 and oil
- Molecular diffusion
- Solubility with water makes contacting water shielded oil easier
- Gives water lower interfacial tension towards oil
- CO_2 increases oil density
- CO_2 causes swelling
- Decreases oil viscosity

Disadvantages of using CO_2 as displacing fluid

In a gravity stable injection gases such as methane has a more favorable density difference than CO_2. CO_2 has acidic properties which can cause corrosion of equipment. With today's technology, CO_2 is expensive to capture. It is also expensive to separate CO_2 from the produced oil, especially if the CO_2 content becomes too high (Morsi et al., 2004). There are natural CO_2 reservoirs; these are however, not always located nearby an oil field. As mentioned, CO_2 has an unfavorable mobility ratio, which causes viscous fingering through the oil. This can lead to early break through and very low macroscopic sweep efficiency. The unfavorable mobility ratio can also cause the CO_2 to flow through high permeable zones, leaving low permeable zones unswept (channeling). The density difference between CO_2 and oil in horizontal flooding can cause gravity segregation, so that the CO_2 only reaches the attic oil. This effect can be reduced if there are higher permeable layers in the bottom than the top of the given formation. Low vertical permeability can also delay the segregation process (Skjæveland and Kleppe, 1992). Although diffusion effects are very effective on a microscopic scale, on a field scale it might not be effective enough to offset the negative effects of bypassed oil due to the unfavorable mobility and density difference (Grogan, 1987).

- Corrosive
- Expensive to capture
- Expensive to separate from produced oil
- Unfavorable mobility ratio
- Higher density difference than water
- availability

2.1.2 Water shielding

A higher saturation of the water phase hinders the CO_2, and has a significant effect on displacing oil in a miscible flood. This is caused by the water shielding the oil from the CO_2 (Zekri et al., 2007). Water causes the oil to be less connected. Water reduces the mass transport of CO_2 to the oil, allowing for less extraction and displacement (Shyeh-Yung, 1991). It has been shown experimentally that the trapping occurs for the non-wetting phase, and thus in an oil-wet porous media virtually none of the oil gets trapped (Walsh et al., 1989). For mixed and oil-wet cores the amount of oil retained is insignificant after large amount of pore volumes of CO_2 are injected(Lin and Huang, 1990). Mas transfer is enhanced under oil-wet media compared to water-wet media, because water occupies the large pores and does not shield the oil thus the oil is more continuous (Wylie and Mohanty, 1999).

Diffusion and oil swelling are important parameters to offset the effect of water shielding. CO_2 can potentially diffuse through the water, and swell the oil face so that it eventually bursts through the water barrier as shown in Figure 2-2. This causes the trapped oil to be come in contact with the CO_2 and thus become recoverable (Grogan, 1987). For less water-soluble gases than CO_2, diffusion rates may be severely reduced by the presence of water. (Skjæveland and Kleppe, 1992) Tertiary oil recovery is less effective than secondary oil recovery for a CO_2 flood at the same conditions (Shyeh-Yung, 1991).

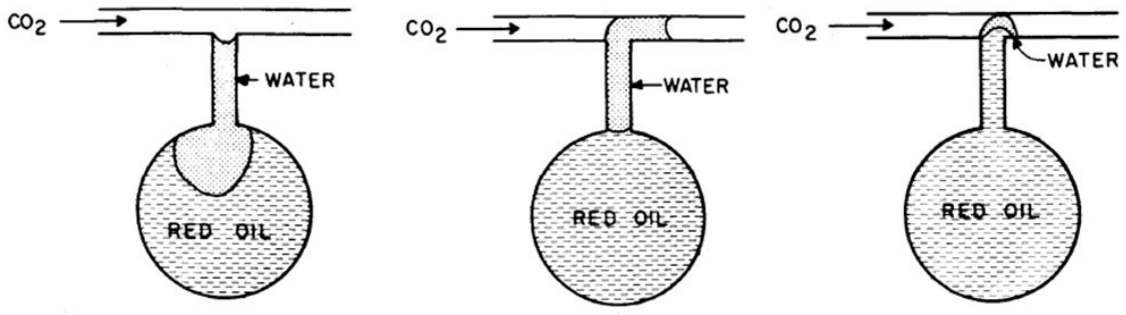

Figure 2-2 – Illustrates CO2 diffusing through the water phase swelling the oil, thus mobilizing the oil. (Campbell and Jr., 1985)

2.1.3 Diffusion during CO_2 flooding in fractured Reservoirs

When miscible carbon dioxide is injected into a fractured reservoir the CO_2 will quickly flow through the high permeable fracture system, which in turn causes all the surfaces of the matrix block to be in contact with the CO_2. The matrix block and fracture will then be in a state of non-equilibrium. This will cause mass transfer to occur between the fracture and the matrix by means of diffusion. The CO_2 will then also start to swell the oil in the matrix block, and oil may swell to as much as twice the original volume (Do and Pinczewski, 1991), causing further mass transfer into the fracture. The diffusion will continue until equilibrium is reached (Karimaie et al., 2007).

In a fractured system the matrix acts as the source of oil, and fractures are the flow conduit. The oil in the matrix gets produced through either gravity forces, or molecular forces. Gravity will become the dominating mechanism if the oil filled matrix columns is tall and permeable. Molecular diffusion will dominate with small and low permeable matrix blocks (Ghedan, 2009). The viscous force becomes negligible if the fluid mainly flows in the fracture and if the matrix block is low permeable (Alavian and Whitson, 2010).

CO_2 can for example contact oil directly, or it can diffuse through water films to contact the oil (Do and Pinczewski, 1991). The diffusion through water films slightly offsets the effect of water shielding. Diffusion rates get lower with increasing water saturations. This is especially governing in tertiary CO_2 injection, where the core/reservoir already has been water flooded (Grogan, 1987). Ultimate recovery has been found to be much lower from CO_2 injection for tertiary recovery (waterflooded before CO_2 injection) compared to secondary recovery(CO_2 injected from the start) (Trivedi and Babadagli, 2006). Water with a high presence of salt can reduce CO_2 solubility significantly, in fact salt levels of around 300 000 ppm reduce CO_2 solubility by as much as 50% (Grogan, 1987). The reduction in water solubility can in turn cause the diffusion rate to be reduced, because of water shielding. Figure 2-3 shows how oil can be mobilized through diffusion on a microscopic scale and mobilizing low permeable zones on a macroscopic scale. On microscopic scale the CO_2 can mobilize the oil in the dead end pore through oil swelling, and extraction. On macroscopic scale the CO_2 can diffuse into the low permeable zone swelling the oil and trading places with the oil.

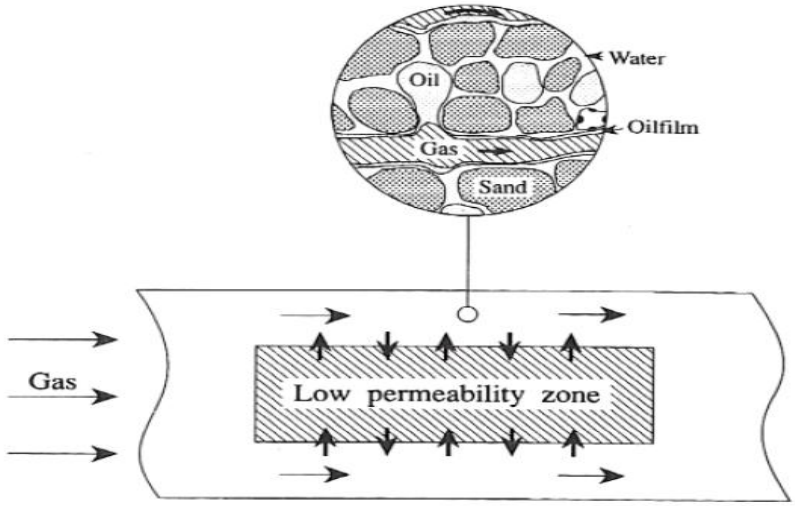

Figure 2-3 – Stagnant oil in a water flooded reservoir getting mobilized by molecular diffusion on a microscopic and macroscopic scale (Skjæveland and Kleppe, 1992).

The stagnant oil in low permeable zones may be mobilized through diffusion. Diffusion of CO_2 into the one meter low permeability zone may be recovered in 3-30 years. Low permeable zones of one meter containing oil may therefore be recovered in a reservoir time scale. (Skjæveland and Kleppe, 1992).

During a CO_2 flooding in a fractured system the lighter components of the oil were produced at an earlier stage then the heavier components. This is due to the higher diffusion rates of the lighter components with CO_2 (Trivedi and Badadagli, 2008).

How foam can increase dispersion rates in fractured reservoirs is discussed in chapter 2.2.5.

2.1.4 Field cases with CO_2 injection

The CO_2 flooding of the Wellman Unit oil-field is one of the most successful CO_2 floods in terms of CO_2 utilization (million cubic feet required to recover one barrel of oil). Over 15 years the Wellman Unit field has produced 7.2 MMbbls of oil by CO_2 flooding, where approximately 42 billion cubic feet CO_2 has been injected. This gives a CO_2 net utilization of 2.25 MCF/bbl. The main causes for such a beneficial utilization are: the reservoir is thick, and steeply dipping with excellent lateral and vertical communication(Schechter et al., 1998). Schecter found that reducing the pressure from well above the minimum miscibility pressure, to a little below the minimum miscibility pressure did not in lab scale give significant reduction in recovery, which meant that the CO_2 injection could be reduced further without high reduction in recovery. CO_2 could mobilize capillary caught oil in the transition zone, which is another beneficial use of CO_2 (Schechter et al., 1998).

In 2009, ADCO instigated the first ever CO_2 EOR pilot in the Middle East. The Reservoir is a heterogeneous limestone reservoir. The pilot was located in an undeveloped part of the field, where the reservoir pressure was above the Minimum Miscibility Pressure (MMP) for CO_2. The pilot consisted of three wells, one production- , one injection- and one observation well. The pilot was supposed to last for one year, but was expanded to evaluate the CO_2 performance of mobilizing oil in the transition zone. It took 60 days before CO_2 breakthrough occurred. It was observed that during injection, the production rate increased gradually by 5-7% before the breakthrough, and production dropped immediately by 30-40% after breakthrough (Al-basry et al., 2011).

The Weyburn Oil field in Canada is the largest horizontal CO_2 injection project in the world. The Weyburn field is a 30 m thick fractured carbonate reservoir at 1400 m depth. The aim of the project is to increase the recovery to over 40% of OOIP. Over the lifetime of the field it is expected to store 20 million tons of CO_2 in the Weyburn Field. All the stored CO_2 will be anthropogenic CO_2 that would otherwise be released into the atmosphere (Mathiassen, 2003).

2.1.5 CO_2 – Physical properties

When flooding cores with CO_2 it is important to understand the properties of CO_2 and the corresponding phase behavior. Figure 2-4 shows the phase diagram for CO_2, and shows CO_2 is liquid at experimental conditions of 20 °C and 90 bars.

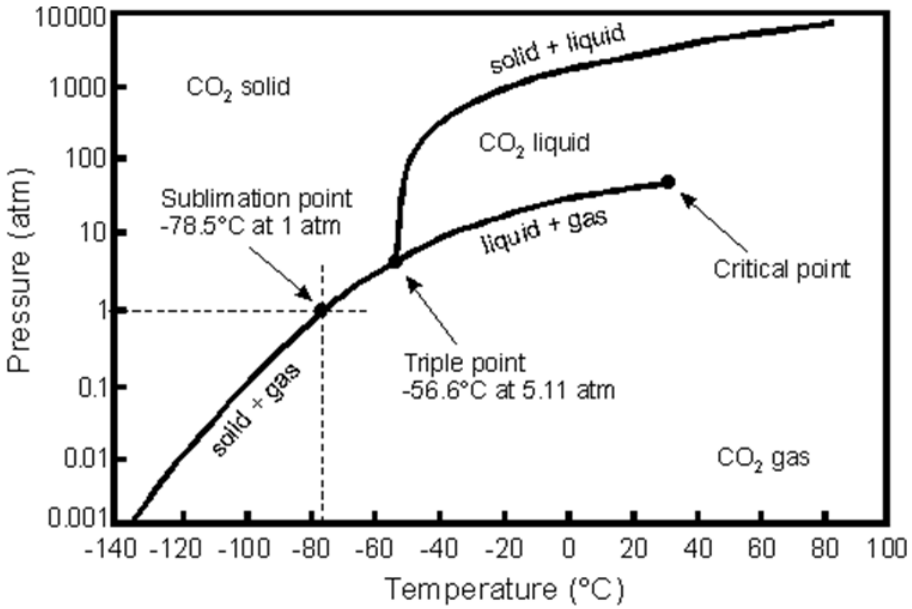

Figure 2-5 – Phase diagram for CO_2 (Picha, 2007)

Figure 2-6 shows viscosity and density as a function of pressure at isothermal conditions of 20 °C.

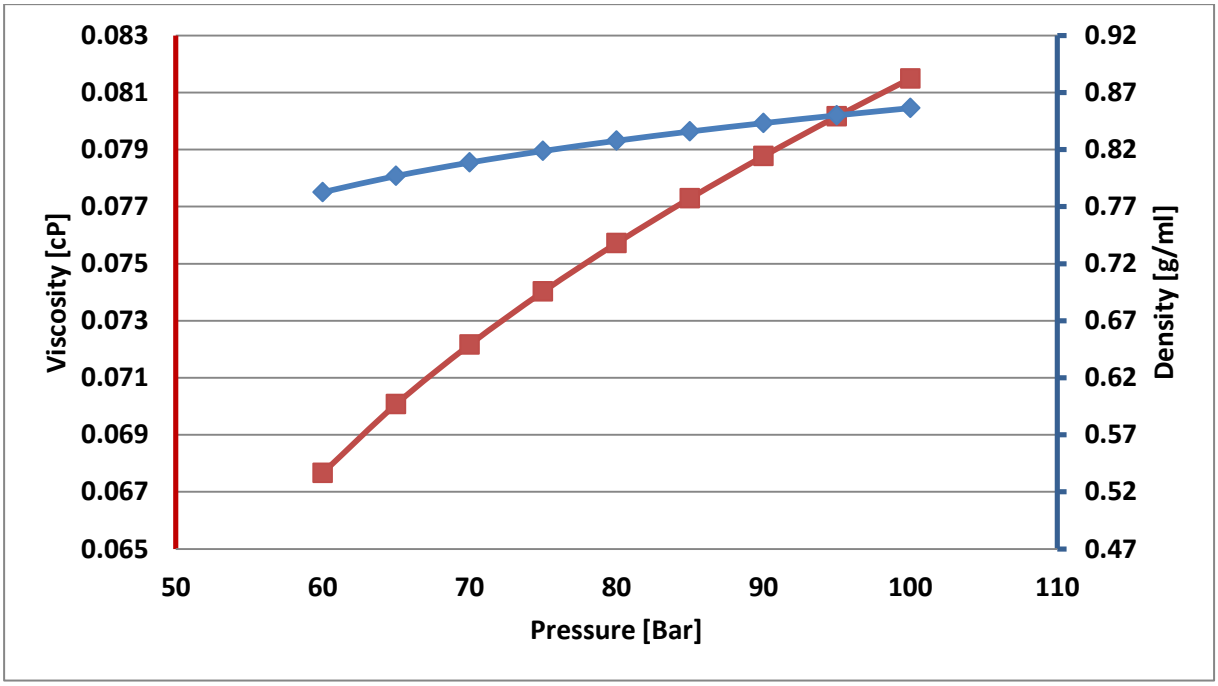

Figure 2-6 – Shows viscosity (red) and density (blue) as a function of pressure at isothermal conditions, 20 °C. (NIST, 2013)

2.2 Foam – mobility control

Foam is advantageous for controlling the mobility of gas in a porous medium. It can be relatively cost effective considering the liquid only needs a concentration in the order of one weight percent. Foam can reduce the effects such as channeling, fingering, and gravity segregation by reducing the displacing fluids mobility. Foam can also reduce the interfacial tension between the fluids. Foam has a selective property of blocking high permeable layers, which means it blocks the high permeable (already swiped zones) layers, leading the fluid to un-swept areas or layers. The selective property of foam targeting high permeable layers can be very beneficial in a heterogeneous porous medium. The implementation of foam as an enhanced oil recovery technique has been hindered because of a lack understanding of the foams behavior in a reservoir. The effectiveness of foam in reservoirs remains unpredictable, because of the complex nature of foam and contradictions in foam studies. In naturally fractured reservoirs foam can be used to create a viscous pressure drop in the fracture, which forces the gas into the oil bearing matrix, thus accelerating oil production (Farajzadeh et al., 2010, Kovscek et al., 1993, Alvarez et al., 1999). Figure 2-7 shows the beneficial effects of foamed gas compared to pure gas.

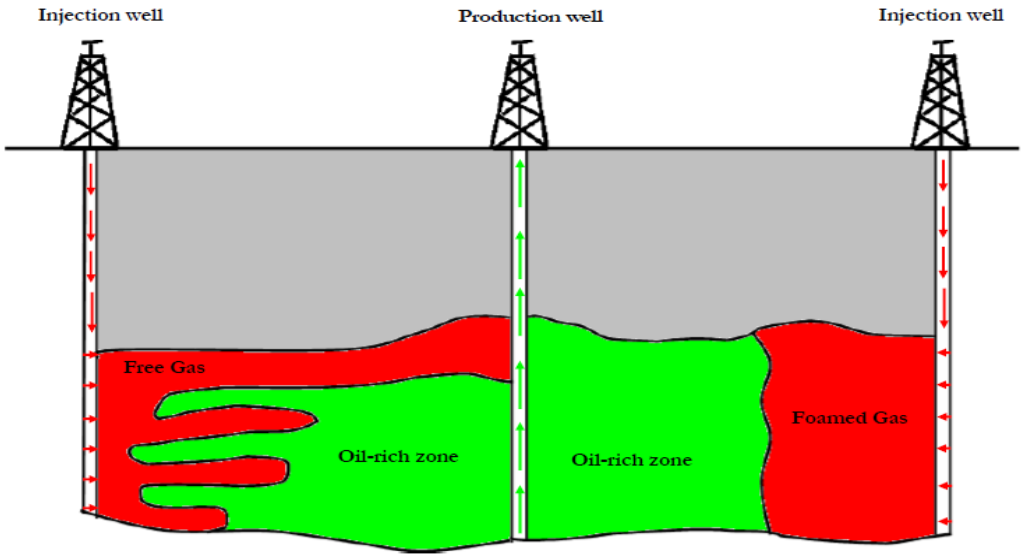

Figure 2-7 Schematic illustration showing effects of gas (on the left side of the illustration) versus foamed gas (on the right side of the illustration) in a horizontal displacement (Farajzadeh et al., 2012)

Definition of foam in porous medium as written by Rossen: "*a dispersion of gas in liquid such that the liquid phase is interconnected and at least some of the gas flow paths are blocked by lamellae.*" (Rossen, 1996). The boundary between the lamellae or a solid is a liquid prismatic region called a plateau border, as shown in Figure 2-8.

Figure 2-8 – A picture showing foam with a plateau border with an oil film. The picture is taken 24 hours after mixing and is enlarged four times. (Vikingstad et al., 2005)

Inside a rock, bubbles are thought to be at least as large as the pore bodies and probably many times larger. The lamellae and its interaction with the pore walls are of central importance when considering foam in a porous rock. There is, however, no way to visually verify the existence of lamellae inside rock, but it can be observed that when a gas is in contact with an aqueous surfactant solution gas mobility is reduced. Concluding that bubbles are as large as or larger than pore bodies is based on the foam size leaving the rock and on the resistance to flow predicted for small bubbles. The explanation for the large bubble size is thought to be due to diffusion of smaller bubbles into bigger bubbles (Rossen, 1996).

There are two types of foam: discontinuous and continuous gas foams. With continuous gas foam, the gas still has an open pathway through the foam, but has to go a longer way to move through the porous rock. This only affects the relative permeability of the CO_2. With discontinuous gas foam the gas does not have a way through the foam as all of the flow paths are blocked by lamellae (Rossen, 1996). Thus for the gas to move through the porous medium it needs to exceed a differential pressure displacing the lamellae in front of it through the porous medium. This affects both the relative permeability of the CO_2 and it gives the CO_2 an apparent viscosity that is higher than the original viscosity. The higher viscosity is caused by the increased flow resistance of the lamellae.

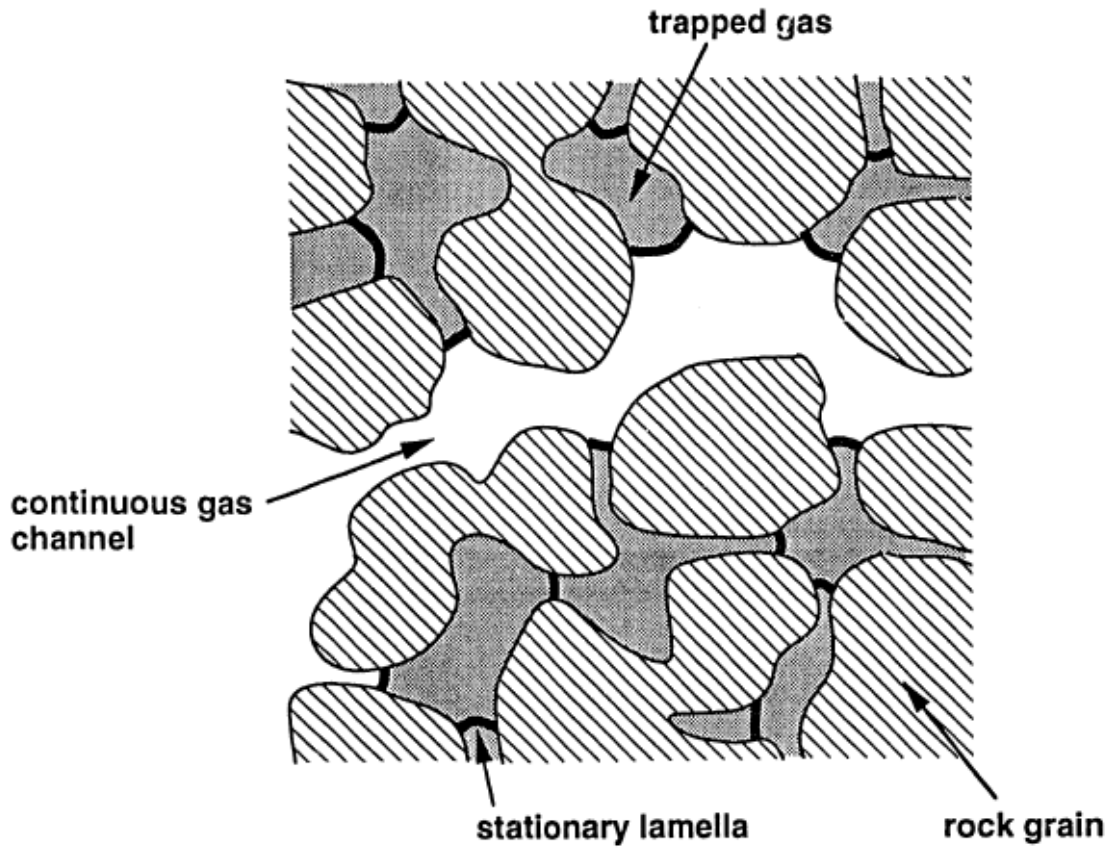

Figure 2-9 - Schematic illustrating discontinuous and continuous gas foam by (Kovscek et al., 1993)

The gas tends to be located in the middle of the largest pores. This however depends on wettability, and on which phases are attracted to each other. The majority of liquid (surfactant) entering the rock with the gas tends to occupy the smaller pores, and is continuous along the pore walls in the larger pores. Only small parts of the liquid are located in the lamellae. In the porous medium the liquid permeability and viscosity is almost unaffected. (Kovscek et al., 1993)

Mobility of gas foam is dominated by foam texture, where the small bubbles greatly reduce gas mobility. If foam texture is kept constant, foams will have a shear thinning effect caused by increase in number of flow paths and by shear thinning behavior along each flow path. Some papers report of shear-thickening behavior which is most probably caused by refinement of foam texture at higher flow rates. (Rossen, 1996)

2.2.1 **Generation of foam**

In the course of its lifetime, lamellae are continuously created and destroyed. The two processes are important factors while talking about foam generation. (Kovscek et al., 1993) For steady, simultaneous injection of liquid and gas for a given surfactant mixture, foam generation depends on injection rate and foam quality (gas volume fraction)(Rossen, 1996). This means the dryer (less liquid, more gas) the injected fluids are, the higher injection rate must be to generate foam. This is showed in Figure 2-10.

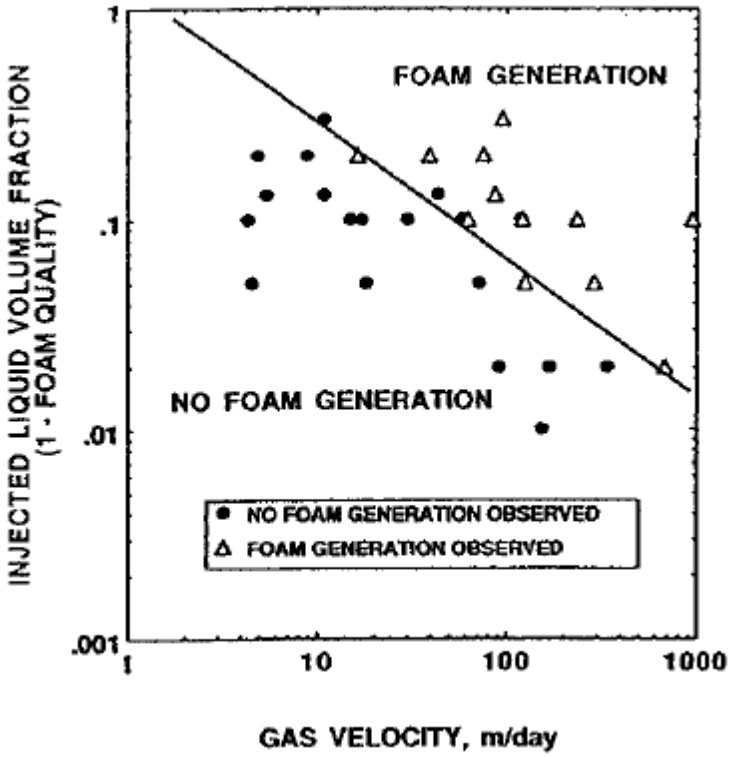

Figure 2-10 - Conditions for foam generation in steady gas/liquid flow (Rossen, 1996)

When generating foam, the creation of lamellae is of central importance and it is a capillary driven process. There are three ways to create lamellae in porous media:

Creating lamellae by Leave-behind:

Leave-behind is a creation process that occurs in pore throats when gas enters from separate directions in adjacent pore bodies as shown in Figure 2-11. The creation of leave-behind lamellae can be very effective in a three dimensional medium, because the of many potential pore throats available for lamellae creation. Albeit an effective creating process, leave-behind has proven not to greatly reduce gas mobility, which means that this is a weak kind of lamellae and a high amount of the lamellae are destroyed. Leave-behind only occurs during a drainage process, when saturation of gas is increasing (Rossen, 1996).

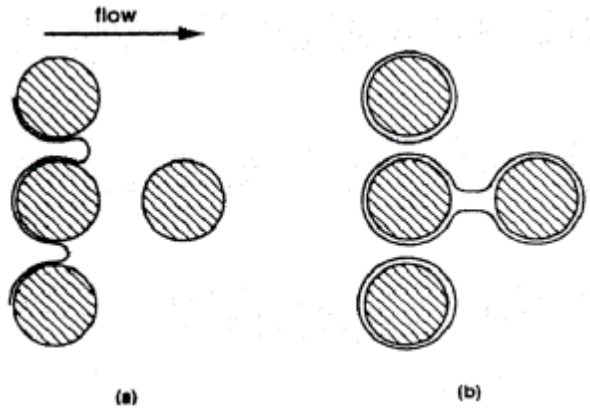

Figure 2-11 - Schematic illustration of the leave-behind process

Creating lamellae by Snap-off:

Figure 2-12 – Showing snap-off caused by decreasing capillary pressure (Rossen, 1996)

Water (surfactant) accumulates at the pore throats and in the small pores where the capillary pressure is higher for a water wet medium. As capillary pressure decreases the water can bridge the gap in the pore throat and create lamellae and is called snap-off, as shown in Figure 2-12.

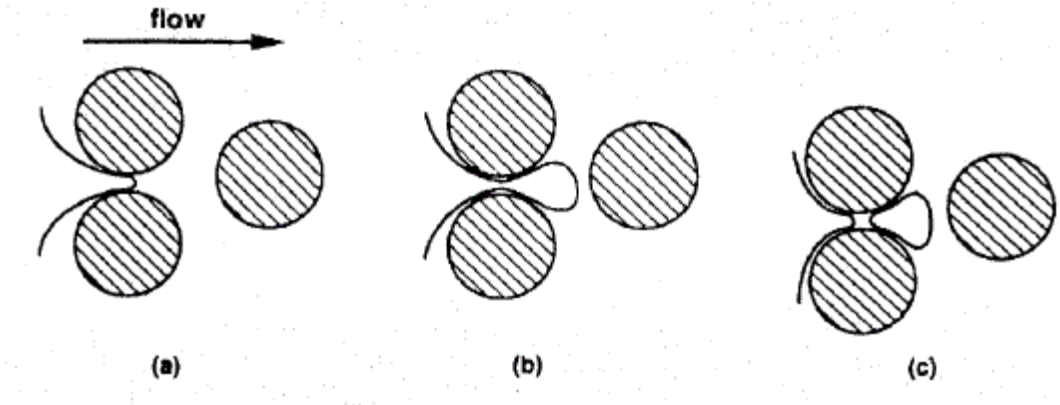

Figure 2-13 – Showing snap-off caused by fluctuations in capillary pressure (Kovscek et al., 1993)

For gas to enter a pore body through a pore throat it needs to exceed a certain capillary pressure to force its way through the pore throat. When the gas enters the pore body, the radius will increase and the capillary pressure will decrease. This fluctuation in capillary pressure can cause a lamella to form in the pore throat as shown in Figure 2-13. This process is called snap-off. (Rossen, 1996)

Creating lamellae by Lamella division:
When a lamella is pushed through a pore system it can suddenly reach a point of several pore throats. The lamella then stretches and either breaks or makes new lamellae in the different pore throats. The lamellae will take the path of least resistance, which means that lamellae are created in the pores of least resistance, forcing gas to take different paths or to displace the lamella. (Rossen, 1996)

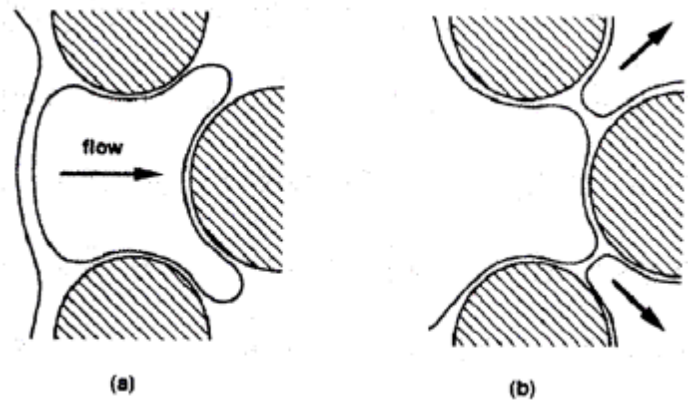

Figure 2-14 – showing lamella division in a pore system (Kovscek et al., 1993)

2.2.2 **Lamella Destruction:**

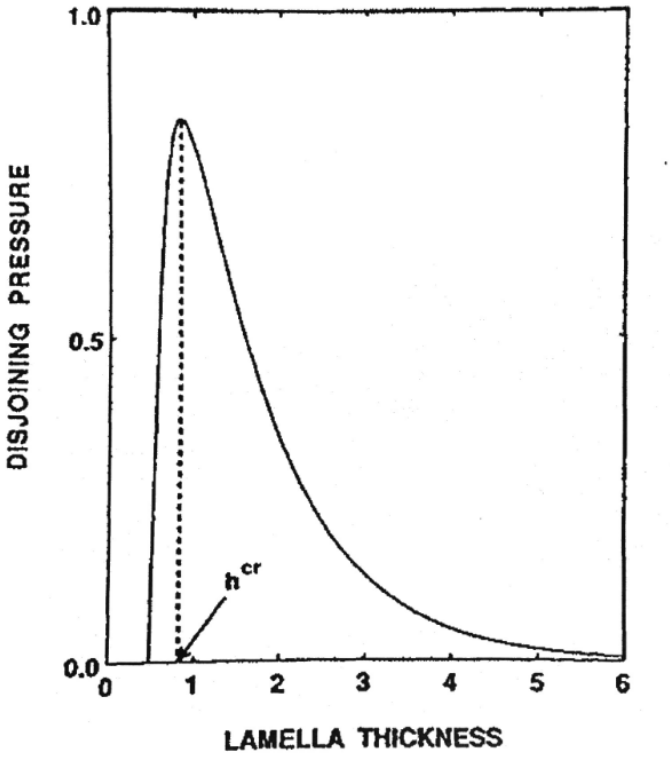

Figure 2-15 - Disjoining pressure as a function of lamella thickness (Rossen, 1996)

Capillary pressure decides the thickness of lamella through disjoining pressure. The two liquid-gas surfaces repel each other, which makes the lamella able to maintain a finite thickness even though the gas pressure is higher, or positive capillary pressure is positive. The higher the capillary pressure, the thinner the lamella will become, which at a critical thickness h^{cr}, causes the lamella to rupture. The closer the lamella is to critical thickness the more sensitive it is to mechanical shock (Rossen, 1996).

Rupturing of lamella depends on capillary pressure and lamella thickness. Lamella can move through the porous medium, and this can cause the lamella thickness to change. For example lamella moves from a pore throats to a pore body the lamella, the lamella will have to stretch because of the increasing area. The stretching causes the thinning of the lamella, which can cause the thickness to go below the critical lamella thickness(Rossen, 1996). Increasing lamella velocity causes the lamella to more easily burs. This happens because the higher the rate of propagation is, the less time the plateau border liquid from has to flow into the lamella and keep it from bursting.

Destruction of lamellae happens more rapidly at the front. A theory of why this occurs: When a lamella enters a pore space that has not been inhabited by foam before, the lamella may need to divide as shown in Figure 2-15. This division causes the lamella to stretch and also jump to cover the whole area. The thinning of the lamella and the mechanical stress caused by jumping can cause the lamella to burst. The rupturing of lamella causes liquid to accumulate on the rock surface, and it can help the next division to divide successfully (Rossen, 1996).

2.2.3 **Effect of oil**

Oils have a degrading effect on foam. It is not clear what causes the degradation foam. Some studies believe that the main cause is the spreading of oil over the lamellae. Spreading oil has a higher degrading effect on foam than non-spreading. The higher degrading effet is because of the local decrease in surface tension and thus producing a thinning effect (Lau, 1988). Oil composition also seems to have an degradation effect; light crudes have a higher degradation effect than heavier crudes (Schramm, 1993). The emulsion effect of oil into the interior foam and the penetration of the aqueous solution both seem to have a destabilizing effect on the foam(Schramm, 1993).

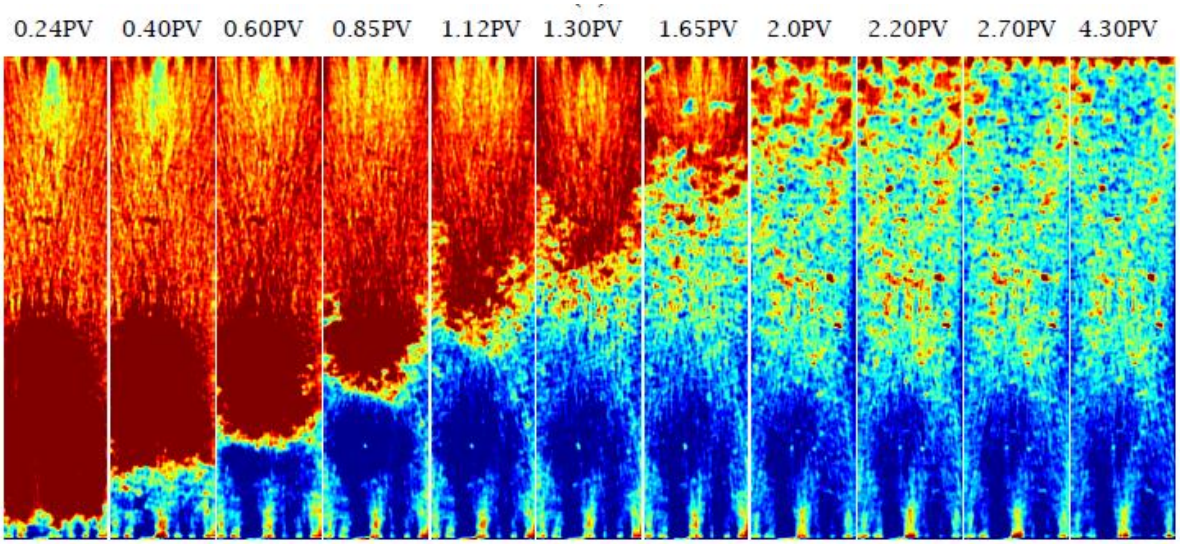

Figure 2-16 – CT pictures showing the detrimental effect of oil on CO_2-Foam. The blue colour is the surfactant and gas solution. Red is only surfactant, orange is residual oil flooded by surfactant. (Farajzadeh et al., 2009)

Initially in the Figure 2-16 the top half of the core is saturated with oil, and surfactant, while the bottom half is only saturated with surfactant. CO_2 is then injected from the bottom. It can be observed that the front is relatively stable until the foam reaches the oil. Fingers are then observed, indicating that the foams mobility control is being reduced. Even though oil has a detrimental effect on foam, and foam is not created in high oil saturated areas, foam can get created in areas where the water saturation is high (already flooded) and cause the gas to divert its flowing path from areas already flooded, to areas where oil has not been recovered (Farajzadeh et al., 2009). Experiments performed at this department have shown that if CO_2-foam is injected into a fully n-Decane saturated chalk core, the foam is destroyed upon entering the core, and the CO2-foam is not stable before the oil saturation is greatly reduced (water saturation is increased) (Baird, 2013).

2.2.4 Effect of wettability

In an oil-wet pore the oil will have a preference to occupy the space along the pore walls. This means that lamellae will find it difficult staying attached to the pore walls. Detached from the pore walls lamella will collapse(Rossen, 1996). In a mixed-wet pore space some of the pores have a water-wet preference and some have an oil-wet preference. This means that creating discontinuous foam is less likely. Discontinuous foams are more effective because they affect both viscosity and relative permeability. Some claim to have created weak foams in oil-wet medium, but this is probably caused by the surfactants ability to change the wettability of rock (Sanchez, 1992).

2.2.5 Foam in fractured Reservoirs

Gas flowing through a fractured reservoir predominantly flows through the fractures, leaving almost all the oil in the matrix behind. Gas will slowly start to diffuse into the matrix, trading places with the oil and forcing the oil into the fracture. This process can be accelerated with the use of foam. Foam creates a viscous pressure drop, forcing the gas into the matrix, contributing with viscous displacement along with the diffusion(Farajzadeh et al., 2010). When gas is forced into the matrix this increases dispersion because mechanical dispersion occurs in addition to the diffusion (Bijeljic and Blunt, 2006). Foam in fractures is expected to behave like bulk foam (bubbles are smaller than the open space confining the foam).The higher the pressure drop, the more gas is forced into the matrix. To get a higher pressure drop, one needs a higher apparent viscosity; this is related to the strength of the foam and the bubble size (smaller bubbles gives stronger foam, which gives a higher pressure drop). (Farajzadeh et al., 2010)

2.2.6 Foam regimes

There are two different foam regimes: the high quality foam regime (dry foam), and low quality foam regime (wet foam). High and low quality foam regime is shown in Figure 2-17. The high quality foam regime the pressure gradient is dependent on liquid velocity and independent on gas velocity and vice versa for the low quality foam regime. The transition from high quality to low quality foam occurs at the point of limiting capillary pressure. Higher than the limiting capillary pressure the foam is in the high quality foam regime, and vice versa. For example if situated in the high quality foam regime and liquid velocity is reduced, the pressure gradient will be reduced because there is too little liquid, which will lead to coarsening of the foam texture. The foam will become too dry. (Osterloh and Jante Jr, 1992).

Chang and Grigg have studied the effect of Injection rate and foam quality for CO2-foam in Berea Sandstone core. They observed that the mobility decreased with increasing foam quality (dryer foam). The foam quality test was only performed up to a four to one ratio on foam quality (the low quality foam regime.) (Chang and Grigg, 1998). The same has behavior has been observed with by Alvarez et al. They observed that for the high quality regime Pc* (limiting capillary pressure) controlled bubble size and thus gas mobility. In the low quality regime bubble size is fixed, and the pressure gradient depends on the porous medium, and less on the surfactants ability to stabilize the foam. In the low quality foam regime, shear thinning behavior is observed. The transition zone is sensitive to both the surfactants ability to stabilize foam and to the porous medium. (Alvarez et al., 1999). Chang and Griggs observe shear thinning behavior for high quality regime, while the opposite is observed by Alvarez et al (Alvarez et al., 1999, Chang and Grigg, 1998). The shear-thinning behavior in the low quality regime is beneficial for injection into a reservoir; this makes the foam more mobile near the

wellbore, increasing injectivity, while further into the reservoir the mobility will be reduced, leading to better macroscopic efficiency. Because of the density of CO_2 injectivity can be a problem. In the low quality foam regime, the liquid rate can be reduced without affecting the pressure drop making it more economic. (Alvarez et al., 1999)

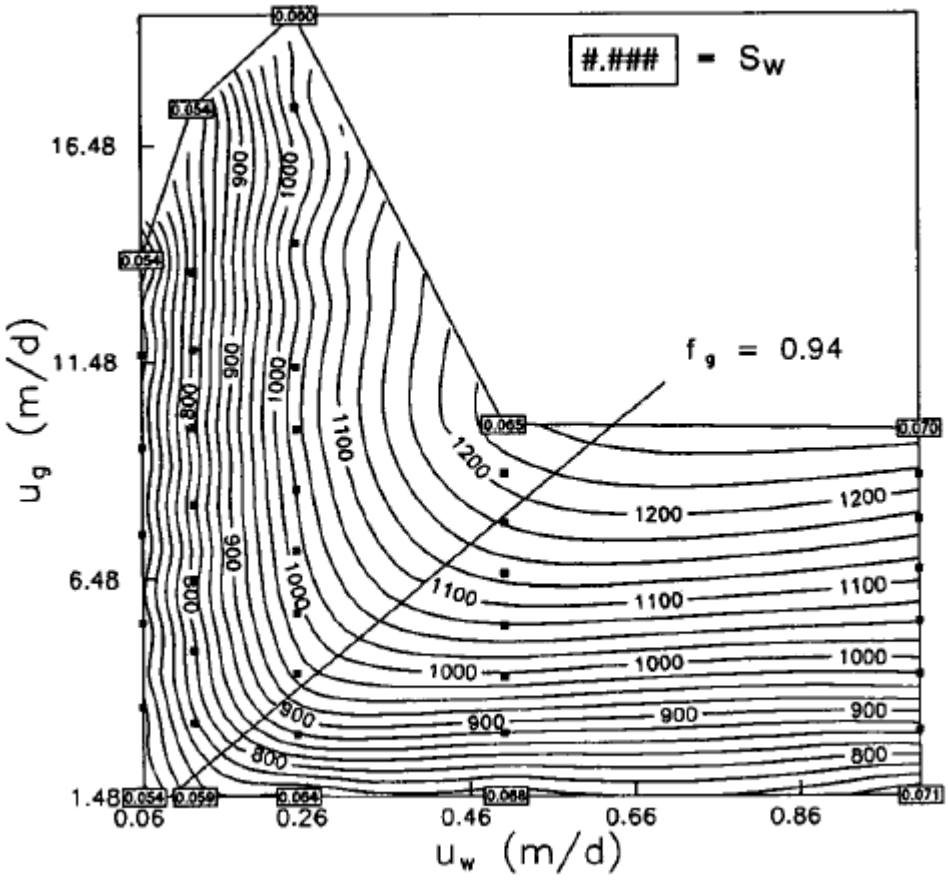

Figure 2-17 – illustration showing high and low quality foam regimes in steady-state foam experiments. The numbered line represents different differential pressures. The line fq shows the transition between low and high quality foam regime (the point of the limiting capillary pressure). The right side of this line is the low quality foam regime, the left side is the high quality foam regime. (Osterloh and Jante Jr, 1992)

2.2.7 **Foam in field scale**

Foam in field application has three flow regimes(Rossen, 1996):

- Surface facilities and the well itself, where turbulent flow may create bulk foam
- The rock face and the region near the face where flow rates and pressure gradients are high
- The formation further from injection rate where pressure gradient and flow rates are much lower.

There are three methods of creating foam in porous media. These include Surfactant alternating gas (SAG), co-injection of gas and liquid and it is possible to dissolve surfactant into supercritical CO_2 Dissolving surfactant in CO_2 is a way to make sure that the surfactant always goes where the CO_2 goes (Xing et al., 2012) (Farajzadeh et al., 2012). If the slugs of the alternating injection are small, then they will mix near the well. The mobility reduction is higher for co-injection of gas and surfactant than surfactant and gas alternating slugs (SAG) for the same gas flowrate (Huh, 1989).

Friedman et al determined that foam propagation rates matched the propagation rate of the surfactant, if gas and liquid was present. This was shown for a pilot test in an oil field. An observation well 12 m from the injection well observed foam at the expected time. There were some problems with the foam propagation to an observation well 20 meters away. The foam at the second observation well arrived several months after predicted arrival (Friedmann et al., 1994). This means that after a while the foam propagation did not keep up with the surfactant propagation, probably caused by the low generation of foam at lower pressures (further from the injection well). Another field pilot test indicated that a 60% increase in apparent viscosity of CO_2 occurred where the foam formed and the foam also blocked high permeability zones, this demonstrates that foams has been successfully implemented on field scale. (Enick et al., 2012).

The Snorre Foam Assisted WAG (FAWAG) is the world's largest application of foam in the oil industry (Skauge et al., 2002). Early gas breakthrough limited the oil production on this field. The trial on the Western fault of the Snorre field was very positive. It showed that gas breakthrough was delayed, and the Gas-Oil-Ratio was also considerably lower prior to the foam treatment. There was an immediate reduction in injectivity after the surfactant was injected, which indicates that foam was created. The effect of foam lasted for a long duration (Skauge et al., 2002).

3. Experimental setup and procedures

CO_2 injection and CO_2-foam injection have been performed on Edwards Limestone core plugs at different initial saturations, wettability, on whole and fractured cores. All the experiments were performed at 20 °C at approximately 90 Bars. Where the CO_2 is liquid, see Figure 2-5.

3.1 Core material

Edwards Limestone is the core material used in all the experiments and is considered a heterogeneous limestone. The porosity ranges 21%-25% from and the permeability ranges from 12-58 mD. Unlike sandstones, carbonates normally display a higher degree of heterogeneity even at core scale. Most of the pore space in the Edwards Limestone is vugular (cavities) caused by dissolution. The Edwards limestone has a relatively narrow pore throat distribution ranging from 0.1 to 10 µm. The relationship between pore bodies and pore throats give an aspect ratio in the range of 50-60 (Morrow and Buckley, 2006).

Figure 3-1 is a CT-scan of a dry core. The dark areas represents low CT-numbers (low density), and the lighter areas represents high CT-numbers (high density). The CT images have a resolution of 40x40x42 µm. The image shows the heterogeneous nature of Edwards Limestone.

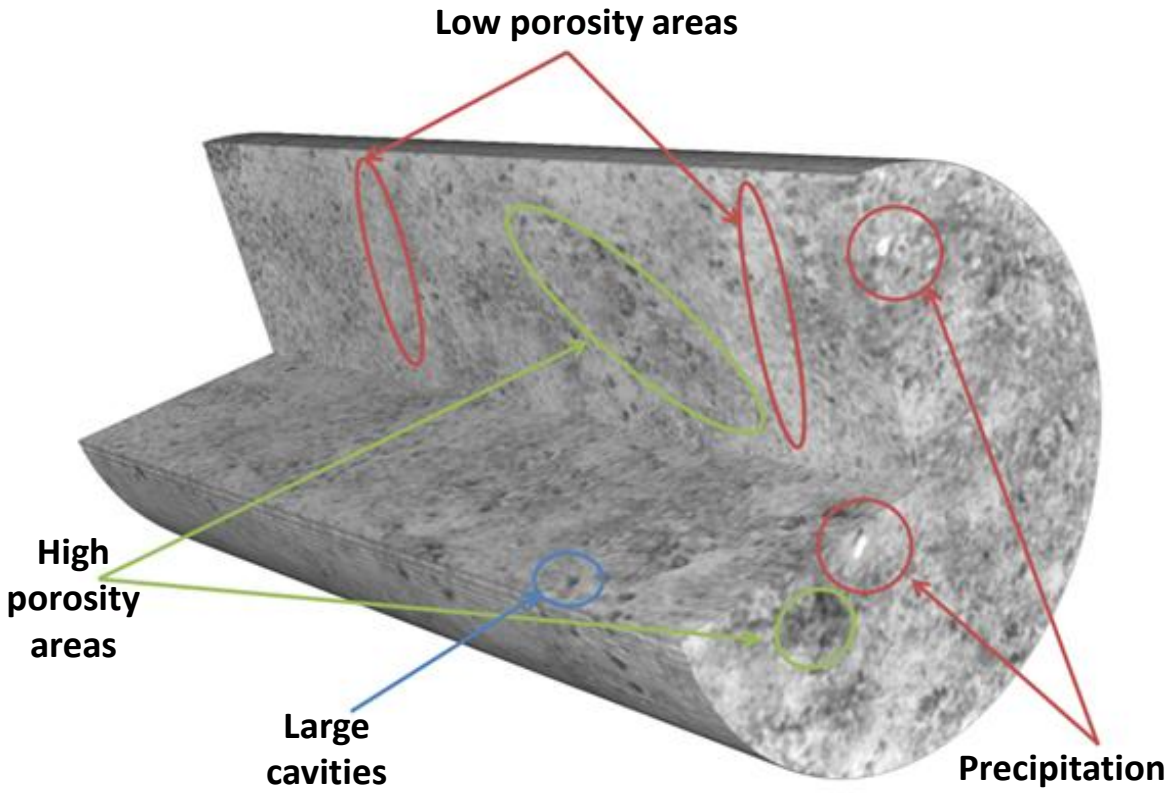

Figure 3-1 - CT scan of Edwards Limestone showing the heterogeneous nature of the rock. Modified from (Christophersen, 2012)

3.2 Fluid Properties

Fluid	Composition	Density 1 bar, 20 °C [g/ml]	Viscosity, 1 bar, 20 °C [cP]	Comments
Synthetic Ekofisk brine	Distilled water 4 weight percent NaCl 3.4 weight percent $CaCl_2$ 0.5 weight percent MgCl	1.05	1.09	Added 0.5 ml NaN_3 to avoid bacterial growth
n-Decane	$C_{10}H_{22}$	0.73	0.91	Purity 95%
Decaline	$C_{10}H_{20}$	0.90	0.85	Purity 95%
Ekofisk Crude	53 weight percent saturated HC 35 weight percent aromatic HC 12 weight percent Rasins 0.9 weight percent Asfaltenes	0.85	14.3 2.7 [80 °C]	Acid number: 0.09 Base number: 1.79
Surfactant: AOS $C_{14/16}$ (petrostep C-1)	Ekofisk brine 1 weight percent P-C1	N/A	N/A	37% active concentration
Liquid CO_2	> 99.9999% CO_2	0.84	0.08	(NIST, 2013) [20 °C, 90 bar]

Table 3-1 – Overview of the different fluid properties and compositions for the fluids used in the experiments (Fernø et al., 2010, NIST, 2013)

3.3 Preparing cores

The cylindrical cores were first drilled out of an outcrop rock. They were drilled to a width of about 2 inches, and varying length from 7-10 cm. The cores were cleaned with distilled water and then placed in a heating cabinet at 90 °C to dry out. After they were dried, the cores length and diameter were measured.

3.4 Porosity measurement

The dry cores were weighed then placed in a vacuum chamber. The container above the core plug was then filled with brine. The container containing the core plug and the container containing brine were then vacuumed until < 10 mbar as shown in Figure 3-2. The core was vacuumed to remove the trapped air in the core to completely saturate the interconnected pore space with brine, because residual air causes the effective porosity to be underestimated. The valve between the two containers was then opened so that the core became submerged with brine, until equilibrium was reached. The fully saturated core was then weighed again. The formula (3.1) shows how the porosity is calculated.

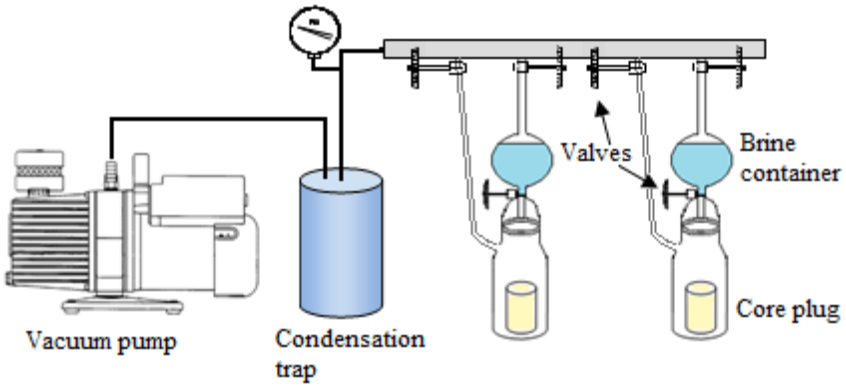

Figure 3-2 - Schematic illustration of the porosity setup (Haugen, 2012)

$$\varphi = \frac{(m_s - m_d)}{\rho \cdot V_b} \cdot 100 \quad (3.1)$$

Where φ is porosity, m_s [g] is the cores saturated weight, m_d [g] is the cores dry weigh, V_b[ml] is the bulk volume of the core and ρ [g/ml] is the density of the brine.

3.5 Permeability measurement

Absolute permeability was determined by injecting the fluid (brine or oil) into the core fully saturated with the injected fluid. The fluid was injected at different constant rates, Q, and the corresponding differential pressure, ΔP, was measured across the core to find the absolute permeability. The absolute permeability was found by plotting the measured data (at least 3 points was needed), and drawing a line between the points, the slope of the curve provides the absolute permeability from Darcy's law equation (1.3) and the slope value shown in Figure 3-3.

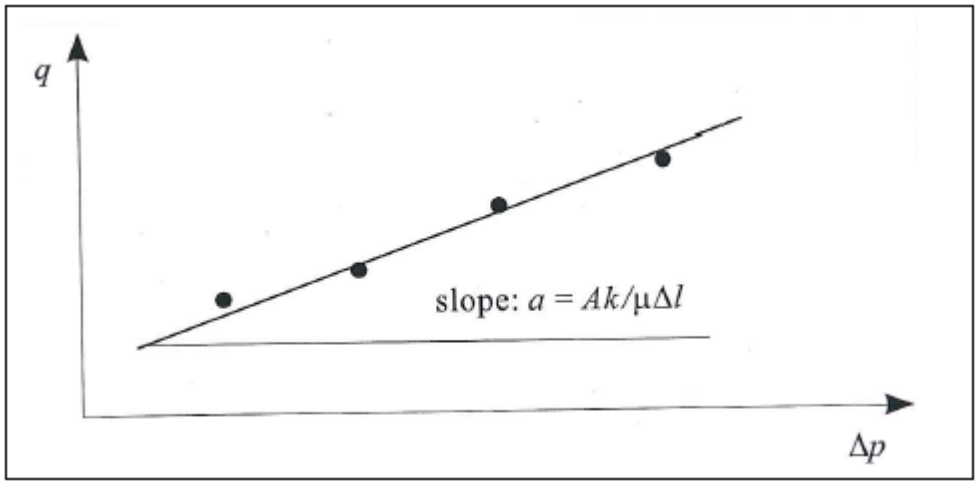

Figure 3-3 - experimental determination of permeability (Zolotukhin, 2000)

Figure 3-4 is a schematic illustration of the experimental setup for the permeability measurements. The confining pressure was kept 20 bars over the differential pressure across the core.

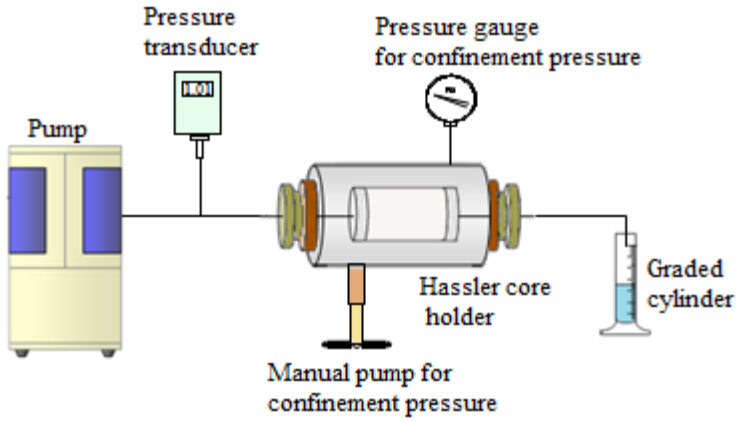

Figure 3-4 - Schematic illustration of the permeability setup (Haugen, 2012)

3.6 Aging of cores

Aging of cores is a process to alter the wettability of the cores. Outcrop rock types are generally water wet and have a preference of imbibing water. There are two kinds of aging techniques: Static and dynamic aging. Static aging is performed by soaking a core in crude oil, and dynamic aging is performed with continuous flooding of crude oil through the core. Both aging techniques are performed at a temperature around 80 °C. Static aging is less effective and slower than dynamic aging (for chalk, not necessarily for limestone) and an aging time more than three times as long when wettability alterations of the core are required to be lower than an Amott-Harvey index of 0.6 (Fernø et al., 2010).

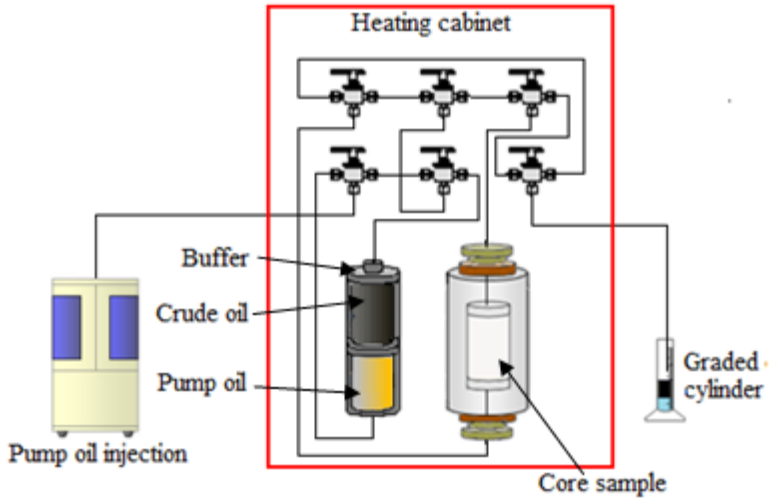

Figure 3-5 - Schematic illustration of the setup used for aging cores (Haugen, 2012)

The aged limestone cores were altered by the use of dynamic aging 80 °C, using Ekofisk crude, composition listed in Table 3-1, and with the setup shown in Figure 3-5. The high temperature is required to prevent precipitation of wax from the crude oil and for the aging to take place. The crude oil was filtered by injecting it through shorter limestone cores (the cores were disposed of after being used as a filter); to make sure the crude oil did not alter the absolute permeability. The filtered crude oil was injected at a constant pressure of 1.5 bar/cm in both directions to make sure the saturation distribution was uniform. 2.5 PV was injected in both directions to eliminate capillary end-effects, and to get uniform saturation distribution after primary drainage. The cores were then flooded with a constant rate of 3 ml/hour for 90 hours. The injection time was chosen based on the experience of Martin Fernø at the University of Bergen to give an Amott-Harvey index close to zero (neutral wettability). The flooding direction was changed halfway through the aging in order to create a uniform wettability distribution. After the preferred wettability was reached, the cores were flooded with 5 pore volumes of Decahydronaphtalene (Decaline), followed by 5 pore volumes of n-Decane. We flooded the cores with Decaline first then with n-Decane, to obtain miscibility and prevent asphaltene precipitation. The cores were then kept in room temperature in an n-Decane filled container.

3.7 Wettability measurement

The wettability measurements were performed using the Amott-Harvey method, described in section 1.4.2. The aged cores at irreducible water saturation were placed in an Ekofisk brine filled imbibition cell as shown in Figure 3-6 (left). When no additional oil was produced during water imbibition, the core was then placed in a Hassler core holder and displaced by Ekofisk brine with an injection pressure of 1.5 Bar/cm for 5 pore volumes each way.

The aged cores at residual oil saturation were now placed in an upside down imbibition cell filled with n-Decane as shown in Figure 3-6 (right). After no more water was produced from spontaneous oil imbibition, the amount of water produced was noted. The cores were then taken out, and flooded back to irreducible water saturation. The wettability was then calculated from the Amott-Harvey equation (1.8).

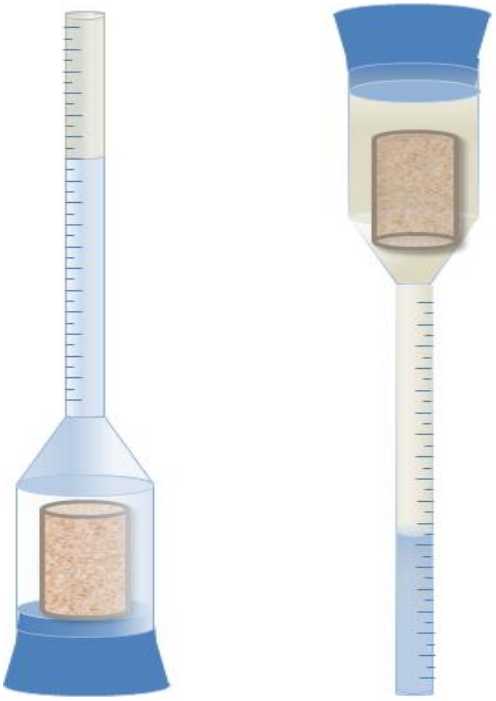

Figure 3-6 - Imbibition cells for wettability measurements – Left: spontaneous water imbibition. Right: spontaneous oil imbibition (Christophersen, 2012)

3.8 Fracturing of cores

To study the effects of liquid CO_2 injection in a fractured reservoir for enhanced oil recovery, experiments have been performed on cores with fractures. This is important to study since a lot of today's proven oil reserves are in naturally fractured reservoirs (Trivedi and Babadagli, 2006). In these fractures spacers has been placed so that the experiments can be performed with a constant fracture through the core as shown in Figure 3-7. The cores were cut with a band saw.

Figure 3-7 – picture to the left showing open core with spacer and picture to the right showing a closed core with spacer in the middle

After the cores were prepared (had the right saturation, wettability, porosity and permeability), the cores were cut with the band saw. The band saw reduced the diameter with about 3 mm, which had to be taken into account because of the change in pore volume. It was assumed that the core had a homogenous saturation distribution.

$$PV_{frac} = PV - (0.3 \cdot D \cdot L \cdot \varphi) \tag{3.2}$$

Where PV_{frac} is the pore volume after the core has been cut, PV is the pore volume for the whole core, 0.3 (3mm) is the width of the core that has been cut away, D is the diameter of the core, L is the length of the core and φ is the porosity.

3.9 Experimental Setups

3.9.1 Liquid CO_2 injections

The experimental setup for the material balance experiments is shown in Figure 3-8. The experiments were performed with an absolute pressure at approximately 90 Bar and at 20 °C, leading to liquid CO_2 conditions.

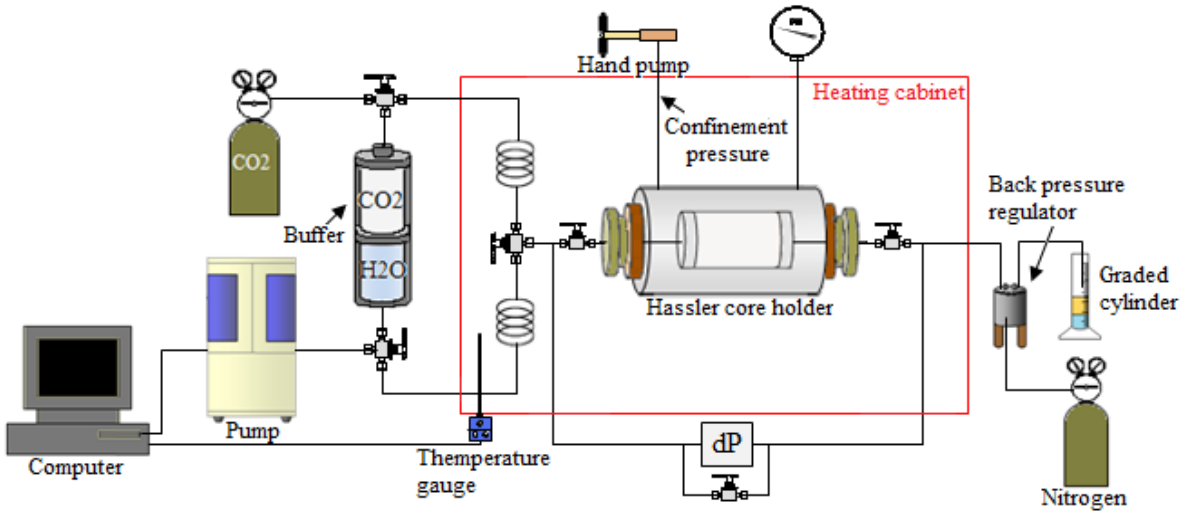

Figure 3-8 - schematic illustration of experimental setup for material balance experiments for liquid and supercritical CO_2 injection (Haugen, 2012)

Equipment used:

- Quizix QX pump
- Hassler core holder with a hand pump controlling the confinement pressure
- CO_2-accumulator
- Validyne DP15 differential pressure
- Swagelok tubing, fittings and valves
- Web camera for taking pictures of the production at regular intervals
- Back pressure regulator supported with nitrogen

Different sets of experiments were performed. Some cores were 100% saturated with n-Decane, while some were drained to S_{wi}. The experiments were done in order to get baseline experiments for CO_2 liquid injection. Experiments were also performed on cores (at S_{wi} and 100% n-Decane saturated) with fractures running through the middle. A spacer was placed in the middle to keep the fractures constant. When CO_2 is in contact with water it reacts and forms carbonic acid. The acid can corrode its way through the rubber sleeve of the Hassler core. Since the CO_2 can corrode the sleeve, the core was wrapped in aluminum foil. The edges of the core were taped with aluminum tape to the end pieces so that there was no contact between the CO_2 and the rubber sleeve as shown in Figure 3-9.

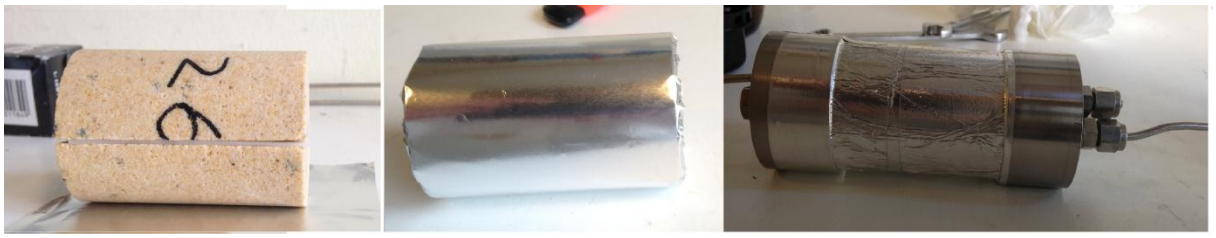

Figure 3-9 - three pictures showing; picture one: core with spacer. Picture two: core wrapped in aluminum foil. Picture three: Aluminum wrapped core taped with aluminum tape to the end pieces.

The fracture permeability was then measured with n-Decane flooding through the fractured core. The cores at S_{wi} will not affect the permeability considering that virtually all the oil goes straight through the fracture.

The CO_2 produces all the oil in the line network because CO_2 is first contact miscible with n-Decane and because the CO_2 causes the oil to swell. To minimize the dead volume the lines not directly between the CO_2 injection and the production outlet were filled with distilled water.

The CO_2-accumulator was pressurized to the desired pressure before the core was placed in the Hassler core holder and n-Decane was injected through the core while confinement pressure was slowly increased to 20 Bar. The n-Decane was continuously injected until all the air downstream in the system was forced out. The air upstream of the system was flushed out before the core was placed in the Hassler core holder. The experimental setup was then pressurized by setting the back pressure to a desired pressure, while keeping the confinement pressure around 20 bars over the line pressure. The amount of oil needed to pressurize the system was added to the dead volume.

When the CO_2 accumulator pressure was equal to the line pressure the injection rate was set to 4 ml/h, and the three-way valve between the accumulator and the core was opened. To start the experiment the oil production, differential pressure and absolute pressure were recorded. The production was then recorded with the help of a web camera.

Comments regarding the CO_2-injection experiments:
The dead volume includes the oil in the tubing in upstream and downstream of the Hassler core holder and the pressurizing dead volume. The pressurizing dead volume is the oil volume attained from pressurizing the system. The dead volume is deducted from the produced oil volume at the start, since over 90% of the dead volume is situated downstream of the core holder.

For the experiments with fractures the dead volume also includes the volume inside the fracture, because in an oil reservoir, fractures scarcely contribute to the total OOIP. In the Ekofisk field the fractures contribute to less than one percent of the pore volume (Skarrestad and Skauge, 2011). In the experiments performed in this thesis the fracture accounts for about 10% of the total OOIP. Therefore we count the fracture as dead volume. The oil in the fracture will get produced instantly, so the dead volume is deducted from the first produced oil.

Our pressurizing dead volume increased when pressurizing fractured cores. This might be caused by some air being left inside the fracture. The air might then be compressed, which gives us a higher dead volume. There is some uncertainty regarding this dead volume. As mentioned earlier the fracture volume was counted as dead volume in our experiments.

3.9.2 Liquid CO_2-foam injection

Figure 3-10 shows the experimental setup used during CO_2-foam experiments performed at Texas A&M University. The experiments were performed at 20 °C, injecting CO_2 simultaneously with surfactant to create foam. Before entering the core, CO_2 and surfactant were co-injected through a glass bead packed foam generator. As a result the foam was formed upon entering the core.

Equipment used:

- 3 ISCO pumps
- Bi-axial (hydrostatic) core holder with a Isco pump controlling the confinement pressure
- 3 Accumulators
- Validyne DP15 differential pressure
- Swagelok tubing, fittings and valves
- Web camera for taking pictures of the production and differential pressure at regular intervals
- Back pressure regulator supported with Nitrogen
- Foam generator (10 cm ¼" Swagelok tubing filled with glass beads)
- Pressure gauges

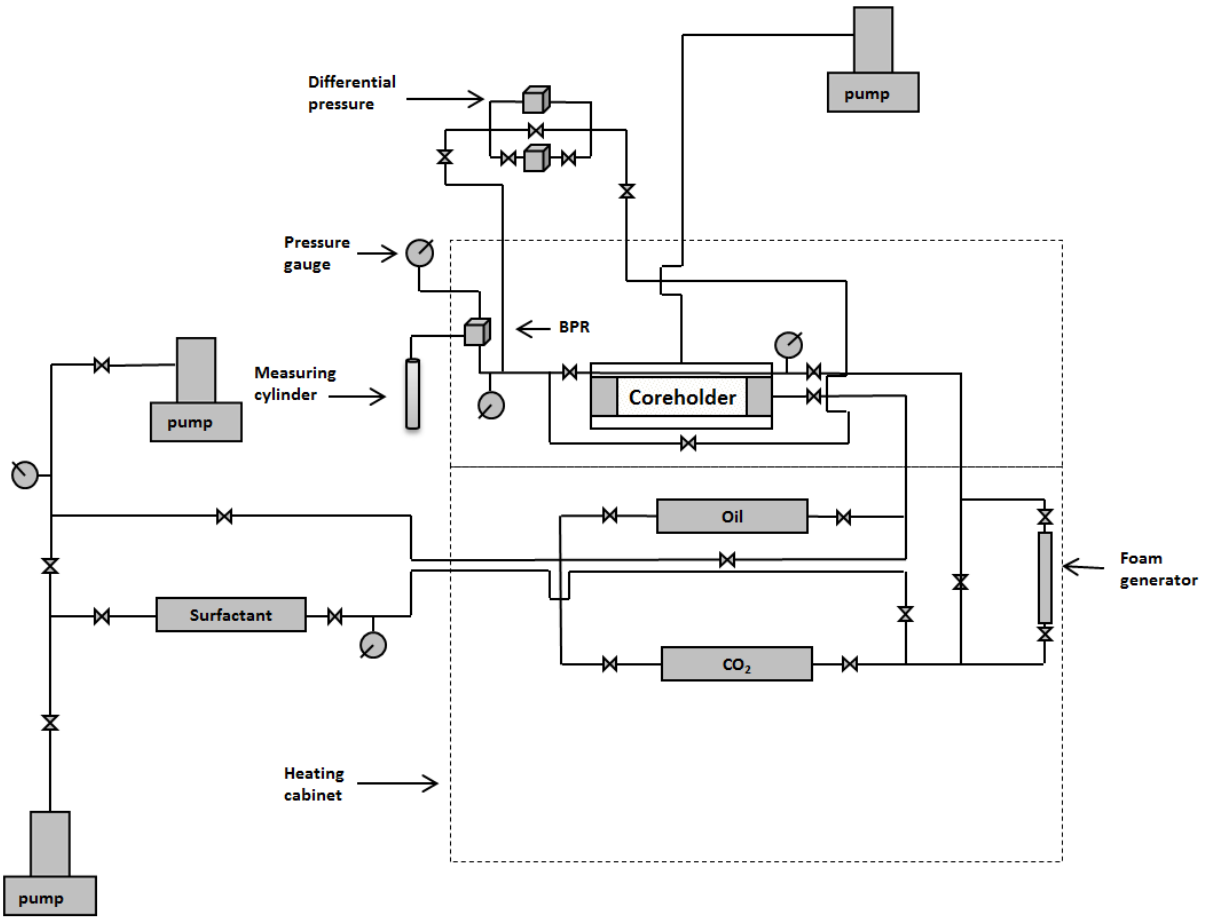

Figure 3-10 Schematic illustration of experimental set-up for the CO_2-foam-experiments at Texas A&M University

Before starting the experiment the lines were flooded with n-Decane, bypassing the foam generator (oil has destabilizing effect on foam). n-Decane was injected through the core at a rate low enough not to drain more water from the core while increasing confining pressure to 20 bars (oil was injected to make sure no air went to the inlet side of the core when confining pressure was increased). The system was pressurized until 90 bars were reached. Confining pressure was kept 20 bars over at all times. The lines were then flooded, bypassing the core, with surfactant (including the foam generator), to flush out the n-Decane, and prepare for the CO_2 injection. CO_2 and surfactant was then co-injected at a rate of 3.72 ml/h for the CO_2 and 0.48 ml/h for the surfactant (9:1 ratio), until the foam had reached the core. The valves leading to the core were then opened to allow the foam too flood the core. The dead volume consists of the n-Decane in the lines around the core, and the compressed n-Decane that comes from the pressurizing of the system. The oil production and differential pressure was recorded with a webcam every half an hour.

Experimental difficulties:

- Blockage of the lines ruining our material balance.
- A BPR that was always increasing, causing the line pressure to always increase.
- Set up the system in another heating cabinet, creating the same set up from scratch twice.

Comments regarding the CO_2 foam experiments:
CO_2-foam injection was performed at a ratio of 9:1, to generate as strong foam as possible (based on the experience of Dr. Martin Fernø (2013)). This in turn would give the highest apparent viscosity. The higher viscosity will give a better mobility ratio, and thus a better sweep efficiency throughout the core. The surfactant solution had one weight percent surfactant, and the rest was Ekofisk brine. Anders Christophersen and Ane Skibenes experienced a high fluctuation with the differential pressure (Christophersen, 2012, Skibenes, 2012). The fluctuating differential pressure was also experienced in this thesis. This was likely caused by the BPR opening and closing because the CO_2 went from liquid to gas state while flowing through the membrane of the BPR (Hirasaki, 2012). The high fluctuations in differential pressure may have affected the foam generation. Our total injection was set to 4.2 ml/h, as close as we could get to 4 ml/h (the injection rate used for the CO_2 injection experiments) while at the same time keeping the 9:1 ratio with our equipment at Texas A&M University.

The dead volume is counted as the volume upstream and downstream of the core holder, and the compression of the fluids (oil volume in the core, oil volume upstream and oil volume downstream of the core holder) caused by pressurizing the system. The dead volume is deducted from the produced oil volume at the start, since over 90% of the dead volume is situated downstream of the core holder

4. Results

4.1 Core data

A total of 51 core samples (limestone, sandstone and chalk) were prepared, and core length, diameter, porosity and permeability were measured. Seven limestone core plugs were aged, and wettability was measured. The Limestone parameters are as given: porosity ranged φ = 0.17-0.25 from and the permeability ranged from 15-59 mD. How the variables were measured is describes in chapter 3.

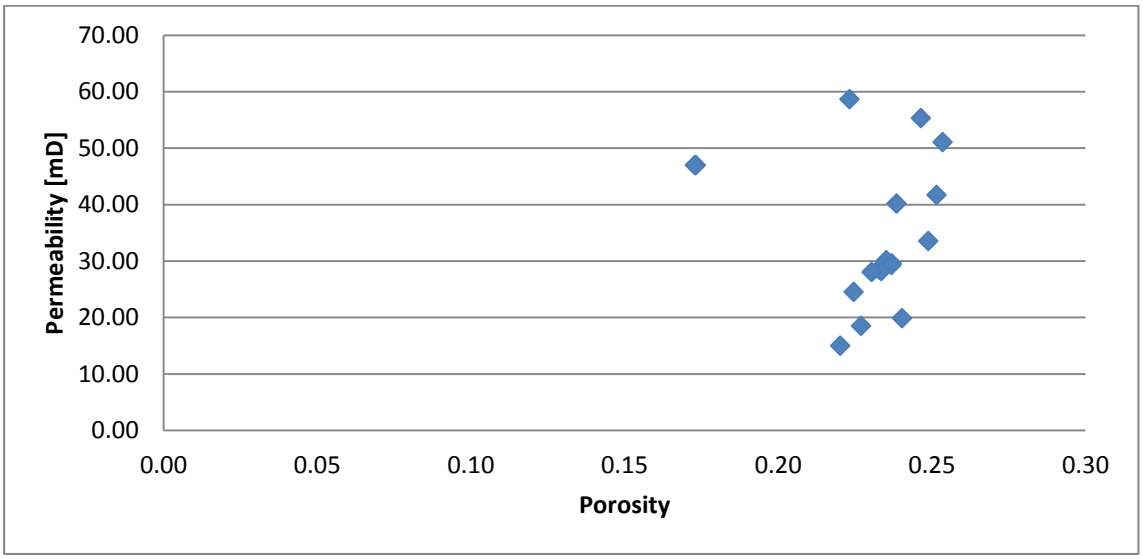

Figure 4-1- Showing permeability as a function of porosity for experiments performed on the Edwards Limestone cores.

Edwards Limestone is a quite heterogeneous rock type as seen from Figure 4-1. In Table 4-1 the pore volume for the fractured cores is the pore volume after fracturing. Formula (3.2) was used to determine the pore volume after fracturing as shown in Chapter 3.8.

Table 4-1 – Overview of basic core properties arranged in numerical order, where Kmatrix is the matrix permeability.

Core	Length [cm]	Diameter [cm]	Pore volume [ml]	Porosity [%]	Kmatrix [mD]
L2	7.38	4.96	33.52	0.24	30.12
L4	7.32	4.96	32.87	0.23	28.56
L6	7.36	4.97	33.82	0.24	29.29
L7	6.74	4.96	29.55	0.23	18.52
L9	7.59	4.99	33.35	0.22	24.53
L10	7.08	4.96	32.39	0.24	29.57
L14	7.27	4.96	32.84	0.23	28.20
L16	7.66	4.95	32.49	0.22	15.00
L17	7.25	5.16	38.40	0.25	51.05
L19	7.03	5.16	35.03	0.24	40.17
L20	6.97	5.16	35.88	0.25	55.34
L21	7.29	5.72	30.32	0.17	46.96
L22	7.34	5.74	30.60	0.17	46.96
L23	7.13	4.98	28.64	0.22	58.68
L25	7.47	4.96	30.65	0.23	28.02
L26	7.29	4.95	32.59	0.25	41.70
L28	7.67	4.96	35.67	0.24	19.88
L33	7.05	4.97	34.01	0.25	33.55
Sandstone	7.76	5.06	36.33	0.23	1000.00

Prepared cores not used

Table 4-2 – Overview of basic core properties arranged in numerical order, L# is Edwards Limestone, S# is sandstone, K# is chalk.

Core	Length [cm]	Diameter [cm]	Pore volume [ml]	Porosity [%]	Kmatrix [mD]
L1	7.37	4.96	32.05	0.23	14.93
L3	7.58	4.98	31.56	0.21	12.48
L5	7.59	4.95	33.76	0.23	22.96
L8	7.26	4.95	30.81	0.22	17.70
L11	7.06	4.96	31.37	0.23	21.12
L12	7.64	4.96	33.43	0.23	14.26
L13	8.03	4.95	33.50	0.22	12.49
L15	7.35	4.96	32.30	0.23	18.57
L18	7.12	5.16	35.82	0.24	49.79
L24	7.06	4.97	31.93	0.23	35.23
L27	7.53	4.96	34.99	0.24	19.88
S1.5"1	8.60	3.75	21.89	0.23	
S1.5"2	9.27	3.75	22.77	0.22	
S1.5"3	8.97	3.75	22.20	0.22	
S1.5"4	9.13	3.75	23.24	0.23	
S2"1	7.76	5.06	36.33	0.23	
S2"2	9.76	5.07	41.67	0.21	
S2"3	9.41	4.96	39.77	0.22	
S2"4	9.74	5.06	42.19	0.22	
S2"5	9.31	5.05	42.49	0.23	
K1	8.01	5.07	72.69	0.45	2.82
K2	7.45	4.95	66.57	0.46	broken
K3	8.00	5.07	74.60	0.46	2.91
K4	7.79	4.94	70.85	0.47	3.51
K5	7.63	4.95	67.72	0.46	2.89
K6	7.25	4.95	65.60	0.47	3.09
K7 (Stevens Chalk)	7.58	5.07	75.27	0.49	6.73
K8	7.66	4.98	68.97	0.46	3.09
K9	7.35	4.95	66.76	0.47	3.11
K10	7.28	4.95	64.78	0.46	2.89
K11	7.50	4.94	67.75	0.47	3.23
K12 (Stevens Chalk)	7.46	5.07	78.06	0.52	6.92

4.2 Wettability measurements

Wettability measurements were performed on all of the aged cores, using the Amot-Harvey method as described in chapter 1.4.2 and chapter 3.7. The Amott-Harvey index was calculated using equation (1.8).

Table 4-3 – Overview of wettability of aged cores arranged the order of Amott-Harvey index (I_{A-H}), aging time and aging method.

Core	Iw	Io	I_{A-H}	Aging time [Hours]	Aging method
L4	0.00	0.02	-0.02	90	Dynamic
L14	0.00	0.06	-0.06	90	Dynamic
L2	0.10	0.00	0.10	90	Dynamic
L7	0.00	0.04	-0.04	90	Dynamic
L15	0.00	0.10	-0.10	90	Dynamic
L1	0.00	0.02	-0.02	90	Dynamic
L16	0.00	0.03	-0.03	90	Dynamic

The moderately oil-wet cores did not imbibe water, and the moderately water-wet cores did not imbibe oil. For this reason they are in this thesis referred to as moderately oil-wet or moderately water-wet, and not as neutrally wet.

Comments on the aging of the cores

As will be discussed in more detail in chapter 4.5.3 the wettability altered cores, might have lost some water at some point of the Amott-Harvey measurements. If this water was lost while the cores were in the imbibition cells, then they should have been shifted even more towards oil-wet wettability. Most likely the water was lost at a different time of the process, because 7 different imbibition cells were used, and there was probably not a problem with all of them. It is however possible some part of the equipment had a leak.

4.3 MMP simulation in CMG Winprop

Numerical simulations to establish the minimum miscibility between CO_2 and n-Decane were performed with the CMG WinProp PVT Simulator. At 20 °C CO_2 had an estimated MMP of 53 Bar. For this reason the line pressure was kept at approximately 90 bars to make sure the displacement was first contact miscible. Knowing that the injecting fluid is first-contact miscible with the oil is an important factor when analyzing what has occurred during the core flooding. Having a miscible displacement leads to an effective microscopic displacement, as discussed in chapter 1.4.1.

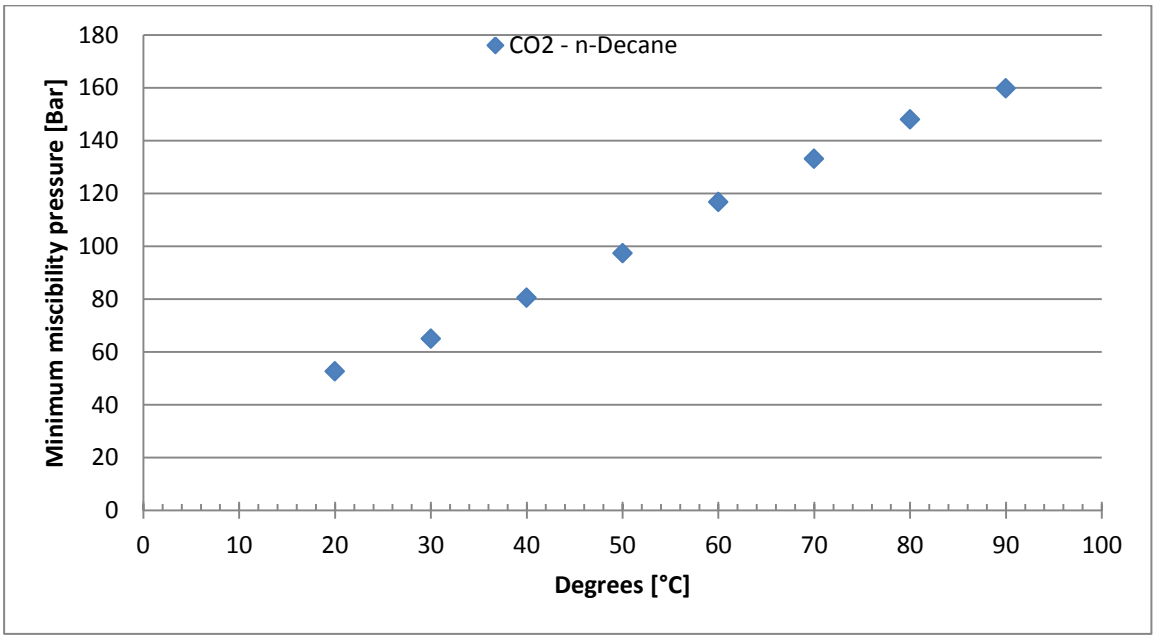

Figure 4-2 – Minimum miscibility pressure for CO_2 and n-Decane as a function of temperature.

4.4 GEM Simulation

In this thesis numerical simulations have been performed to reproduce experimental results and use this to further explain different phenomena surrounding CO_2 injection and CO_2-foam injection. The simulations have been performed with CMG GEM simulator, which is an advanced compositional and unconventional reservoir simulator and has options to simulate complex behavior during CO_2 flooding.

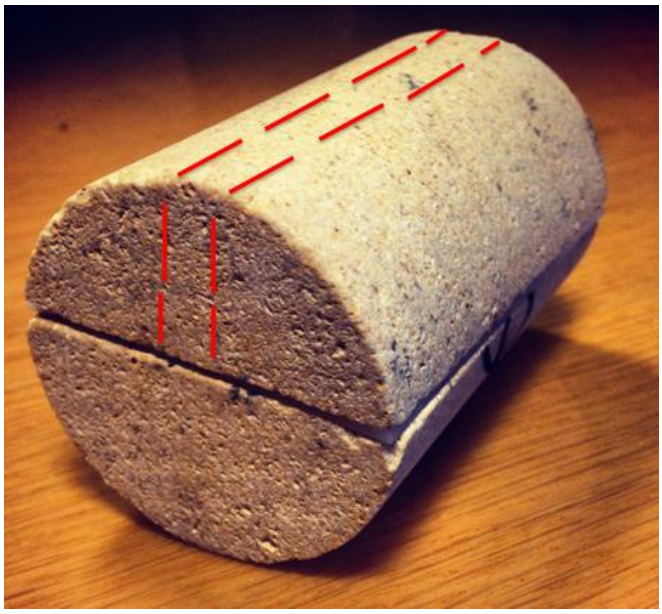

Figure 4-3 – the area within the red dashed lines is showing the part of the core that was simulated.

Figure 4-3 shows the area that was simulated to simplify the simulation. The grid was built in the CMG Builder without wells and the grid was made into blocks of 34x21x1. Instead of placing wells two areas were made: the matrix area representing the core, and the fracture area representing the fracture and end pieces, as shown in Figure 4-4. The end pieces were included because as shown from CT images showing diffusion from a fracture (see Figure 4-24), there is a significant CO_2 concentration contribution from the end pieces used in the experiments in this thesis, which increases the diffusion of oil. This is discussed in more detail in chapter 4.6.3. The fracture area was made a lot larger than the matrix area, so that the saturation in the fracture area would continuously have close to 100% CO_2.

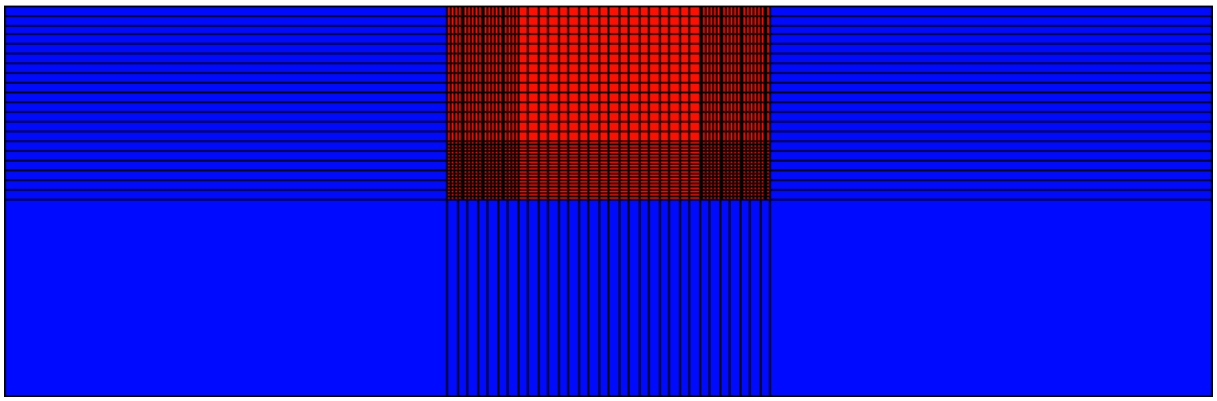

Figure 4-4 – The red part of the grid represents the matrix area (the core), the blue represents the fracture area (the end pieces on the right and left side, the fracture below).

The permeability in the fracture was set to 500 000 mD. The high fracture perm and constant concentration is done to represent the effect of CO_2 being continuously injected through the fracture. The simplification causes everything to be diffusion driven, with no viscous forces present. This has been done because Edwards Limestone core plugs are low permeable (in the range of approximately 30 mD). The simplification will not be far from reality since viscous force becomes negligible if the fluid mainly flows in the fracture and if the matrix block is low permeable (Alavian and Whitson, 2010). The part of the matrix area (blue), closest to the fracture area (red) was refined (split into smaller cells) to reduce numerical problems. Refinement in boundary areas between two phases can reduce the simulation time and the numerical problems effectively. This was also done in Schlumberger's *Eclipse* simulator on the Troll field by Statoil in the area close to the gas-oil contact. The problems are caused by large saturation variations in small timesteps (Nybø, 2012).

The core properties are then defined, such as; porosity, permeability, irreducible water saturation, relative permeability curve and capillary pressure curve. The relative permeability curve and capillary pressure curve were taken from literature values for chalk. Component properties for CO_2 and n-Decane were imported from the CMG WinProp PVT Simulator. Oil swelling was not included in order to reduce simulation time. This factor is then incorporated in the diffusion coefficient that we found by trying to replicate the experimental results. There were a lot of problems encountered concerning simulation time and numerical problems (numerical problems resulted in stopped simulations). A lot of time was spent fine tuning the numerical controls to reduce the simulation time. In the beginning it would take 4-5 days to simulate 2 days of CO_2 injection.

The simulations were run with three different diffusion keywords: `*DIFCOR-OIL SIGMUND`, `*DIFCOR-OIL WILKE` and `*DIFFC-OIL`. `*DIFCOR-OIL SIGMUND` specified the Sigmund correlation for molecular diffusion (Sigmund, 1976). `*DIFCOR-OIL WILKE` specifies the Wilke-Chang correlation for oil phase molecular diffusion (Wilke, 1955). `*DIFFC-OIL` specifies the Lake correlation for molecular diffusion(Lake, 1989). After several simulations, `*DIFFC-OIL` was chosen as the diffusion keyword to be used for further simulations in this thesis. `*DIFFC-OIL` was chosen because the two other keywords, exaggerated the oil recovery, and it was not possible to change the diffusion coefficient. With the keyword `*DIFFC-OIL` it was possible to change the diffusion coefficient. The simulations were run several times to find a diffusion coefficient in the right range.

Since CO_2 and oil are miscible at the pressure and temperature used in the simulations and since both are in the liquid phase, the simulator counted both as components in the oil phase. The only way we could estimate the production was by plotting the oil components moles of CO_2 and oil as a function of time in the matrix region from the CMG Results Graph, exporting the plot to excel, and then calculating from moles to saturation.

Results from these simulations are discussed in the discussion part of this thesis, in chapter 5.5.

4.5 Experimental overview

All experiments were performed at approximately 90 bars and 20 °C, i.e. at liquid CO_2 conditions and CO_2 fully miscible with n-Decane. The CO_2 injection experiments were performed with the experimental setup in chapter 3.9.1 and the foam injection experiments were performed as shown in the experimental setup in chapter 3.9.2. The fracturing was conducted as shown in chapter 3.8. The pore volume (time) shown in the results has been adjusted to account for the dead volume. The pore volume (time) starts from the point after the dead volume has been produced, since all the production before that is not from the core. Less than 10% of the dead volume is behind the core, but has been taken into account as if it was in front of the core.

Comments regarding the figures in the results and the discussion section

The saturation curves and recovery factor curves shown in this thesis will have a linear curve initially when plotted as a function of pore volumes injected. This means that the amount of liquid injected equals the amount of liquid produced (compressibility is negligible when liquid is produced and injected). When this linearity stops it means breakthrough has occurred, and oil production will become less effective. Curves for the fractured cores may not have a linear curve initially, because breakthrough occurs almost instantly.

Table 4-4 – Overview of performed experiments arranged in the order of wettability, irreducible water saturation, injection fluid and core state. H&P is the huff and puff experiment. SWW = strongly water wet, OW = moderately oil-wet.* Estimated values

Core	Description	CO2/Foam	State	Swi	Kmatrix	Kfracture	Sor, w	Sor, co2	RF
L17	SWW, 100% oil	CO2	Whole	0.00	51.0	-	-	0.00	1.00
L19	SWW, 100% oil	CO2	Whole	0.00	40.2	-	-	0.05	0.95
L20	SWW, 100% oil	CO2	Whole	0.00	55.3	-	-	0.00	1.00
L21	SWW, 100% oil	CO2	Fractured	0.00	47.0*	1080	-	0.07	0.93
L22	SWW, 100% oil	CO2	Fractured	0.00	47.0*	1080*	-	0.08	0.92
L6	SWW, Swi	CO2	Whole	0.14	29.3	-	-	0.11	0.87
L9	SWW, Swi	CO2	Whole	0.23	24.5	-	-	0.07	0.91
L10	SWW, Swi	CO2	Whole	0.20	29.6	-	-	0.00	1.00
L28	SWW, Swi, Foam	Foam	Whole	0.24	19.9	-	-	0.27	0.65
L33	SWW,Swi Foam	Foam	Whole	0.29	33.5	-	-	0.06	0.91
L23	SWW, Swi	CO2	Fractured	0.13	58.7	1342	-	0.22	0.75
L26	SWW, Swi	CO2	Fractured	0.23	41.7	1318	-	0.12	0.84
L25	SWW, Swi, H&P	CO2	Fractured	0.26	28.0	1366	-	0.05	0.93
L7	OW, Swi	CO2	Whole	0.32	18.5	1255	-	0.00	1.00
L4	OW, Swi	CO2	Whole	0.32*	28.6	-	-	0.00	1.00
L16	OW, Swi	CO2	Whole	0.38*	15.0	-	-	0.15	0.77
L2	OW, Swi	CO2	Fractured	0.32*	30.1	1255	-	0.24	0.59
L14	OW, Swi	Foam	whole	0.34	28.2	-	-	0.01	0.98
EDW6	OW, Swi	Foam	Fractured	0.19	27.5	1980	-	0.07	0.91
EDW32	OW, Swi	Foam	Fractured	0.17	21.0	265	-	0.07	0.92
EDW39	OW, Swi	Foam	Fractured	0.11	11.6	1021	-	0.16	0.82
EDW15	SWW, Swi, Tertiary	Foam	Fractured	0.26	19.3	1365	0.58	0.31	0.58
EDW34	SWW, Swi, Tertiary	Foam	Fractured	0.23	31.6	285	0.44	0.19	0.76
EDW16	SWW, Swi	Foam	Fractured	0.32	26.4	117	-	0.24	0.64
EDW33	SWW, Swi	Foam	Fractured	0.19	28.5	261	-	0.17	0.78
E5	SWW, Swi, Tertiary	CO2	Whole	0.27	15.2	-	0.52	0.41	0.56
E6	SWW, Swi, Tertiary	CO2	Whole	0.30	9.3	-	0.55	0.45	0.65
E8	SWW, Swi, Tertiary	CO2	Whole	0.34	9.5	-	0.57	0.47	0.71

4.5.1 Liquid CO_2 injection in cores fully saturated with n-Decane

Table 4-5 shows core and production data for experiments performed with 100% oil saturated cores. SWW expresses that the core is strongly water wet, S_{wi} is the initial water saturation, Kmatrix is the matrix permeability, Kfracture is the fracture permeability, "Sor, CO_2" is the residual oil after a CO_2 flood, and RF is the recovery factor OOIP (oil in place after flooding/oil in place initially).

Table 4-5 – Overview of experiments performed on cores fully saturated with n-Decane arranged in the order of wettability wettability. *estimated values.

Core	Description	CO2/Foam	State	S_{wi}	Kmatrix [mD]	Kfracture [mD]	Sor, w	Sor, CO_2	RF
L17	SWW, 100% oil	CO2	Whole	0,00	51,0	-	-	0,00	1,00
L19	SWW, 100% oil	CO2	Whole	0,00	40,2	-	-	0,05	0,95
L20	SWW, 100% oil	CO2	Whole	0,00	55,3	-	-	0,00	1,00
L21	SWW, 100% oil	CO2	Fractured	0,00	47,0*	1080	-	0,07	0,93
L22	SWW, 100% oil	CO2	Fractured	0,00	47,0*	1080*	-	0,08	0,92

Whole

Table 4-6 – Recovery factor for given pore volumes during CO2 injection in three water-wet, whole limestone core plugs fully saturated with n-Decane.

Core	RF @ 1 PV	RF @ 2 PV	RF,total	PV @ RF,total
L17	0.68	0.92	1.00	2.8
L19	0.48	0.72	0.95	4.6
L20	0.60	0.77	1.00	4.8

Three secondary liquid CO_2 injection experiments were performed on whole cores fully saturated with n-Decane. Experiments were performed above the minimum miscibility pressure (Core L17: 92 bar, Core L19: 91 bar, Core L20: 94 bar), which means the experiments were first-contact miscible. All three experiments end up with a high recovery; Core plugs L17 and L20 with 100% oil recovery, and core plug L19 with 95% oil recovery. L19 might also have reached 100% if the experiment had continued.

As shown in Figure 4-5 and Figure 4-6, the curves for L17 and L20 follow each other and show similar recovery curves in the beginning. Both have CO_2 breakthrough after approximately 0.3 PV. They diverge at approximately 0.65 PV. The divergence may be caused by a reduction in confining pressure so that the CO_2 is allowed to flow around the core along the sleeve of the core holder. If the divergence is caused by the confining pressure getting close to the line pressure, then core L17 is the most correct and more experiments should be done to confirm this. Core L17 seems to have a kink at around 1.3 pore volumes, this is caused by the production tube being submerged in the produced oil in the production beaker, and CO_2 then creating disturbances in the produced oil, making it difficult to get an exact reading of oil production from the webcam. This lasts until 2.1 pore volumes.

Looking at Figure 4-5 and Figure 4-6 for core L19 the curve looks a bit different than the other two. This might be caused by the fact that L19 has an early break through at 0.1 pore volume, which might be caused by the confining pressure getting close to the line pressure, letting CO_2 slip around the edges of the core. The confining pressure is increased after around 0.5 pore volume (this can be seen from

the recovery factor curve). The production then normalizes and catches up with core L20. The reason it catches up, might be because L20 also has confinement problems.

The dead volume was not measured for L20. Because the pore volume of L19 is similar to L20, we estimated that the dead volume for L20 would be similar to L19.

Figure 4-7 shows recovery factor as a function of the square root of time. Recovery factor is plotted as a function of the square root of time because the penetration depth of diffusion, is proportional to the square root of the time if there is a constant concentration at the boundary, which makes saturation and thus recovery factor proportional to the square root of time if diffusion is the only recovery mechanism, detailed in 1.8 (Cussler, 1997). The closer to linear the recovery factor curve is when plotted as a function of the square root of time the more dominating diffusion is as recovery mechanism. The two fractured cores have close to linear shapes, which indicate that the oil recovery is mainly diffusion driven. Compared to core L17, the slope diverges further from the linear line, which indicates that the recovery process is more viscous driven. Core L19 and Core L20 however do not have the same shape as L17, another indication that the confining pressure has gotten close to the line pressure at different times. When the confining pressure has gotten close to the line pressure the CO_2 will go around the core, and the recovery will be caused by diffusion from outside of the core, and in to the matrix. The CO_2 will not go through the core (because of higher resistance), thus viscous recovery will not take place. Core L19, where the confining pressure was increased after 0.5 pore volumes seems to become viscous driven, because the shape becomes more like the shape of Core L17. Figure 4-14 shows CO_2 injection on whole cores with irreducible water saturation, these cores should behave similarly although these cores contain water which will cause water shielding (Zekri et al., 2007). Figure 4-14 shows that the whole core curves at S_{wi} behave similarly to Core L17. This confirms the suspicions that core L19, and core L20 do not behave as they should, and thus in the discussion part of this thesis only core L17 will be included to represent CO_2 injection in fully saturated whole cores. The ultimate recovery for core L19 and L20 will be included in the discussion, because this will not be affected by the low confining pressure.

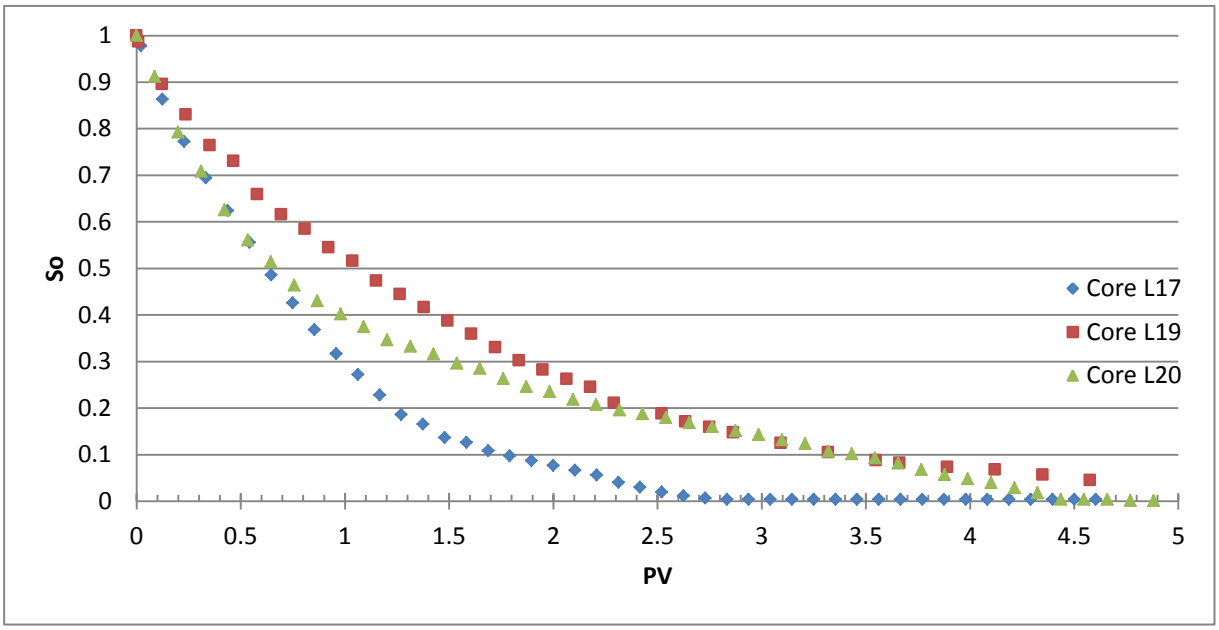

Figure 4-5 – Average oil saturation as a function of time during CO2 injection in three water-wet, un-fractured limestone core plugs fully saturated with n-Decane.

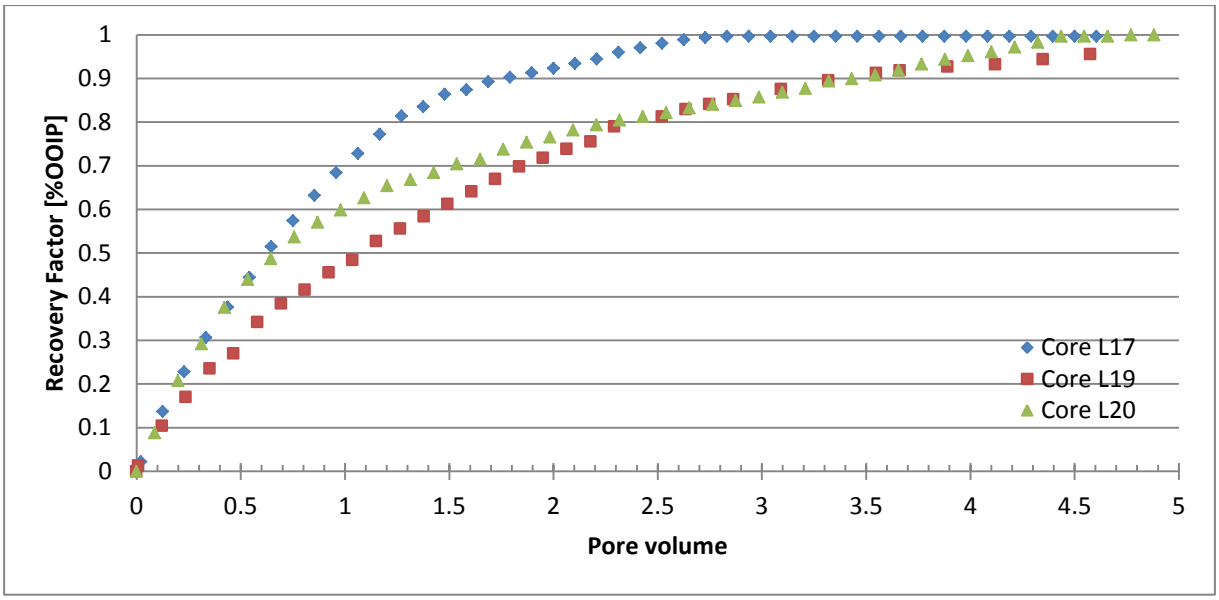

Figure 4-6 – Recovery factor as a function of time during CO2 injection in three water-wet, whole limestone core plugs fully saturated with n-Decane.

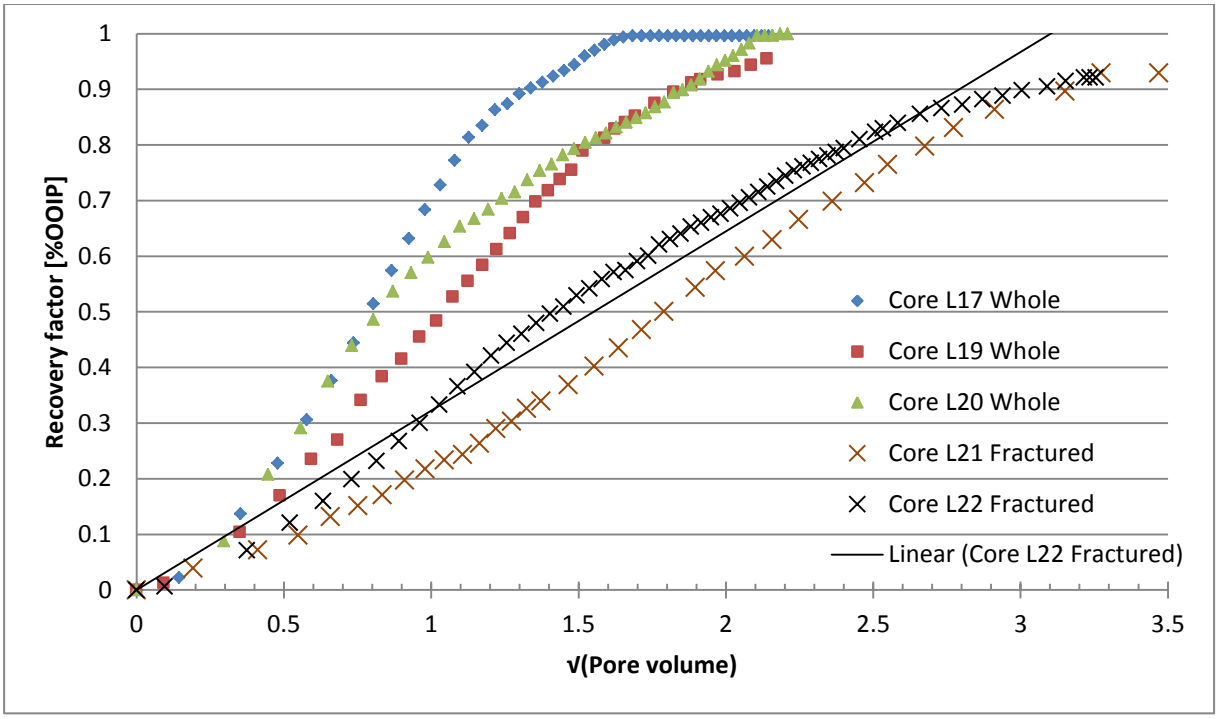

Figure 4-7 – Recovery factor as a function of the square root of time during CO2 injection in three water-wet, whole and two water-wet, fractured limestone core plugs fully saturated with n-Decane.

Fractured core plugs

Table 4-7 – Recovery factor for given pore volumes during CO_2 injection in three water-wet, fractured limestone core plugs fully saturated with n-Decane.

Core	RF @ 1 PV	RF @ 2 PV	RF,total	PV @ RF,total
L21	0.22	0.34	0.93	12
L22	0.33	0.50	0.92	10.6

Two secondary liquid CO_2 injection experiments were performed on fractured cores fully saturated with n-Decane. Experiments were performed above the minimum miscibility pressure (Core L21: 92 bar, Core L22: 97 bar) which means the experiments were first-contact miscible. Both experiments ended up with a high oil recovery, above 90%, although they might have reached 100% if allowed to continue since the curves have not flattened out.

The matrix permeability for L21 and L22 was not measured, because the cores were cut (fractured) in dry condition. The matrix permeability was set to the average permeability of the cores L23 and L24, because they were drilled out of the same area of the outcrop rock.

The fracture permeability was not measured for L22. Since L21 and L22 have similar properties we estimated that the fracture permeability would be the same. The dead volume was not measured for L21. Because the pore volume of L22 is similar to L21, we estimated that the dead volume for L21 would be comparable to L22.

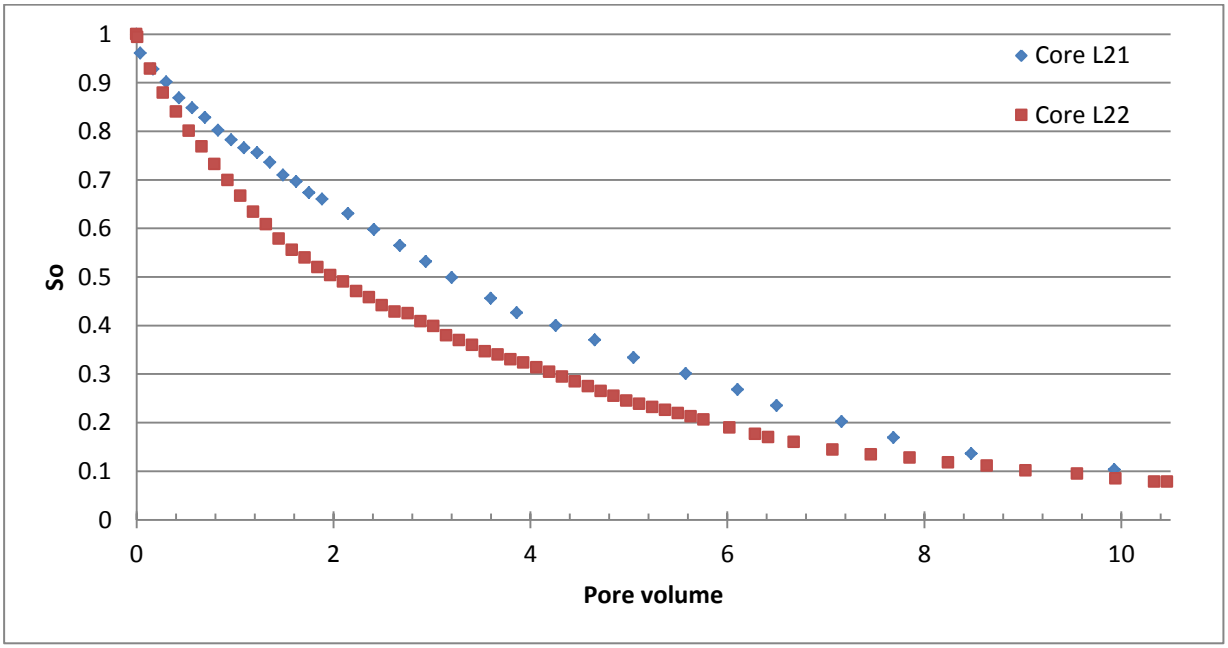

Figure 4-8 - Average oil saturation as a function of time during CO2 injection in two water-wet, fractured limestone core plugs fully saturated with n-Decane.

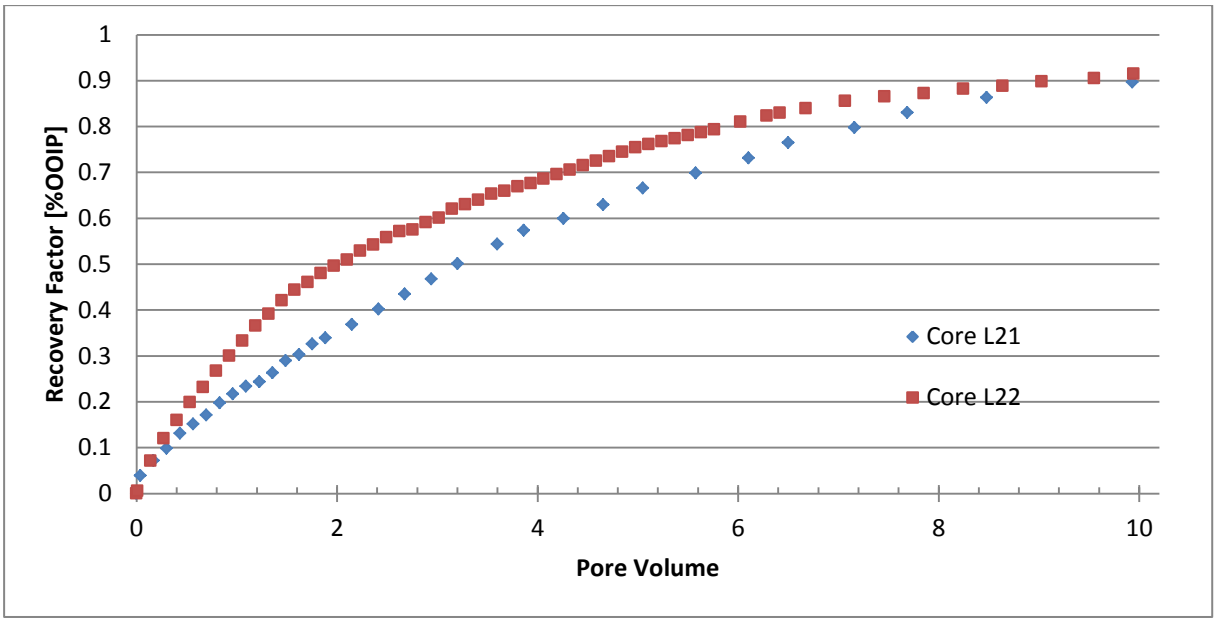

Figure 4-9 - Recovery factor as a function of time during CO2 injection in two water-wet, fractured limestone core plugs fully saturated with n-Decane.

Sandstone whole core

One secondary liquid CO_2 injection experiments was performed on a whole sandstone cores fully saturated with n-Decane. The experiment was performed above the minimum miscibility pressure (Core sandstone 87 bars) which means the experiments were first-contact miscible. The experiment ended up with a high oil recovery, above 90%.

Table 4-8– Recovery factor for given pore volumes during CO2 injection in a whole sandstone core plug fully saturated with n-Decane.

Core	RF @ 1 PV	RF @ 2 PV	RF,total	PV @ RF,total
Sandstone	0.49	0.59	0.92	6.1

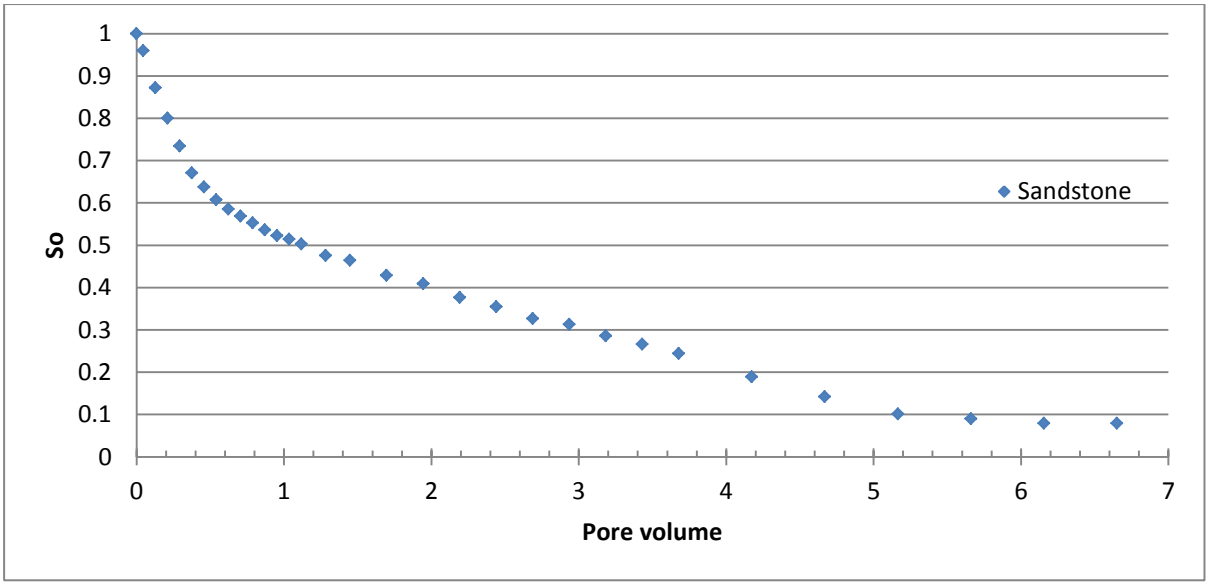

Figure 4-10 - Average oil saturation as a function of time during CO2 injection in a whole, fully oil saturated sandstone core plug.

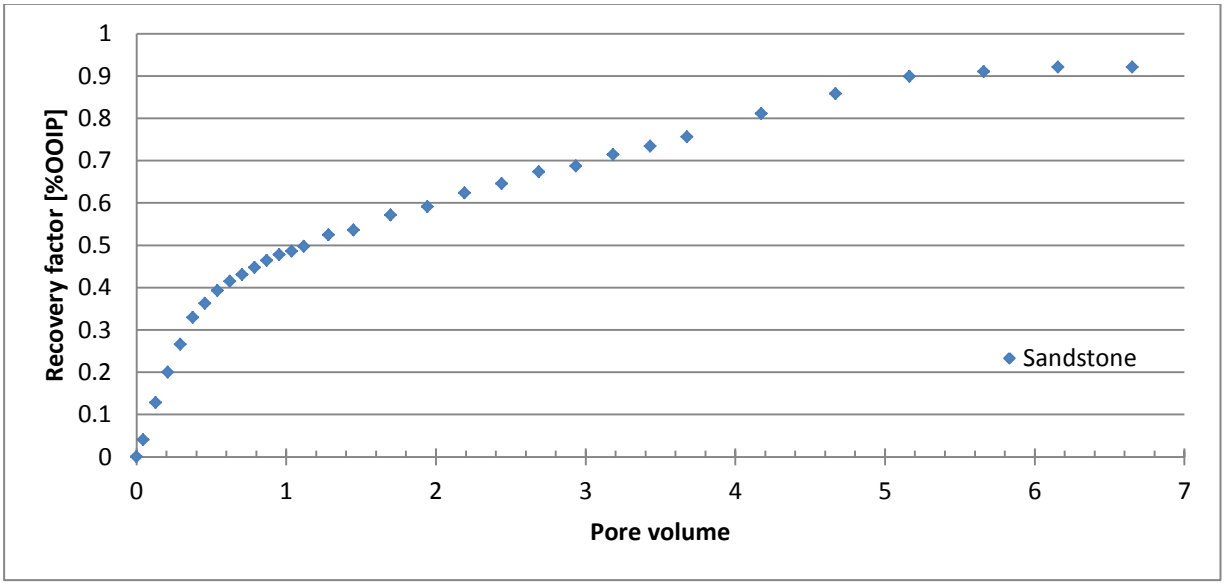

Figure 4-11 – Recovery factor saturation as a function of time during CO2 injection in a whole, fully oil saturated sandstone core plug.

4.5.2 Liquid CO_2 injection in strongly water-wet cores at irreducible water saturation.

Table 4-9 - Overview of experiments performed on cores at irreducible water saturation arranged in the order of wettability. H&P = Huff and Puff experiment. *dead volume was not measured

Core	Description	CO2/Foam	State	Swi	Kmatrix [mD]	Kfracture [mD]	Sor, w	Sor, co2	RF
L6	SWW, Swi	CO2	Whole	0.14	29.3	-	-	0.11	0.87
L9	SWW, Swi	CO2	Whole	0.23	24.5	-	-	0.07	0.91
L10	SWW, Swi	CO2	Whole	0.20	29.6	-	-	0.06*	0.92*
L23	SWW, Swi	CO2	Fractured	0.13	58.7	-	-	0.22	0.75
L26	SWW, Swi	CO2	Fractured	0.23	41.7	1318	-	0.12	0.84
L25	SWW, Swi, H&P	CO2	Fractured	0.26	28.0	1366	-	0.05	0.93

Whole core plugs

Table 4-10 – Recovery factor for given pore volumes during CO2 injection in three water-wet, whole limestone core plugs at irreducible water saturation.

Core	RF @ 1 PV	RF @ 2 PV	RF,total	PV @ RF,total
L6	0.64	0.81	0.87	4.3
L9	0.74	0.89	0.91	3.5
L10	0.69	0.86	0.92	3.2

Three secondary liquid CO_2 injection experiments were performed on whole cores at irreducible water saturation. Experiments were performed above the minimum miscibility pressure (Core L6: 91 bar, Core L9: 86 bar, Core L10: 80 bar) which means the experiments were first-contact miscible. The three core plugs ended up with a high oil recovery, above 87%. The cores flatten after approximately 3 pore volumes. All the cores reach around the same recovery factor at 1 and 2 pore volumes.

The pressurizing dead volume was not measured for core L10, and it was set equal to L9 because they had the most similar parameters. This gave us 100% recovery (in reality the dead volume was likely larger and thus total recovery lower). The core seems to behave as the other two cores except for the end point. The three core plugs used around the same amount of time (3 PV) to reach ultimate recovery. This seems to support that the dead volume is the only fault with core plug L10. All other parameters are in the same area. Core L10 also had some fluctuations in pressure (between 77-85 bar), which might affect the curve slightly. For this reason the pressurizing dead volume for core L10 which was initially set equal to L9, was increased, so that core L10 got a more realistic end point. Therefore when studying the curve of L10, the end point should not be taken into account.

Core plug L6 was left confined for 48 hours after 0.35 pore volumes because the accumulator ran out of CO_2. There did not seem to be any increase or decrease in recovery after the confinement period, see Figure 4-12 and Figure 4-13. An increase in recovery was expected because the core was left for 48 hours, letting the CO_2 to diffuse throughout the core, but the recovery seemed unaffected. The direction of diffusion is controlled by the concentration gradient. The reason there was no increase in recovery might be because the highest concentration of CO_2 will be at the inlet of the core, unlike a fractured core where the highest concentration will be in the middle, and will force the oil to diffuse from the matrix into the fracture, and then be produced. High concentration at the inlet will only force CO_2 and oil to mix, and some of the oil would diffuse in the direction of the inlet, away from

production(in the direction of highest CO_2 concentration). The shut in might reduce the effect of fingering, since CO_2 would have time to smooth out the fingers (Skarrestad and Skauge, 2011).

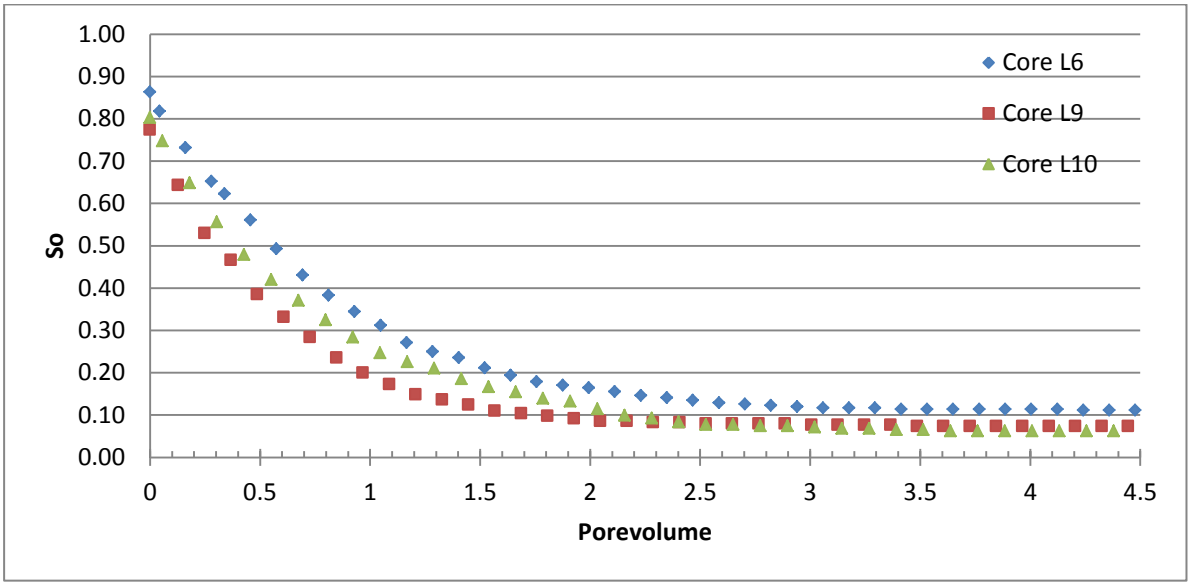

Figure 4-12 - Average oil saturation as a function of time during CO_2 injection in three water-wet, un-fractured limestone core plugs at irreducible water saturation.

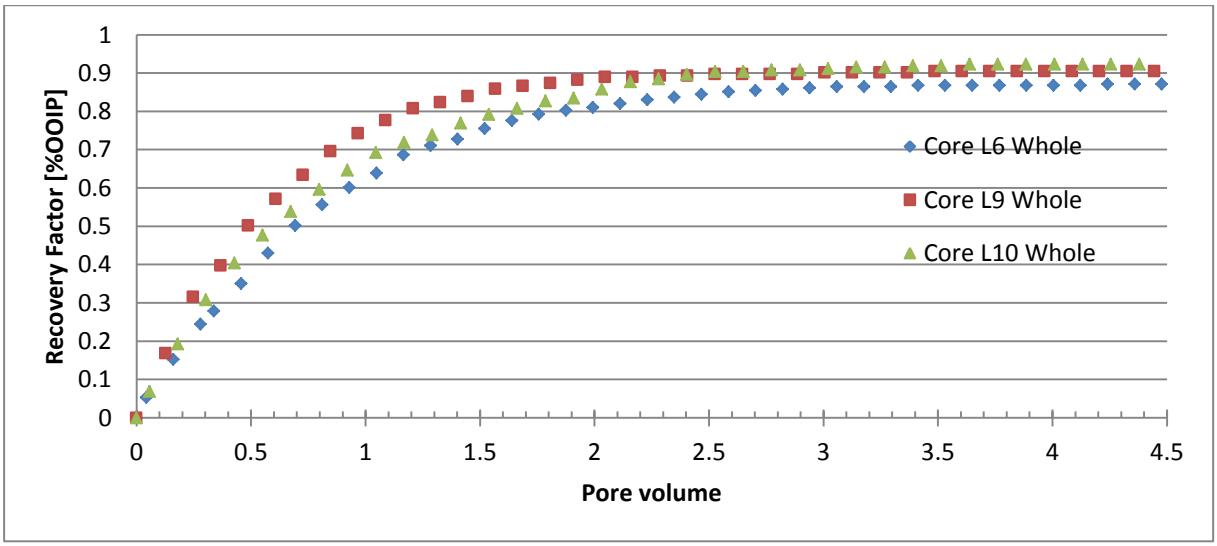

Figure 4-13 - Recovery factor as a function of time during CO_2 injection in three water-wet, whole limestone core plugs at irreducible water saturation.

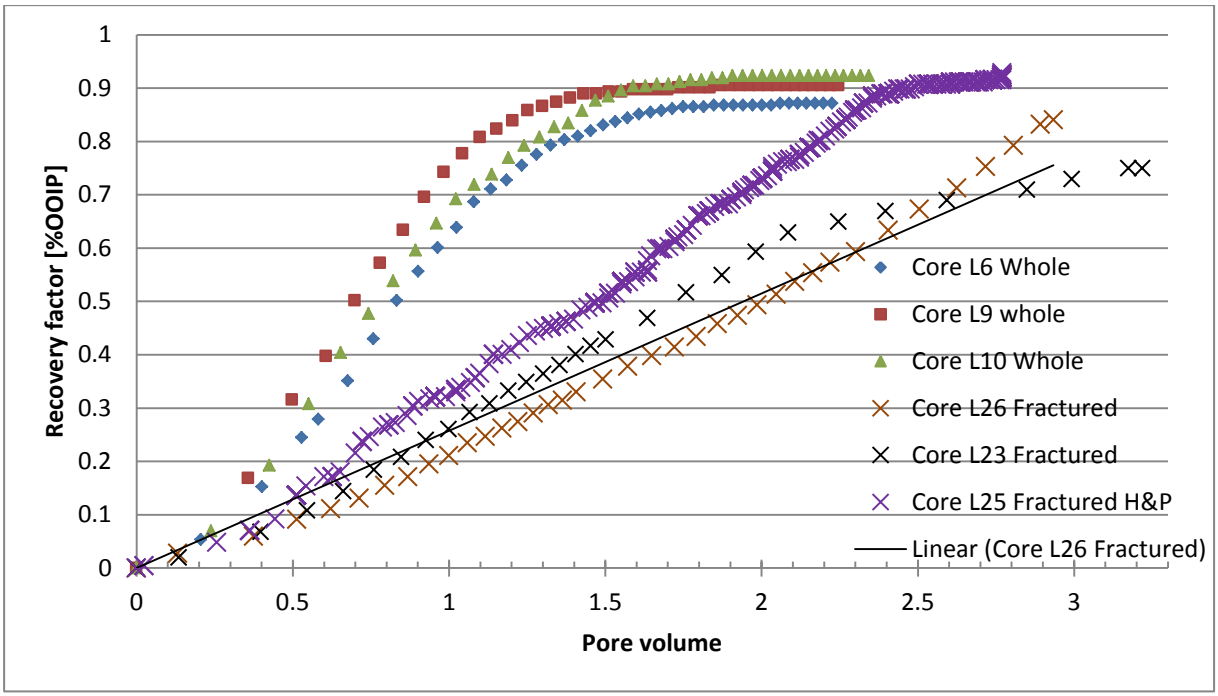

Figure 4-14 – Recovery factor as a function of the square root of time during CO_2 injection in three water-wet, whole and two water-wet, fractured limestone core plugs at irreducible water saturation.

Fractured core plugs

Table 4-11 – Recovery factor for given pore volumes during CO2 injection in three water-wet, fractured limestone core plugs at irreducible water saturation. H&P = huff and puff experiment

Core	RF @ 1 PV	RF @ 2 PV	RF,total	PV @ RF,total
L23	0.26	0.40	0.75	10
L25 H&P	0.33	0.48	0.93	8.6
L26	0.21	0.33	0.84	7.7

Three secondary liquid CO_2 injection experiments were performed on fractured cores at irreducible water saturation. Experiments were performed above the minimum miscibility pressure (Core L23: 97 bar, Core L26: 91 bar, Core L25: 98 bar) which means the experiments were first-contact miscible. The three core plugs ended up with a high oil recovery, above 75%, although core plug L23 would likely reach a higher recovery than 75% if the experiment had continued, the same might be true for L26.

Observing the trend in Figure 4-15 and Figure 4-16, Core L23 and Core L26 were most likely not finished recovering all the oil. If left for longer they would probably reach a higher ultimate recovery. The slope of L23 seems to start to flatten out very early after 4.3 pore volumes. The ultimate recovery for core plug L23 is lower than L26, which is illogical since the water saturation is lower for L23, which should lead to less water shielding effects. This might be caused by a decrease in confining pressure, since we had issues with the confining pressure dropping for other experiments. Line pressure seems to be stable in the area of 4 pore volumes, where L23 starts to flatten out, indicating that the problem is not caused by the pressure going below MMP.

For Core L23 fracture permeability was not measured. The fracture permeability was estimated (by calculating the average fracture permeability of L26 and L25) to be close to L26 and L25, because the same spacer was used and because Core plugs L26 and L25 had fracture permeabilities in the same region (1.3 Darcy). The fracture permeability of L23 was set to equal the average of core L26 and core L25.

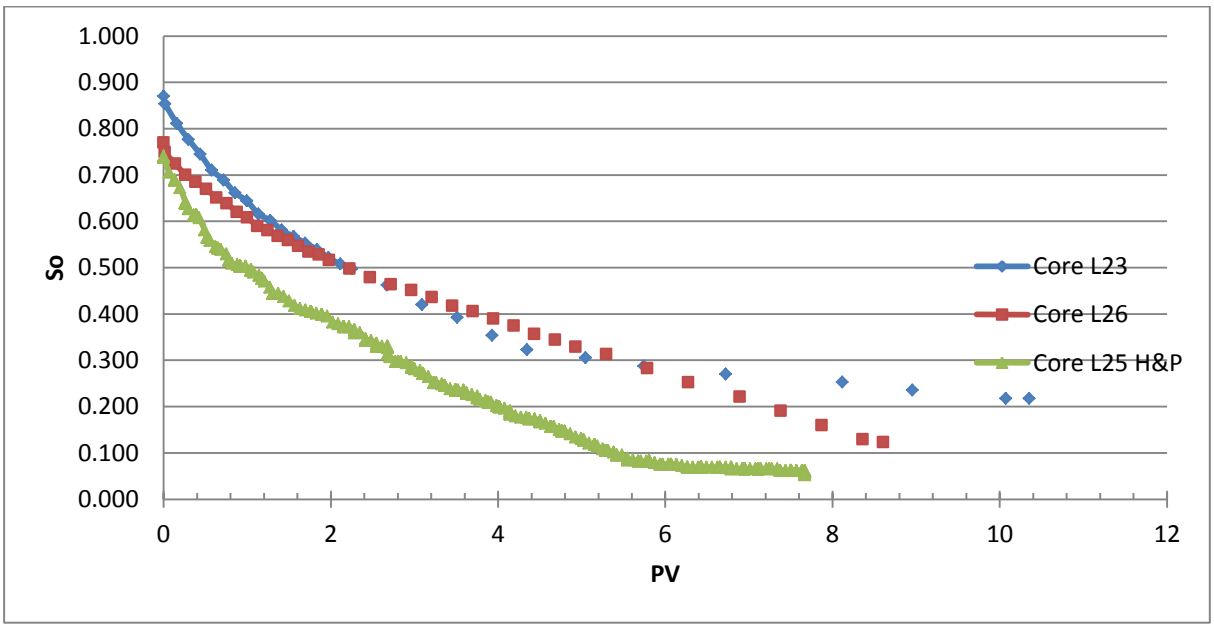

Figure 4-15 - Average oil saturation as a function of time during CO2 injection in three water-wet, fractured limestone core plugs at irreducible water saturation. H&P is an abbreviation for a huff and puff experiment.

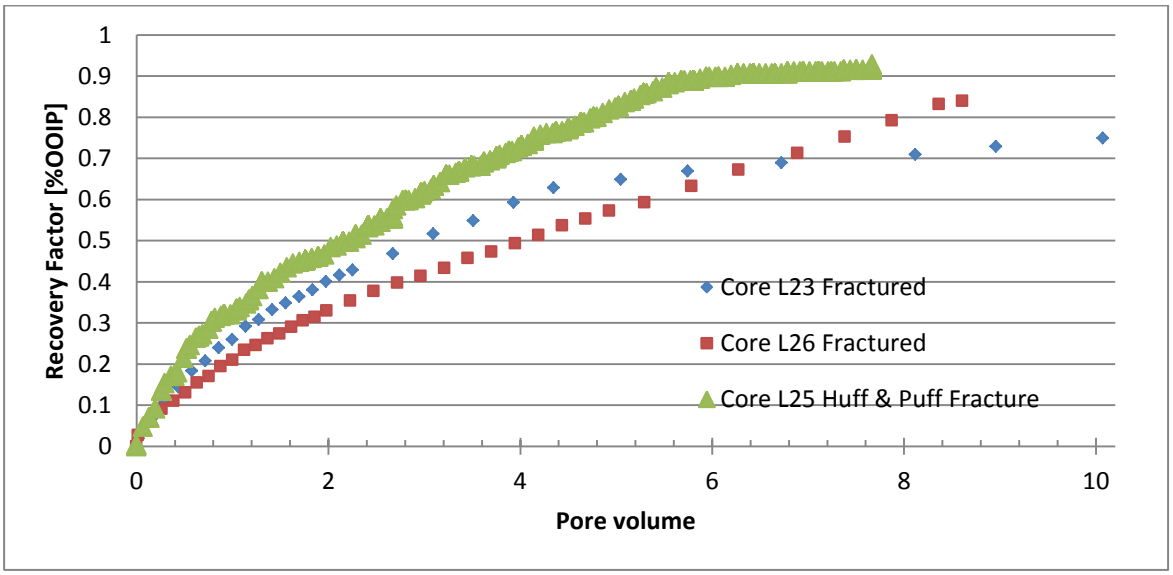

Figure 4-16 - Recovery factor as a function of time during CO2 injection in three water-wet, fractured limestone core plugs at S_{wi}.

Huff and Puff

Core L25 H&P was a huff and puff experiment where CO_2 was injected for one hour with an injection rate of 4 ml/h, then stopped for two hours (giving the CO_2 time to diffuse from the fracture and into the matrix for). This was done periodically every day. The core was stopped through the night, since injection had to be set manually. The experiment was run for a total of 15 days; almost 8 pore volumes were injected over the whole experiment.

4.5.3 Liquid CO_2 injection in moderately oil-wet cores at irreducible water saturation.

Table 4-12 - Overview of experiments performed on cores at irreducible water saturation arranged in the order of wettability, irreducible water saturation, injection fluid and core state. *estimated values

Core	Description	CO2/Foam	State	Swi	Kmatrix [mD]	Kfracture [mD]	Sor, w	Sor, co2	RF
L7	OW, Swi	CO2	Whole	0.33*	18.52	-	-	0.00	1.00
L4	OW, Swi	CO2	Whole	0.39*	28.56	-	-	0.00	1.00
L16	OW, Swi	CO2	Whole	0.33*	15.00	-	-	0.15	0.77
L2	OW, Swi	CO2	Fractured	0.32	30.12	1254	-	0.24	0.59

Whole cores

Table 4-13 – Recovery factor for given pore volumes during CO2 injection in moderately oil-wet, whole limestone core plugs at irreducible water saturation.

Core	RF @ 1 PV	RF @ 2 PV	RF,total	PV @ RF,total
L16	0.23	0.41	0.77	5
L4	0.46	0.69	1.00	4.8
L7	0.35	0.55	1.00	4.1

Three secondary liquid CO_2 injection experiments were performed on moderately oil-wet (see chapter 4.2 for a description of the Amott-Harvey index), whole cores at irreducible water saturation. Experiments were performed above the minimum miscibility pressure (Core L7: 92 bar, Core L4: 96 bar, Core L16: 80 bar) which means the experiments were first-contact miscible. Core L4 and L7 ended up with 100% oil recovery. Core L16 ended up with 77% oil recovery but had not finished producing when the experiment stopped. The experiment stopped because the line pressure went over 100 bars, triggering a release valve. The cores L4 and L7 recoveries flatten out around 4 pore volumes.

Figure 4-17 and Figure 4-18 shows average oil saturation and recovery factor for the core plugs; L4, L6 and L16. L7 follows L4 until suddenly L7's oil recovery drops at around 0.7 pore volume. The drop in oil recovery is likely caused by a loss of confining pressure, letting the CO_2 flow around the edges of the core reducing oil production. The CO_2 will follow the path of least resistance. Flowing around the edges, the CO_2 will displace a lot less oil, because recovery is now only diffusion driven, not viscous. Low confining pressure will have the same effect as having a fracture in the matrix, except that CO_2 shoots around the edges of the matrix, and not through the inside of the matrix as would happen with a fracture. At around 1.1 pore volumes the confining pressure is adjusted, and core plug L7 starts to catch up with L4. Core L4 has likely the most accurate curve. Only the ultimate recovery will be included from Core plug L7.

Looking at Figure 4-17 and Figure 4-18 the curve of L16 is only linear until approximately 0.02 PV, which indicates early breakthrough. This indicates that confining pressure has dropped for this experiment, because breakthrough after 0.02 is unlikely quick in an un-fractured core. As shown in Figure 4-19, when recovery is plotted as the square root of time for core L16 the slope of the curve is close to linear, indicating diffusion driven recovery. This further confirms the suspicion that confining pressure has dropped close to the line pressure, letting the CO_2 go around the sleeve, instead of through the core. For this reason only L4 will be taken into account in the discussion.

The aged cores had unlikely higher water saturations than expected as discussed in chapter 4.2. From weighing core L1 and L2 (also neutrally-wet), the actual S_{wi} could be estimated. Each of these cores had a lower S_{wi} from weighing than from the material balance estimates, which means water has been lost at some point of the experiment. The average difference in water saturation was calculated for core L1 and L2 (S_{wi} material balance – S_{wi} weighed), and deducted the average difference from the S_{wi} material balance for core L7, L16, and L4, since these cores were not weighed before the CO_2 injection experiments.

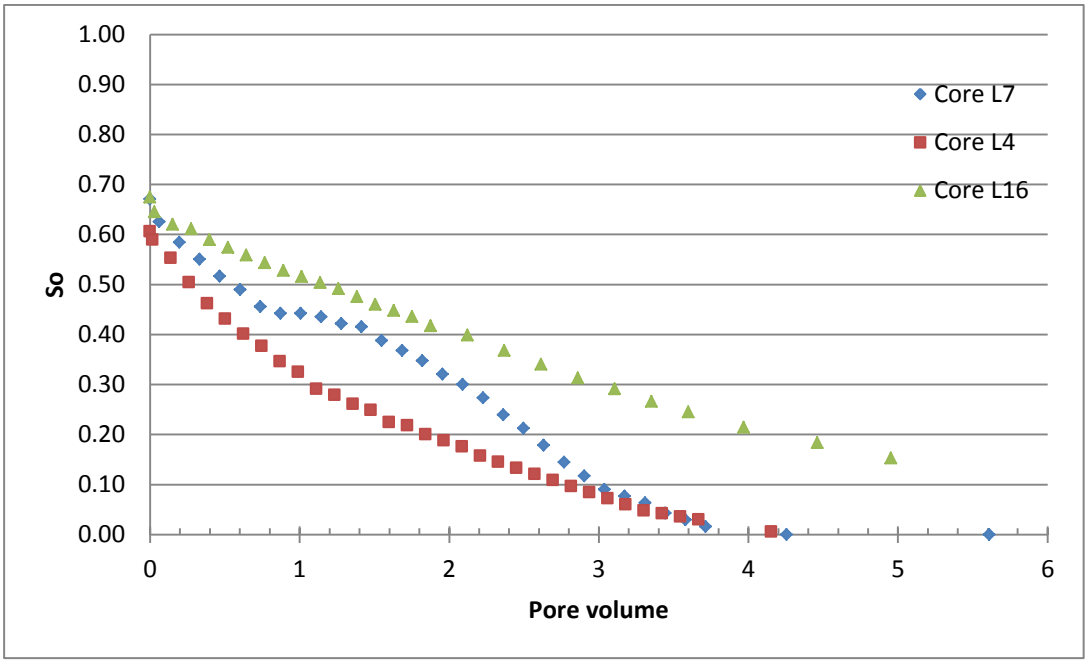

Figure 4-17 - Average oil saturation as a function of time during CO_2 injection in three moderately oil-wet, un-fractured limestone core plugs at irreducible water saturation.

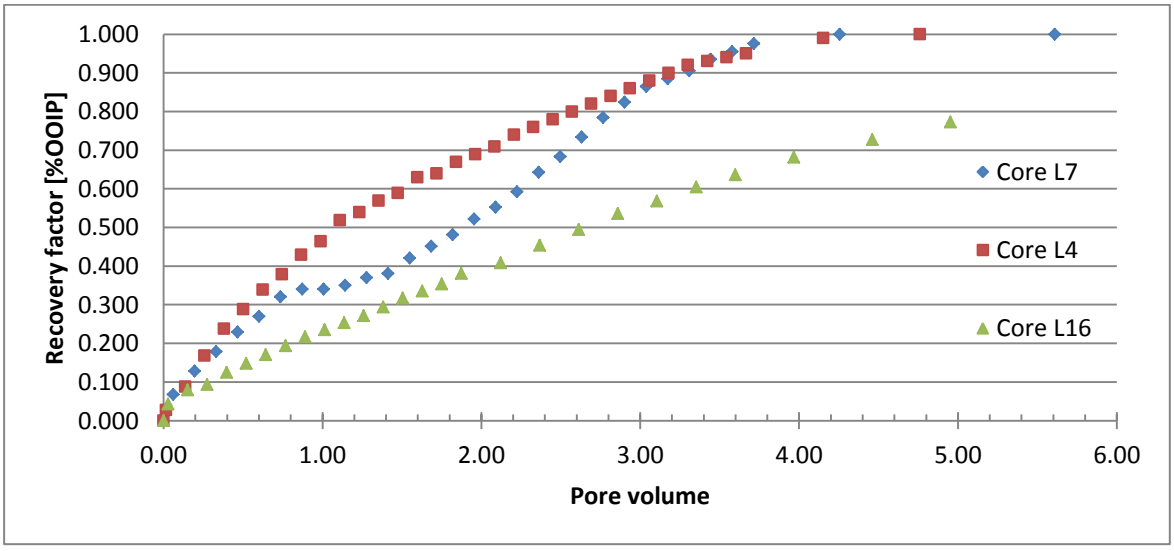

Figure 4-18 - Recovery factor as a function of time during CO2 injection in three oil-wet, whole limestone core plug at irreducible water saturation.

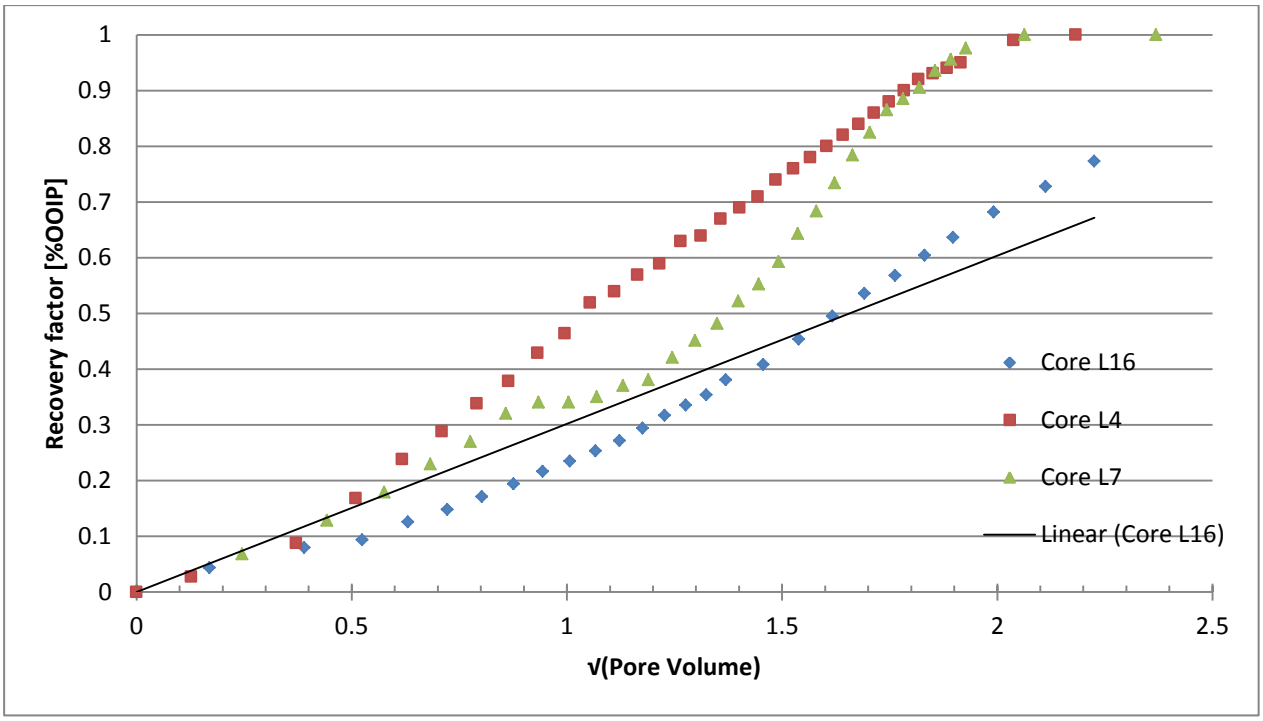

Figure 4-19 – Recovery factor as a function of the square root of time during CO2 injection in three oil-wet, whole limestone core plugs at irreducible water saturation.

Fractured cores

Table 4-14 – Recovery factor for given pore volumes during CO2 injection in moderately oil-wet, whole limestone core plugs at irreducible water saturation.

Core	RF @ 1 PV	RF @ 2 PV	RF,total	PV @ RF,total
L2	0.11	0.16	0.59	17.2

One secondary liquid CO_2 injection experiments was performed on a moderately oil-wet (see chapter 4.2 for Amott-Harvey index), whole core at irreducible water saturation. The experiment was performed at 93 bar, which means the experiment was first-contact miscible.

As shown in Table 4-14, the ultimate recovery after 17.2 pore volumes injected was 59 %. This low recovery is illogical because a higher oil recovery is expected for oil-wet cores, compared to water-wet cores, because of reduced effect of water shielding. Experiments have shown that the trapping occurs for the non-wetting phase, and thus in an oil-wet porous media virtually none of the oil gets trapped (Walsh et al., 1989). For mixed and oil-wet cores the amount of oil retained is insignificant after large amount of pore volumes of CO_2 are injected(Lin and Huang, 1990). The core was weighed (which means the S_{wi} is correct). Any clear reason for the low recovery cannot be found. The experimental results cannot be trusted and will not be included in the discussion.

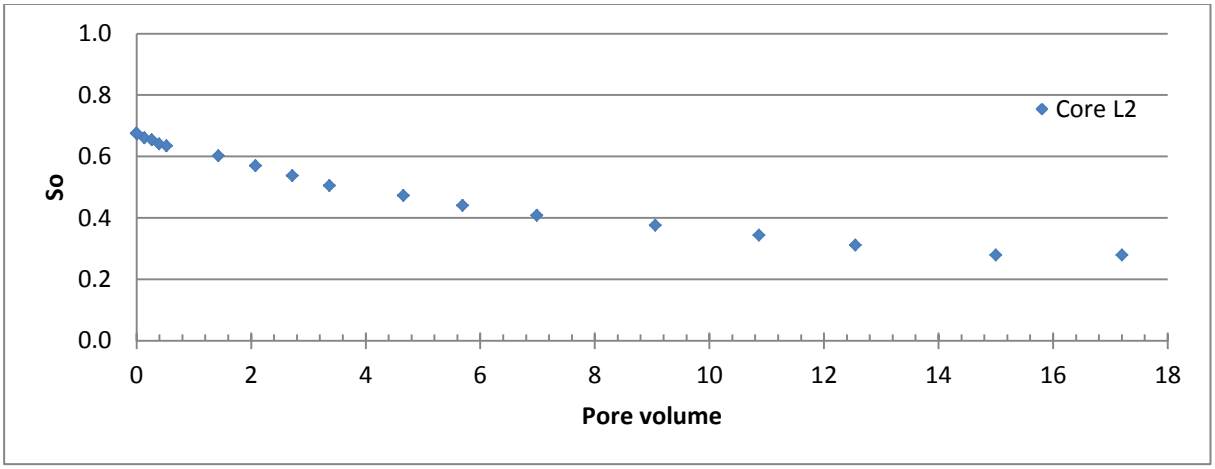

Figure 4-20 - Average oil saturation as a function of time during CO2 injection in one moderately oil-wet, fractured limestone core plugs at irreducible water saturation.

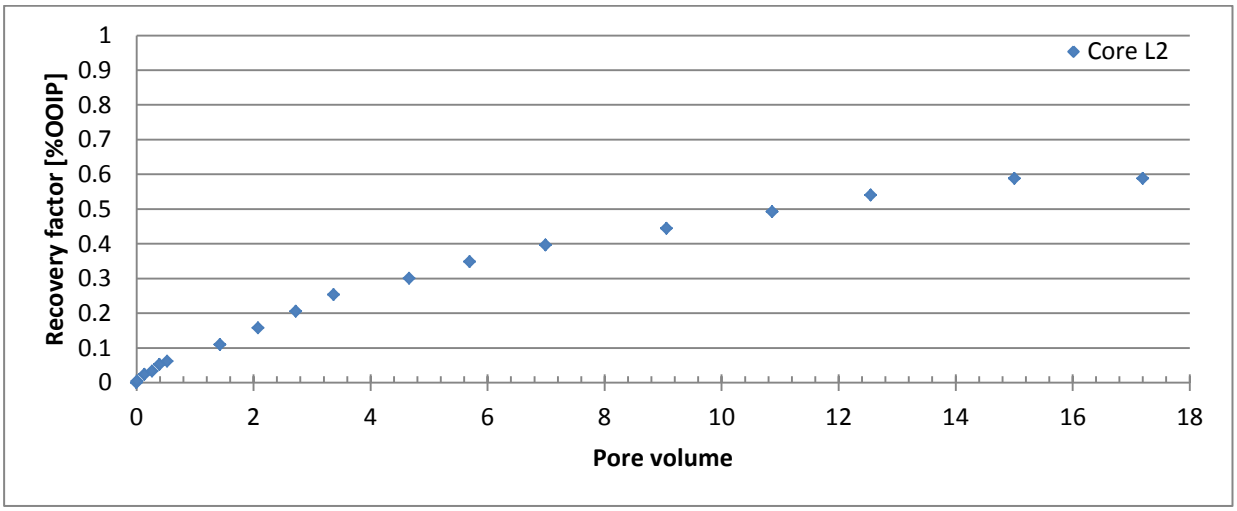

Figure 4-21 - Recovery factor as a function of time during CO2 injection in an oil-wet, fractured limestone core plug at irreducible water saturation.

4.5.4 **Liquid CO_2-foam injection with cores at irreducible water saturation.**

Table 4-15 - Overview of experiments performed on cores at irreducible water saturation arranged in the order of wettability, irreducible water saturation, injection fluid and core state.

Core	Description	CO2/Foam	State	Swi	Kmatrix [mD]	Kfracture [mD]	Sor, w	Sor, co2	RF
L28	SWW, Swi, Foam	Foam	Whole	0.24	19.9	-	-	0.27	0.65
L33	SWW,Swi Foam	Foam	Whole	0.29	33.5	-	-	0.06	0.91
L14	OW, Swi	Foam	whole	0.34	28.2	-	-	0.01	0.98

Table 4-16 – Recovery factor for given pore volumes during CO_2-Foam injection in two water-wet and one moderately oil-wet, whole limestone core plugs at irreducible water saturation.

Core	RF @ 1 PV	RF @ 2 PV	RF,total	PV @ RF,total
L28	0.58	-	0.65	1.4
L33	0.70	0.89	0.91	2.1
L14	0.75	0.92	0.98	2.2

Three secondary liquid CO_2-foam injection experiments were performed on two water-wet whole cores and one moderately oil wet whole core (see chapter 4.2 for Amott-Harvey index), at irreducible water saturation. Experiments were performed above the minimum miscibility pressure (Core L28: 99 bar, Core L33: 98 bar, Core L14: 99) which means the experiments were first-contact miscible. As shown in Figure 4-22 the differential pressure for the two water-wet cores are in the same range, and Core plug L33 starts to increase as oil saturation is reduced. This indicates creation of stronger foam as oil saturation is reduced. The differential pressure of the oil-wet core is approximately 1-2 orders of magnitude smaller than for the two water-wet cores. This indicates that there is either no foam created, or weaker foam is created in the oil wet core. 1-2 orders of magnitude higher differential pressure difference proves that foam has definitely been created in the water-wet cores.

As shown in Table 4-16, in Figure 4-22 and in Figure 4-23 the cores L33 and L14 reached a very high oil recovery above 90%, and might recover more oil if the experiment had been continued for a longer time. The two water-wet cores (L28 and L33) have the same oil recovery profile up to 0.65 pore volumes where they diverge. Core L28, does not recover more than 65%, which is an unlikely low oil recovery, and such different results indicate that the material balance is incorrect. The experiment was performed for 24 more hours than the other two foam experiments, and did not recover more than 65%, which is another indication that there was more water, and less oil than estimated (from the material balance) in the core, or oil was lost during the experiment. For this reason the results on Core L28 cannot be trusted, and will not be included in the discussion.

With L33 the dead volume is slightly larger because a valve was left open, leaving an oil filled line in contact with the CO_2, which got produced through diffusion after a certain time.

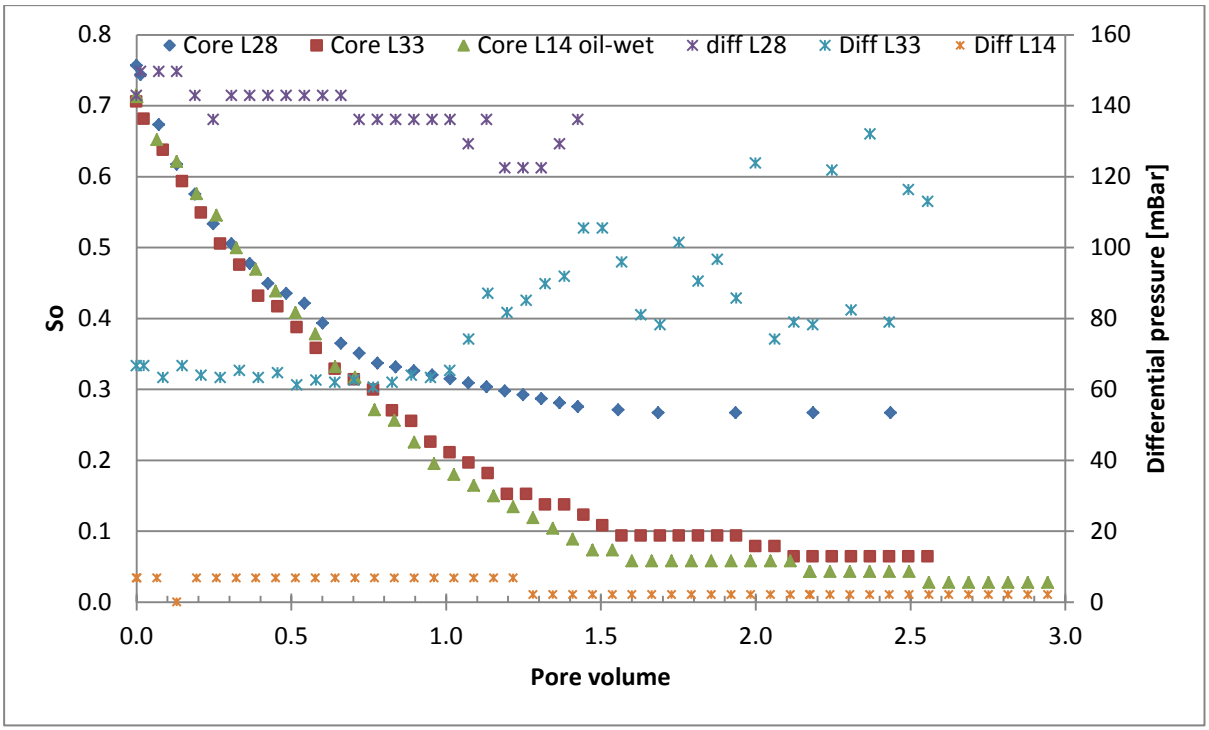

Figure 4-22 - Average oil saturation and differential pressure as a function of time during CO_2-foam injection in two water-wet and one moderately wet, un-fractured limestone core plugs at irreducible water saturation.

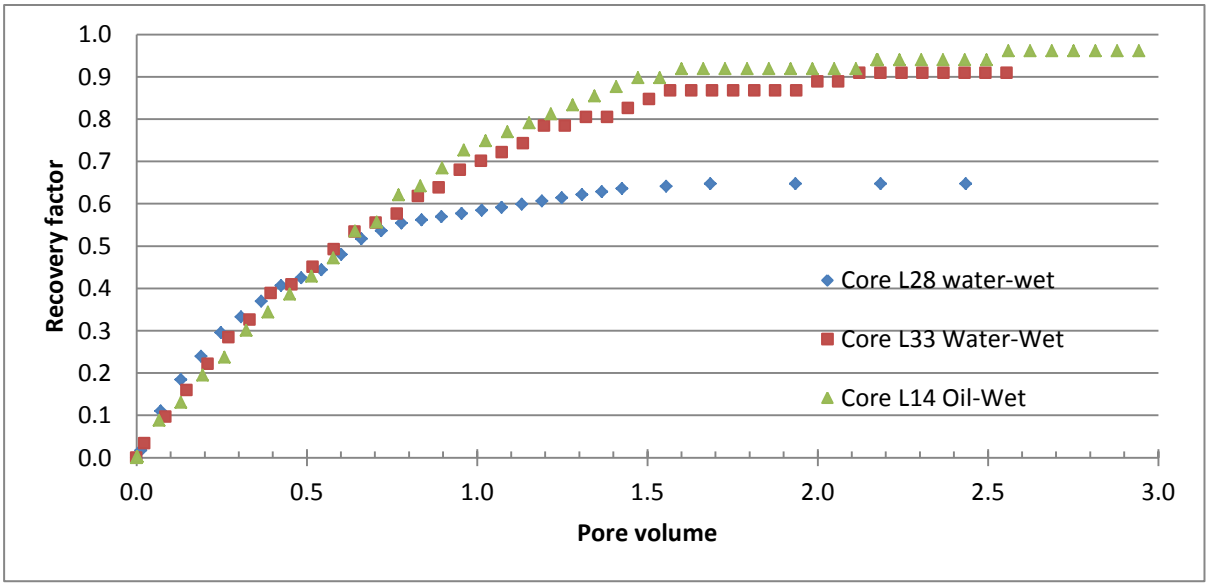

Figure 4-23 - Recovery factor as a function of time during CO2-foam injection in one oil-wet and two water-wet, whole limestone core plug at irreducible water saturation.

4.6 Reference experiments

In this chapter experimental results previously performed at the Department of Physics and Technology, University of Bergen in 2011- 2013. The experimental setup is shown in Figure 3-10, and performed at approximately 90 Bar and 20 °C on Edwards Limestone core plugs. At these conditions CO_2 and n-Decane is first contact miscible. In the discussion these results are compared to the experimental results presented in chapter 4.5. Experiments by Svenningsen (Svenningsen, 2011), were performed on 1.5 inch cores with an injection rate of 2 ml/h. Experiments by Christophersen and Skibenes were performed on 2 inch cores with an injection rate of 3 ml/h.

Table 4-17 – Overview of basic core properties arranged in numerical order, where Kmatrix is the matrix permeability. Experiments marked EDW# performed by Anders Christophersen (2012) and Ane Skibenes (2012). Experiments marked E# performed by Sondre Svenningsen (2011).

Core	Length [cm]	Diameter [cm]	Pore volume [ml]	Porosity	Kmatrix [mD]
EDW6	7.19	4.92	31.50	0.23	27.50
EDW15	7.61	4.96	33.37	0.23	19.30
EDW16	7.77	4.96	35.10	0.23	26.40
EDW32	7.19	4.92	30.57	0.22	21.00
EDW33	7.17	4.91	32.30	0.24	28.50
EDW34	7.15	4.91	32.77	0.24	31.60
EDW39	6.85	3.81	18.04	0.23	11.60
E5	5.91	3.81	17.21	0.26	15.16
E6	6.36	3.81	16.49	0.23	9.29
E8	7.18	3.81	17.55	0.21	9.47

Table 4-18 – Overview of experiments performed on cores arranged in the order of wettability, irreducible water saturation, injection fluid and core state. Experiments marked EDW# performed by Anders Christophersen (2012) and Ane Skibenes (2012). Experiments marked E# performed by Sondre Svenningsen (2011).

Core	Description	CO2/Foam	State	Swi	Kmatrix [mD]	Kfracture [mD]	Sor, w	Sor, co2	RF
EDW6	OW, Swi	Foam	Fractured	0.19	27.5	1980	-	0.07	0.91
EDW32	OW, Swi	Foam	Fractured	0.17	21.0	265	-	0.07	0.92
EDW39	OW, Swi	Foam	Fractured	0.11	11.6	1021	-	0.16	0.82
EDW15	SWW, Swi, Tertiary	Foam	Fractured	0.26	19.3	1365	0.58	0.31	0.58
EDW34	SWW, Swi, Tertiary	Foam	Fractured	0.23	31.6	285	0.44	0.19	0.76
EDW16	SWW, Swi	Foam	Fractured	0.32	26.4	117	-	0.24	0.64
EDW33	SWW, Swi	Foam	Fractured	0.19	28.5	261	-	0.17	0.78
E5	SWW, Swi, Tertiary	CO2	Whole	0.27	15.2	-	0.52	0.41	0.56
E6	SWW, Swi, Tertiary	CO2	Whole	0.30	9.3	-	0.55	0.45	0.65
E8	SWW, Swi, Tertiary	CO2	Whole	0.34	9.5	-	0.57	0.47	0.71

4.6.1 Liquid CO_2-foam injection fractured core plugs

Table 4-19 - Overview of experiments performed on cores arranged in the order of wettability, irreducible water saturation, injection fluid and core state. Experiments performed by Anders Christophersen (2012) and Ane Skibenes (2012).

Core	Description	CO2/Foam	State	Swi	Kmatrix [mD]	Kfracture [mD]	Sor, w	Sor, co2	RF
EDW16	SWW, Swi	Foam	Fractured	0.32	26.4	117	-	0.24	0.64
EDW33	SWW, Swi	Foam	Fractured	0.19	28.5	261	-	0.17	0.78
EDW6	OW, Swi	Foam	Fractured	0.19	27.5	1980	-	0.07	0.91
EDW32	OW, Swi	Foam	Fractured	0.17	21.0	265	-	0.07	0.92
EDW39	OW, Swi	Foam	Fractured	0.11	11.6	1021	-	0.16	0.82

All the experiments were performed above the minimum miscibility pressure (Core EDW16: 95 bar, Core EDW33: 96 bar, Core EDW6: 96 bar, Core EDW32: 96 bar, Core EDW39: 96 bar). So in all the experiments CO_2 was first-contact miscible with n-Decane.

Table 4-20 – Recovery factor for given pore volumes during CO2-foam injection in water-wet and moderately oil-wet, fractured limestone core plugs at irreducible water saturation.

Core	RF @ 1 PV	RF @ 2 PV	RF,total	PV @ RF,total
EDW16 - SWW	0.53	0.63	0.64	4.9
EDW33 - SWW	0.49	0.66	0.78	4.5
EDW6 - OW	0.45	0.68	0.91	4.2
EDW32 - OW	0.55	0.81	0.92	3.45
EDW39 - Ow	0.39	0.62	0.82	6

4.6.2 Tertiary, liquid CO_2 injection core plugs.

Table 4-21 - Overview of experiments performed on cores arranged in the order of, irreducible water saturation, injection fluid and core state. Experiments performed by Sondre Svenningsen (2011).

Core	Description	CO2/Foam	State	Swi	Kmatrix [mD]	Kfracture [mD]	Sor, w	Sor, co2	RF
E5	SWW, Swi, Tertiary	CO2	Whole	0.27	15.2	-	0.52	0.41	0.56
E6	SWW, Swi, Tertiary	CO2	Whole	0.30	9.3	-	0.55	0.45	0.65
E8	SWW, Swi, Tertiary	CO2	Whole	0.34	9.5	-	0.57	0.47	0.71

All the experiments were performed above the minimum miscibility pressure at around 82 bar. All the experiments CO_2 were first-contact miscible with n-Decane.

Table 4-22 – Recovery factor for waterflood and tertiary CO2-injection. Experiments performed by Sondre Svenningsen (2011)

Core	RF @ 1 PV	RF @ 2 PV	RF,total	PV @ RF,total
E5	0.28	0.44	0.44	0.9
E6	0.22	0.35	0.35	0.7
E8	0.13	0.29	0.29	0.4

4.6.3 **Diffusion in a fractured chalk core**

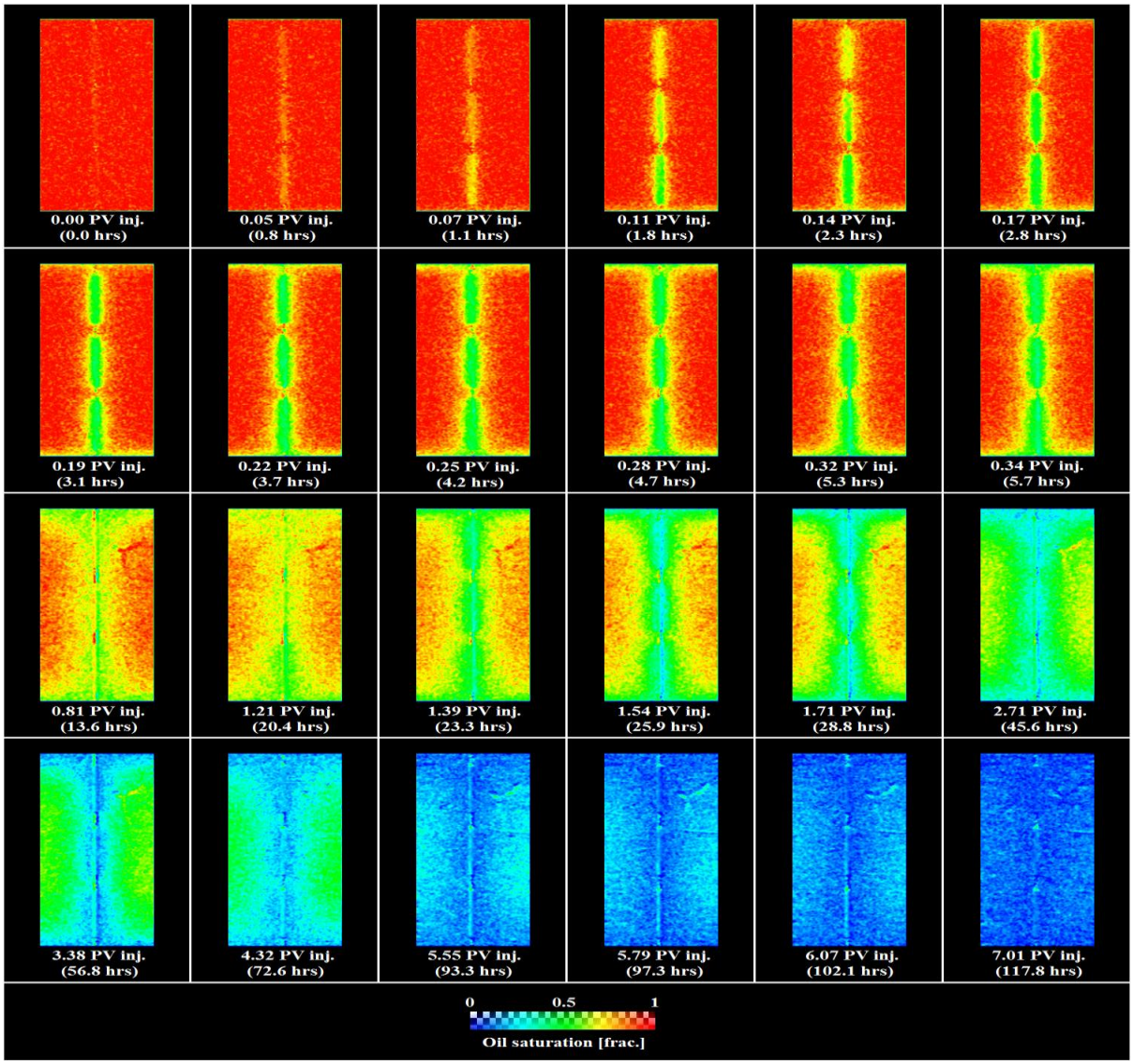

Figure 4-24- CT images showing development of oil saturation during CO2 injection into chalk core. Injection from bottom to the top. The core was digitally sliced perpendicular to the fracture plane with each image representing one time step at the same location. Warm colors represent high oil saturation while cold colors represent low oil saturation. (Baird, 2013)

Figure 4-24 is from a medical CT and was included to illustrate the diffusion mechanism in a fractured core. Chalk and limestone are both carbonates and low permeable rock types, and the recovery process is likely similar, although chalk is more homogenous. The fracture is an open fracture with a spacer (the same kind of spacer used in the experiments in this thesis). As shown in Figure 4-24 the CO_2 displaces all the oil in the fracture instantly (viscous displacement). After the CO_2 breaks through, diffusion is the dominating recovery mechanism. The CO_2 diffuses from the fracture and from end pieces into the matrix of the chalk. Diffusion from the end pieces occurs because, diffusion is controlled by the concentration gradient, and there is a significant concentration of CO_2 located at the end pieces. Similar experiments were done by Haugen (2012) with an MRI, but with a closed fracture. From those MRI images the end pieces had such a dominant concentration gradient that the majority of the diffusion drive came from the end pieces, because the closed fracture has a low volume of CO_2 compared to the end pieces. Ideally there should be no diffusion contribution from the end pieces to get a good picture of how CO_2 diffuses from a fracture and into the matrix.

5. Discussion

In this discussion chapter 5.1 will discuss pure CO_2 injection in general, the effect of water on whole cores during CO_2 injection, secondary CO_2 injection compared to tertiary CO_2 injection, and the effect of wettability. 5.2 will discuss the impact of fractures on pure CO_2 injection. Chapter 5.3 will discuss how to increase the CO_2 utilization, when pure CO_2 is injected into a fractured core. 5.4 will discuss CO_2 foam as mobility control to mitigate the negative effects of fractures. The start of chapter 5.4 deals with how foam generation can be confirmed in the experiments, because foam generation should be established before discussing the effects of foam. The effect of wettability on foam will be discussed in this chapter. Chapter 5.5 discusses the simulations that were run, and if the simulations can be used in future work.

5.1 CO_2 EOR

In this thesis CO_2 has showed excellent recovery in the range of 90%, see Table 5-1. Water injection performed by Svenningsen (2011) showed recovery in the range of 20%. The low water recovery occurs because of the low injection rate of 2 ml/h, which gives a low capillary number (detailed in chapter 1.7). This comparison shows the potential of CO_2 injection for enhanced oil recovery.

Table 5-1 shows final recovery for pure CO_2 injection and water injection. Only cores that reached ultimate recovery were included. Water injection was performed on 1.5 inch cores at a rate of 2 ml/h. Pure CO_2 injection was performed on 2 inch cores at a rate of 4 ml/h.

Table 5-1 – showing final recovery for pure CO_2 injection and water injection. Core E# were performed by Svenningsen (2011)

CO2	Final recovery
L6 - Swi Whole	0.87
L9 - Swi Whole	0.91
L10 - Swi whole	0.92
L17 – 100% oil	1.00
L19 – 100% oil	0.95
L20 – 100% oil	1.00
L21 - Swi fracture	0.93
L22 - Swi fracture	0.92
L25 - Swi,fracture H&P	0.93
Average CO2	0.94
Water injection	Final recovery
E5	0.28
E6	0.22
E8	0.13
Average water injection	0.21

5.1.1 Water impact during pure CO_2 injection

This section shows the effect of water present during CO_2 injection on whole cores and it compares three cores at S_{wi} (L6, L9 and L10) and one fully oil saturated core (L17). Water shielding primarily affects the ultimate recovery and the recovery rate approaching the end of production (predominantly affecting the diffusion). Key numbers are tabulated in Table 5-2.

Figure 5-1 and Figure 5-2 shows average oil saturation and recovery factor as a function of pore volumes of CO_2 injected. Only the end point is included for core L19 and L20 due to problems with confining pressure, as discussed in chapter 4.5.1.

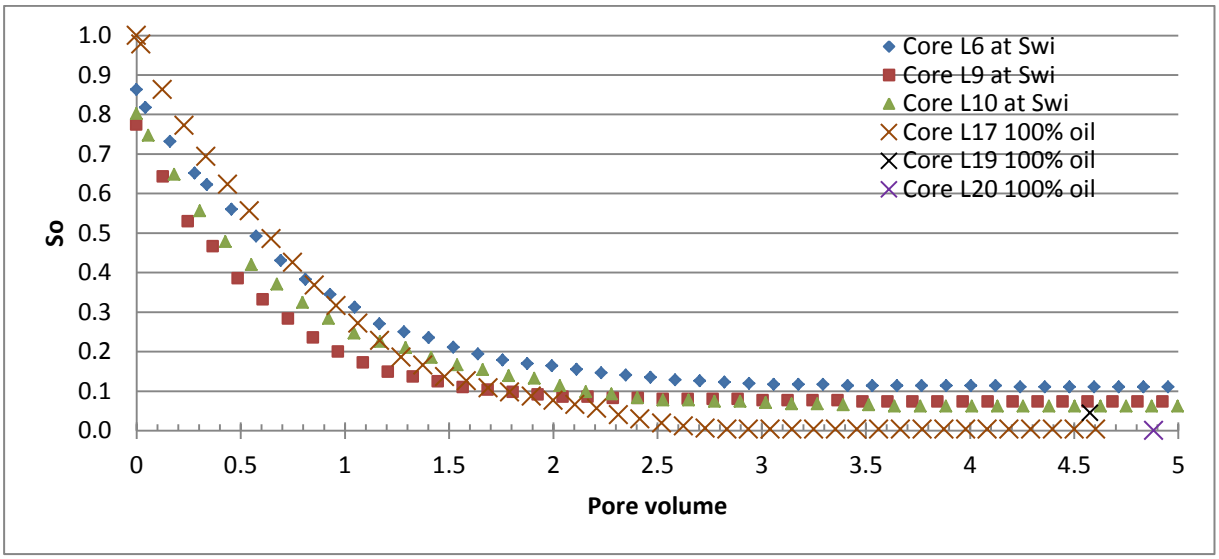

Figure 5-1 - Average oil saturation as a function of time during CO2 injection in water-wet, un-fractured limestone core plugs either fully saturated with oil or at irreducible water saturation.

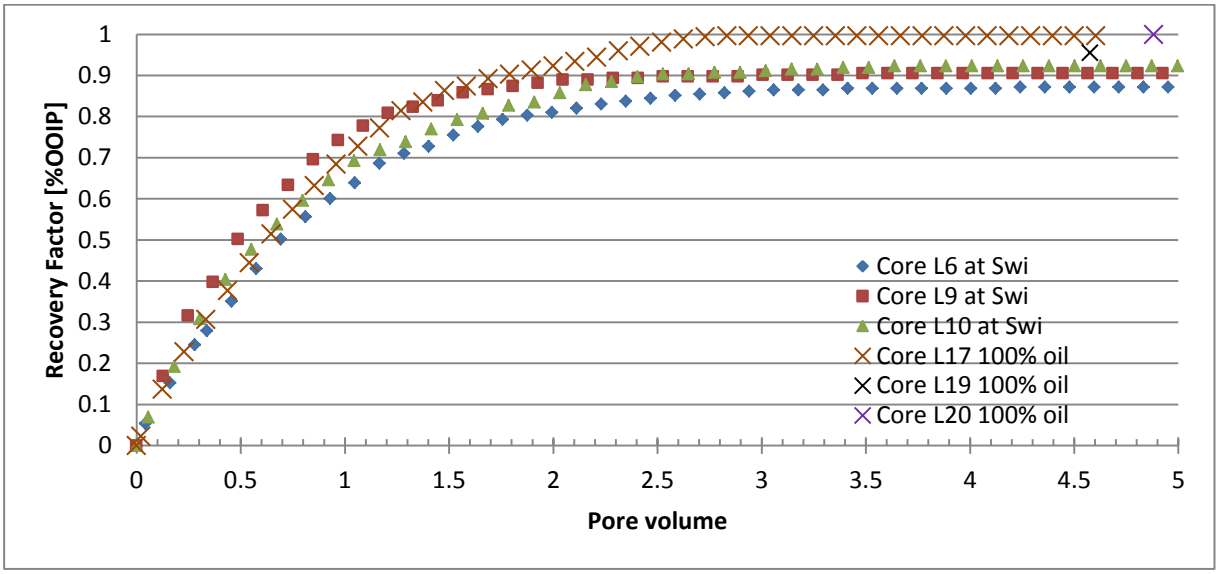

Figure 5-2 – Recovery factor as a function of time during CO2 injection in water-wet, un-fractured limestone core plugs either fully saturated with oil or at irreducible water saturation.

Table 5-2 - Comparing effect of water on oil recovery for CO2 injection on whole cores. Only the end points taken in account core cores L19 and L20.

	RF @ 1 PV	RF @ 2 PV	RF,total	PV @ RF,total
L6 - Swi	0.64	0.81	0.87	4.3
L9 - Swi	0.74	0.89	0.91	3.5
L10 - Swi	0.69	0.86	0.92	3.6
Swi average	0.69	0.85	0.90	3.80
L17 – 100% oil	0.68	0.92	1.00	2.8
L19 – 100% oil			0.95	
L20 – 100% oil			1.00	
100% oil average	0.68	0.92	0.98	2.80

As shown in Table 5-2, Figure 5-1 and Figure 5-2 the oil recovery with irreducible water present were similar compared to the fully oil saturated cores during the first pore volume (S_o=1 : 69% OOIP at 1 pv ; S_{wi}: 68% OOIP at 1 pv). At 2 pore volumes the fully saturated core L17 has a higher average oil recovery (92% OOIP) than the cores at irreducible water saturation (85% OOIP). Two of the fully oil saturated cores get 100% ultimate recovery, while L19 reaches 95%, but did not finish producing, see chapter 4.5.1. In the three cores at S_{wi} ultimate recovery was around 90 %. The difference in oil recovery of 10% OOIP is likely caused by water shielding. Water blocks the CO_2 from the oil. Given a large enough time, the CO_2 might be able to recover all the oil by diffusing through the water barrier, and swelling the oil, detailed in chapter 2.1.2 (Zekri et al., 2007, Shyeh-Yung, 1991, Grogan, 1987). From Table 5-2, Figure 5-1 and Figure 5-2, water shielding seems to primarily affect the ultimate recovery and the recovery rate at the end of the recovery when all the viscously recoverable oil has been produced. After this the oil is recovered by diffusion.

5.1.2 Secondary compared CO_2 injection to tertiary CO_2 injection

This section discusses secondary CO_2 injection compared to tertiary CO_2 injection on whole cores. It compares secondary injection on three cores (L6, L9 and L10) and tertiary injection on three cores (E5, E6 and E8). The total oil recovery is higher for secondary CO_2 injection compared to tertiary CO_2 injection. Tertiary CO_2 injection has potential to increase oil recovery after waterflooding. Key numbers are tabulated in Table 5-3.

Figure 5-3 and Figure 5-4 shows average oil saturation and recovery factor as function of pore volumes liquid injected. It is important to note that the tertiary recovery experiments were performed on 1.5 inch cores.

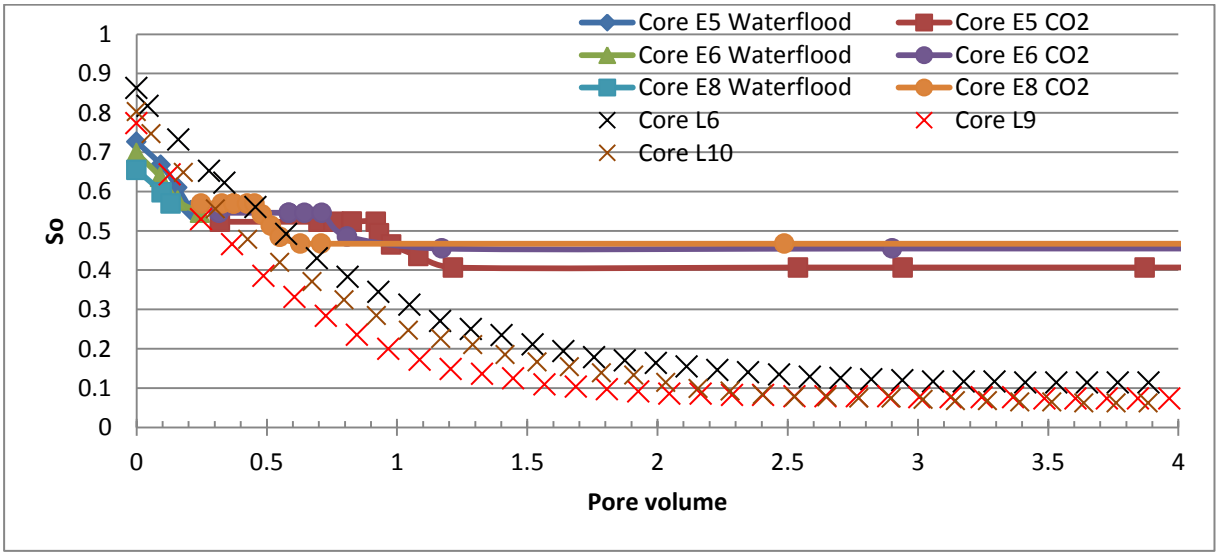

Figure 5-3 - Average oil saturation as a function of time during CO2 injection compared to tertiary CO_2-injection in water-wet, whole limestone core plugs at irreducible water saturation. Cores marked E# have been performed by Sveningsen (2011)

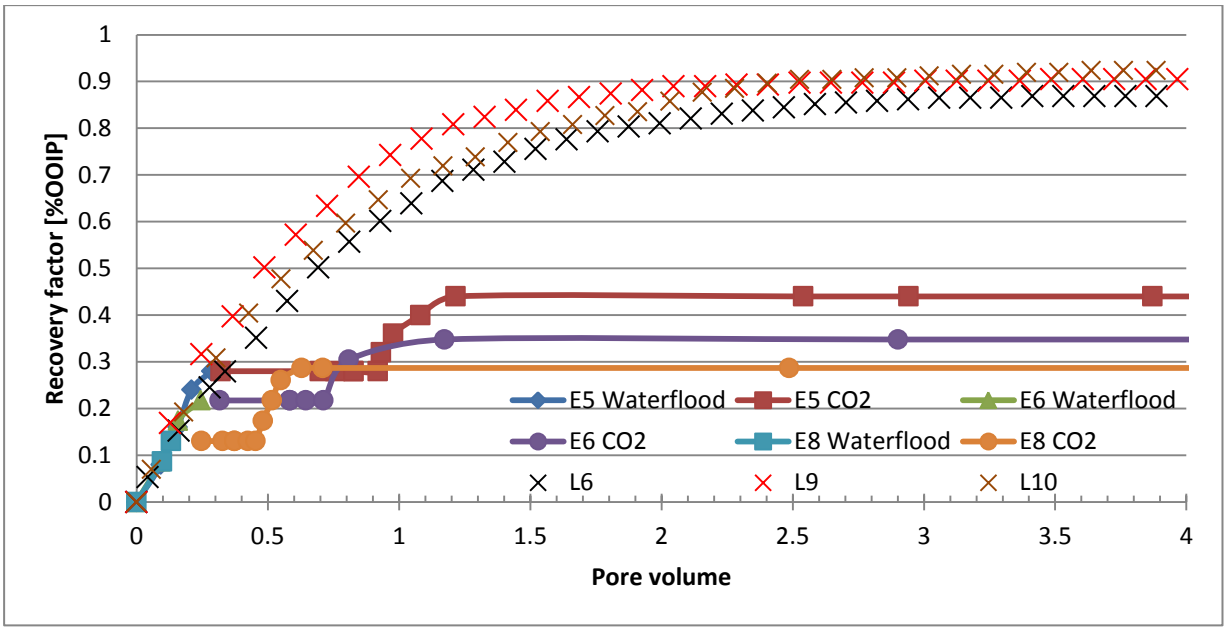

Figure 5-4 – Recovery factor as a function of time during CO_2 injection(2 inch cores) compared to tertiary CO_2-injection(1.5 inch cores) in water-wet, whole limestone core plugs at irreducible water saturation. Cores marked E# have been performed by Sveningsen (2011)

Table 5-3 – Comparing secondary to tertiary CO_2 recovery. The pore volumes signify amount of CO_2 injected

Core	Rf after waterflood	RF @ 1 PV	RF @ 2 PV	RF,total	PV @ RF,total	Tertiary CO_2 injection ΔRF
L6		0.64	0.81	0.87	4.3	
L9		0.74	0.89	0.91	3.5	
L10		0.69	0.86	0.92	3.6	
E5	0.28	0.44	0.44	0.44	0.9	0.16
E6	0.22	0.35	0.35	0.35	0.7	0.13
E8	0.13	0.29	0.29	0.29	0.4	0.16

The total oil recovery for secondary CO_2 injection is higher compared to tertiary CO_2 injection as shown from Table 5-3, Figure 5-3 and Figure 5-4, which was expected (Shyeh-Yung, 1991). After water injection in a water-wet core, oil appear as discontinuous oil blobs surrounded by water, caused by the snap-off effect(Roof, 1970). This leaves a large amount of oil behind walls of water, which makes it harder for the CO_2 to contact, and thus mobilize the oil. CO_2, if given enough time, can diffuse through the water because CO_2 is soluble in water. CO_2 solubility in water is highly dependent on the salinity of the water (higher salinity, less soluble). In the beginning of the tertiary CO_2 injection, an oil bank starts to form (because of the CO_2 being able to mobilize some of the oil). Because of the snap-off effect all the oil ahead of the oil bank is immobile, which is why water is produced first (Grogan, 1987, Skjæveland and Kleppe, 1992, Shyeh-Yung, 1991, Zekri et al., 2007, Trivedi and Babadagli, 2006). This can be seen from Figure 5-3 and Figure 5-4, the oil recovery does not start immediately.

Although secondary CO_2 injection is more effective than tertiary CO_2 injection in lab scale, there are several reasons why in field scale, tertiary CO_2 injection might be the favored recovery method. CO_2 is more expensive than water, water is less mobile (better macroscopic sweep efficiency for horizontal flooding), and CO_2 has higher investments and risks. This is discussed in more detail in chapter 2.1.1.

This of course depends on the field. In a steeply dipping reservoir with good vertical permeability, gravity stable CO_2 injection would be an effective recovery mechanism and a situation where CO_2 injection would have good macroscopic sweep efficiency. So even though secondary CO_2 injection might give a higher recovery, it may not necessarily give a higher profit. For this reason tertiary CO_2 injection can be a good way to increase the field's lifetime, and increase the ultimate recovery of the oil field (Dong et al., 1999, Gozalpour et al., 2005, Enick et al., 2012, Skjæveland and Kleppe, 1992).

From Figure 5-4 and Table 5-3 it can be observed that less than one pore volume of CO_2 is needed to reach the ultimate recovery during tertiary CO_2 injection. Given a large amount of time, the CO_2 would likely mobilize more oil by diffusing through the water phase and swelling the oil (Campbell and Jr., 1985, Grogan, 1987). The water injection has been performed with the same injection rate as the CO_2 in the tertiary experiments (2 ml/h), which gives a very low differential pressure, and a low capillary number (capillary number detailed in chapter 1.7), leading to low oil recovery from the waterflood. Water injection would be more effective with a higher differential pressure.

From Table 5-3, it can be shown that CO_2 injection increases the oil recovery by approximately 16% OOIP for core E5 and E8, and 13% OOIP for core E8 after 0.9, 0.4 and 0.7 pore volumes respectively. On average 0.7 pore volumes were injected to reach ultimate recovery for tertiary injection. This CO_2 amount is low compared to secondary CO_2 injection which needed an average of 3.8 pore volumes of CO_2 to reach ultimate recovery. This indicates that if the waterflood had been more effective, then tertiary CO_2 injection might be an effective recovery mechanism, increasing recovery with a small amount of CO_2 needed for tertiary CO_2 injection compared to secondary CO_2 injection. The oil recovery does show that CO_2 injection has potential to enhance oil recovery after a waterflood.

For example, had the water flood reached 50% recovery, and the CO_2 flooding had the same effect as with core E8, and increased recovery by 16 % after 0.4 pore volumes injected, then final recovery would be 66% with only 0.4 pore volumes of CO_2 injected. This could be an effective utilization of CO_2. However a higher water recovery would lead to more dominating water shielding effects, and CO_2 injection after waterflooding would most likely be less effective. More experiments should be done on tertiary CO_2 injection with more effective waterflooding, to see how dominating the water shielding effect would become, and if CO_2 could effectively increase recovery with few pore volumes of CO_2 injected. Tertiary CO_2 injection experiments should also be performed on fractured cores.

5.1.3 Effect of wettability on CO2 injection

This section discusses the effect of wettability during CO_2 injection on whole cores, and compares three water-wet cores (L6, L9 and L10) and two moderately oil-wet core (L4 and L7). Total oil recovery is on average higher for the oil-wet cores compared to the water-wet cores. Key numbers are tabulated in Table 5-4.

Figure 5-5 and Figure 5-6 show average oil saturation and recovery factor as a function of pore volumes injected during pure CO_2 injection in water-wet and oil-wet cores.

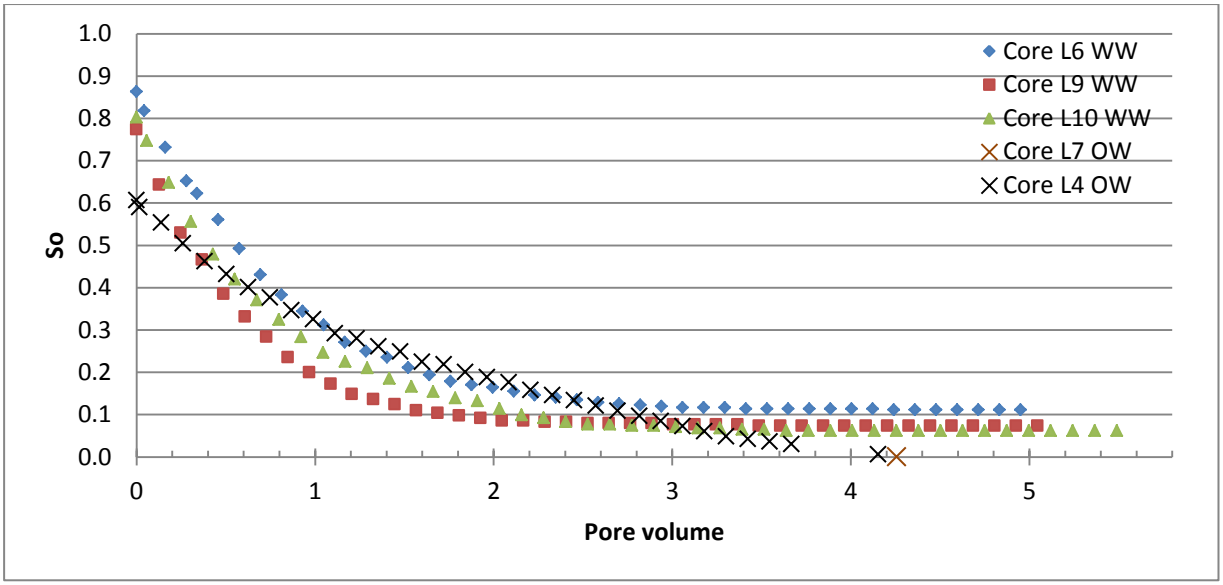

Figure 5-5 – Average oil saturation as a function of time during CO2 injection in either water-wet or oil-wet, whole limestone core plugs at irreducible water saturation.

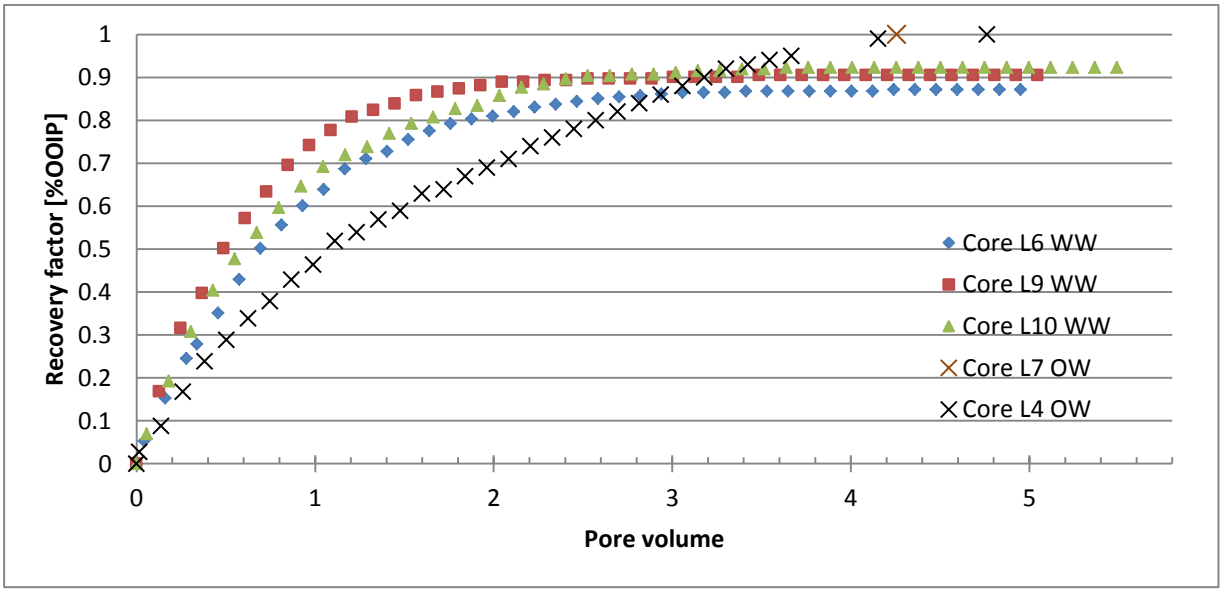

Figure 5-6 – Recovery factor as a function of time during CO2 injection in either water-wet or oil-wet, whole limestone core plugs at irreducible water saturation.

Table 5-4 - Comparing effect of wettability on oil recovery for CO2 injection on whole cores.

	RF @ 1 PV	RF @ 2 PV	RF,total	PV @ RF,total
L6 – Water-wet	0.64	0.81	0.87	4.3
L9 - Water-wet	0.74	0.89	0.91	3.5
L10 - Water-wet	0.69	0.86	0.92	3.2
L4 – Oil-wet	0.46	0.69	1.00	4.8
L7 – Oil-wet	-	-	1.00	-

As shown in Table 5-4 the oil-wet cores L4 and L7 recover 100% of the oil. There is however a large uncertainty regarding the irreducible water saturation (and OOIP), as discussed in chapter 4.5.3. As shown in Table 5-4, Figure 5-5 and Figure 5-6 the recovery rate for the oil-wet core L4 is slower than for the water-wet cores for the first 3 pore volumes. There is approximately twice as high water saturation for core L4 compared to the water-wet cores, and this might delay the CO_2 in contacting the oil. In a fractionally-wet system some pores might have preference for both phases, see chapter 1.4.2, even though the water does not completely block the oil from the CO_2, the water might hinder the CO_2 so that the CO_2 has to mobilize some of the oil through diffusion. Oil is not completely blocked from the water because 100% ultimate recovery is reached for both oil-wet cores L4 and L7. (Skjæveland and Kleppe, 1992, Bijeljic and Blunt, 2006).

Because of all the uncertainties regarding the water saturation, and regarding at what point the water was lost (which could alter the Amott-Harvey index if water was lost in the imbibition cell), more experiments should be done on the effect of wettability on CO_2 injection.

A high final recovery is expected because trapping occurs for the non-wetting phase, and thus in an oil-wet porous media virtually none of the oil gets trapped (Walsh et al., 1989). For mixed and oil-wet cores the amount of oil retained is insignificant after large amount of pore volumes of CO_2 are injected(Lin and Huang, 1990). Even if water affects oil recovery initially in the oil-wet cores, all the oil gets recovered in the end for pure CO_2-injection.

5.2 The impact of fractures on CO_2 EOR

Fractures dramatically decrease oil recovery rate, and limits viscous displacement in the matrix. In chapter 5.2.1 oil recovery is compared between fully oil saturated whole cores and fractured cores. Chapter 5.2.2 the same comparison is made for cores at irreducible water saturation. Then chapter 5.2.3 discusses the impact of water on fractured cores.

5.2.1 Fully oil saturated cores

This section discusses the presence of fractures during CO_2 injection in fully oil saturated cores, and compares whole core (L17) and two fractured cores (L21 and L22). Fractures significantly decrease the oil recovery rate and limit the viscous displacement in the matrix. Key numbers are tabulated in Table 5-5. Figure 5-7 and Figure 5-8

Figure 5-7 and Figure 5-8 shows average oil saturation and recovery factor as function of pore volumes of CO_2 injected. The oil recovery rate is significantly reduced for the fractured cores. Figure 5-15 displays recovery factor as function the square root of pore volumes of CO_2 injected, and shows that the fractured cores have close to linear shape. This indicates that diffusion is the dominating recovery mechanism, explained by Fick's second law of diffusion, detailed in chapter 1.8. Figure 5-15 shows that the oil recovery for the whole Core L17 is influenced by viscous forces in addition to diffusion.

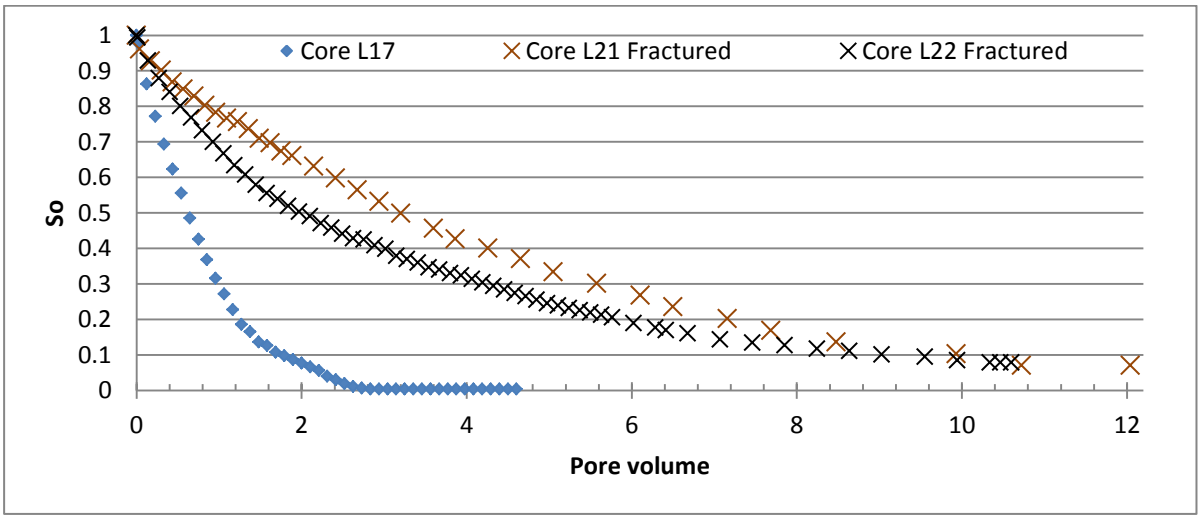

Figure 5-7 - Average oil saturation as a function of time during CO2 injection in water-wet, either whole or fractured limestone core plugs fully saturated with oil.

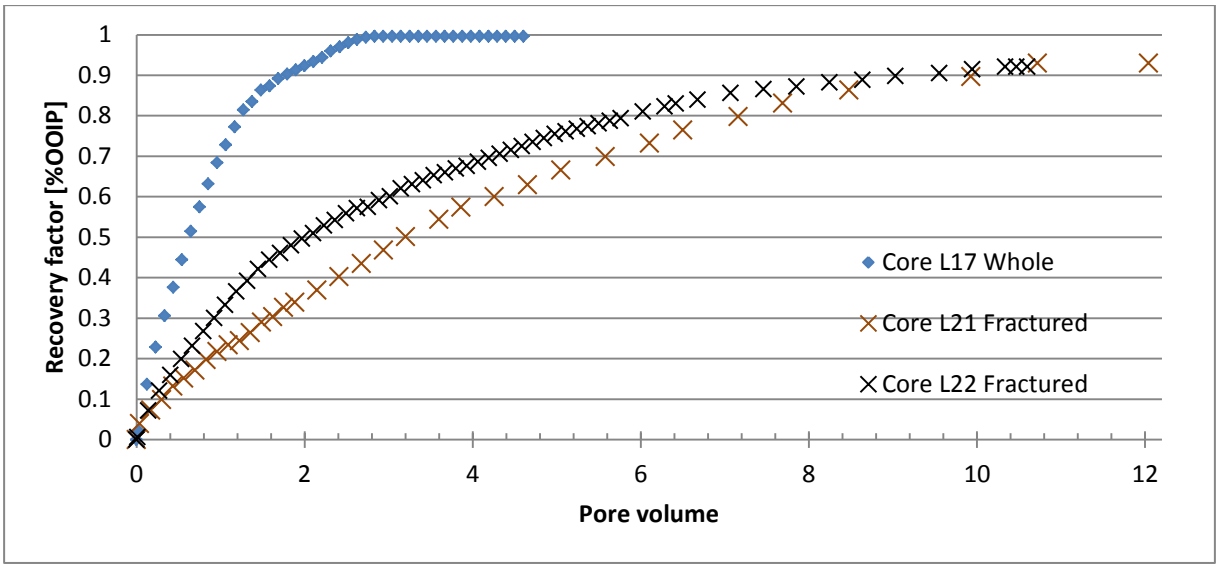

Figure 5-8 – Recovery factor as a function of time during CO2 injection in water-wet, either whole or fractured limestone core plugs fully saturated with oil.

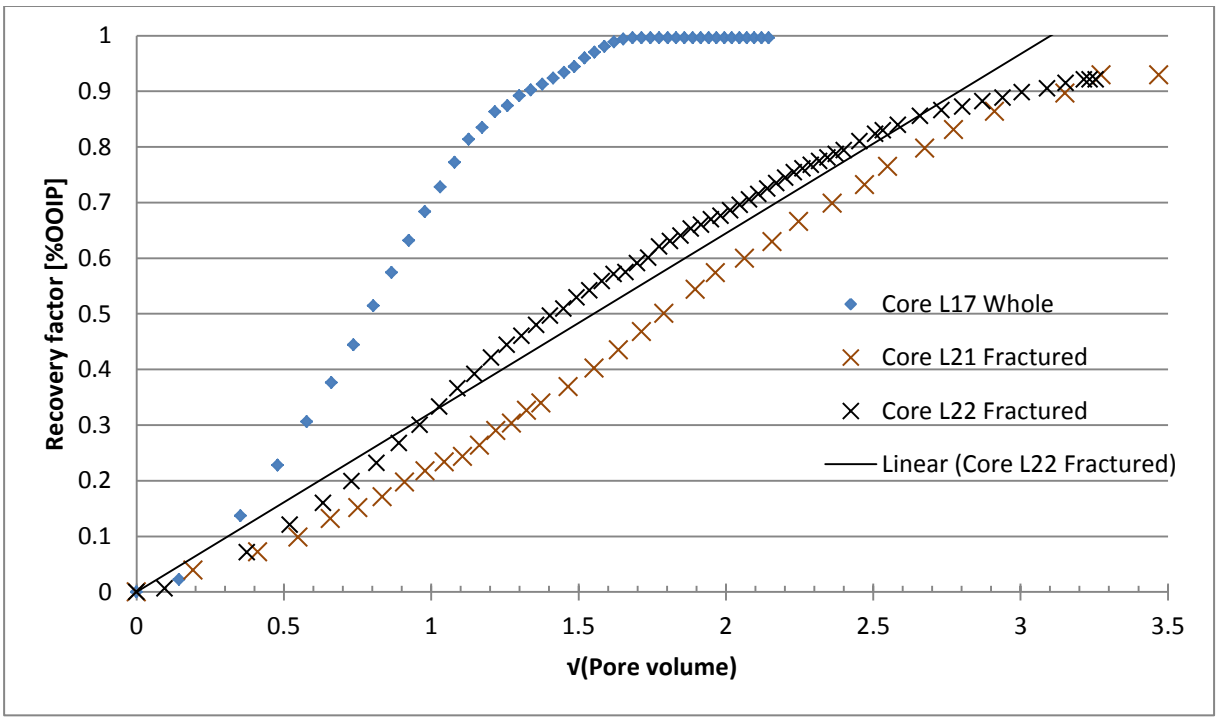

Figure 5-9 – Recovery factor as a function of the square root of time during CO2 injection in a water-wet, whole and two water-wet, fractured limestone core plugs fully saturated with n-Decane.

Table 5-5 - Comparing effect of fractures on oil recovery for CO2 injection. Core L17 is whole. Core L21 and L22 are fractured fully saturated with oil.

	RF @ 1 PV	RF @ 2 PV	RF,total	PV @ RF,total
L17 – Whole	0.68	0.92	1.00	2.8
L21 – Fractured	0.22	0.34	0.93	12
L22 - Fractured	0.33	0.50	0.92	10.6

As shown in Table 5-5, Figure 5-7 and Figure 5-8 the recovery rate for fractured cores was lower than for whole cores. At 1 pore volume the whole core has an oil recovery of 68% OOIP compared to 27.5 % OOIP for the fractured cores. At 2 pore volume the whole has an oil recovery of 92% OOIP compared to an average of 47 % OOIP for the fractured cores. The oil recovery for fractured cores takes 5 times longer than whole cores to reach approximately 90%.

The reduction in the recovery rate occur because a core with a fracture, virtually all the CO_2 will go through the fracture and to the outlet, producing all the oil in the fracture but not the oil in the matrix. The CO_2 will follow the path of least resistance, and the great permeability difference (in this case approximately 40 times larger for the fracture), will cause the CO_2 to flow through the fracture.

The only recovery mechanism in the matrix with a fracture presents is diffusion and CO_2 oil swelling, and negligible contribution from viscous forces, if the matrix is low permeable compared to the fracture. The slope of the fractured curves in Figure 5-9 shows that the curves are close to linear, indicating the oil recovery is mainly diffusion driven, as expected since the matrix permeability is low compared to the fracture permeability. Figure 5-7 shows that the production for the fractured cores has not flattened out and not reached final recovery. The diffusion will continue until equilibrium is reached between the fracture and the matrix. (Ghedan, 2009, Alavian and Whitson, 2010, Do and Pinczewski, 1991)

As discussed earlier in chapter 4.6.3, CO_2 injection into a fractured chalk core produced oil from the fracture instantly, and the oil in the matrix was produced through diffusion and oil swelling. In experiments in this thesis, the diffusion effect will be exaggerated compared to what happens in a reservoir, due to the volume of the fracture being over 10% of the total OOIP. In the fractured oil field Ekofisk, the total volume of fractures compared to the matrix is less than 1% (Skarrestad and Skauge, 2011). In addition to the fracture volume, the CO_2 concentration in both end pieces contributes to recovery because diffusion is driven by the concentration gradient (Darvish, 2007).

5.2.2 **Cores at irreducible water saturation**

This section discusses the presence of fractures during CO_2 injection in cores at irreducible water saturation, and compares three whole cores (L6, L9 and L10) and two fractured cores (L23 and L26 Fractures significantly decrease the oil recovery rate and limit the viscous displacement in the matrix. Water seems to enhance the heterogeneity effect that a fracture has on a core plug. Key numbers are tabulated in Table 5-6.

Figure 5-10 and Figure 5-11 show average oil saturation and recovery factor as function of pore volumes of CO_2 injected. The oil recovery rate is significantly reduced for the fractured cores. Figure 5-12 displays recovery factor as function the square root of pore volumes of CO_2 injected, and shows that the fractured cores have a close to linear shape. This indicates that diffusion is the dominating recovery mechanism, explained by Fick's second law of diffusion. Figure 5-15 shows that the oil recoveries for the whole cores are influenced by viscous forces in addition to diffusion.

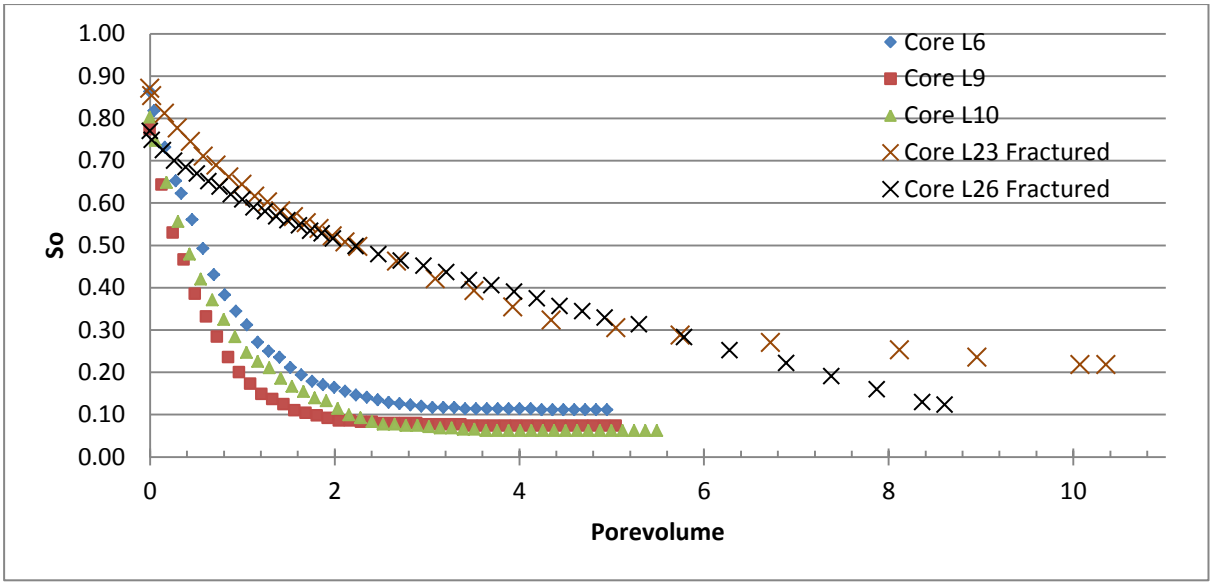

Figure 5-10 - Average oil saturation as a function of time during CO2 injection in water-wet, either whole or fractured limestone core plugs at irreducible water saturation.

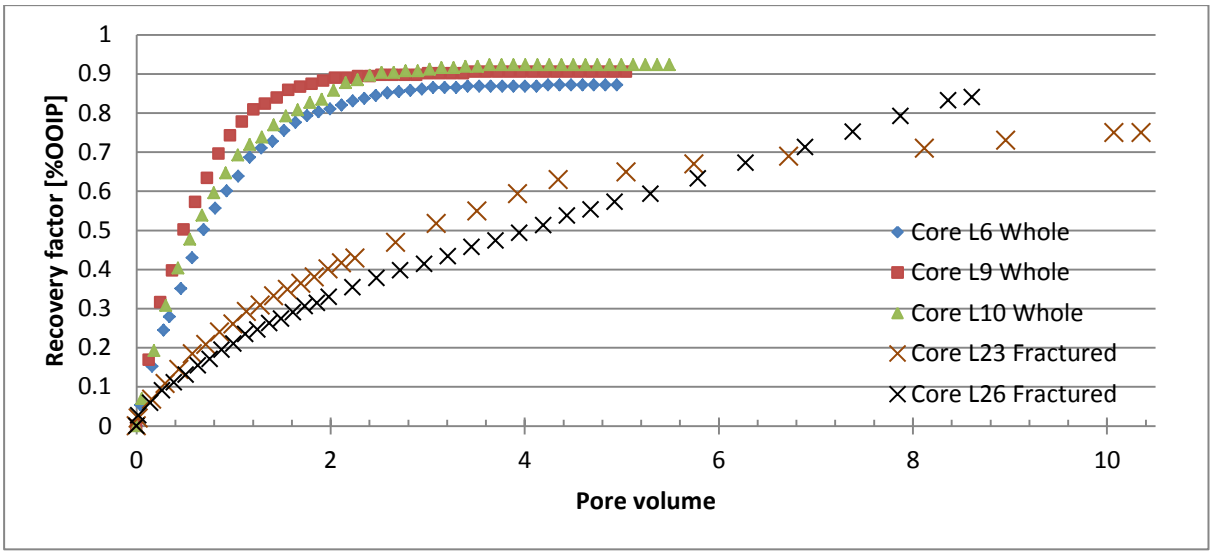

Figure 5-11 – Recovery factor as a function of time during CO2 injection in water-wet, either whole or fractured limestone core plugs at irreducible water saturation.

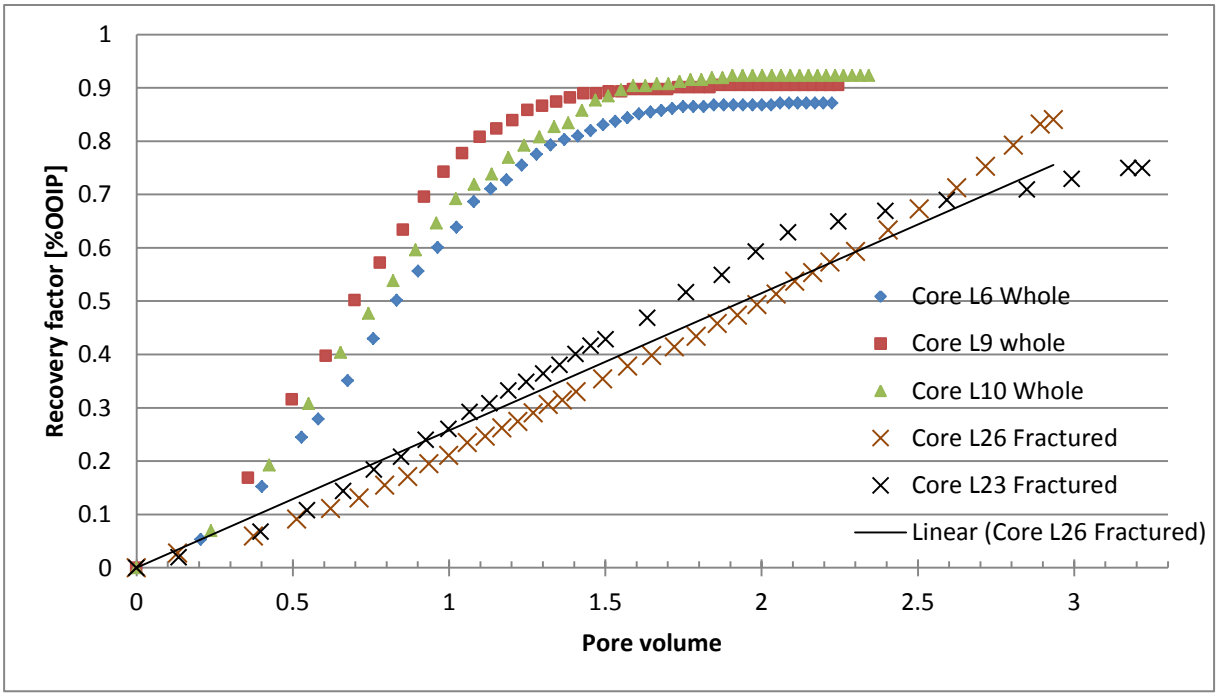

Figure 5-12 – Recovery factor as a function of the square root of time during CO2 injection three a water-wet, whole and two water-wet, fractured limestone core plugs at S_{wi}.

Table 5-6 - Comparing effect of fractures on oil recovery for CO2 injection. Core L6, L9 and L10 is whole. Core L23 and L26 are fractured at S_{wi}.

	RF @ 1 PV	RF @ 2 PV	RF,total	PV @ RF,total
L6	0.64	0.81	0.87	4.3
L9	0.74	0.89	0.91	3.5
L10	0.69	0.86	0.92	3.2
L23	0.26	0.40	0.75	10
L26	0.21	0.33	0.84	7.7

As shown in Table 5-6, Figure 5-10 and Figure 5-11 the recovery rate for fractured cores is dramatically reduced. The presence of water influenced final recovery and the rate of recovery during CO_2 injection, and enhanced the unfavorable effect from fractures. After 1 pore volume injected, the oil recovery in whole cores was 147% higher compared to fractured cores, without water present. With an irreducible water phase, the oil recovery in whole cores was 193% higher compared to fractured cores. The corresponding number was 119% and 132% after 2 pore volume injected. This can be explained by the fact that water shields the oil, and blocks or slows down the oil in the matrix, preventing the oil from diffusing into the fracture, reducing the relative permeability of oil (Zekri et al., 2007, Shyeh-Yung, 1991, Grogan, 1987).

Figure 5-10 shows that the curves for the two fractured cores had not flattened out, indicating that final recovery was not reached, therefore the effect of water shielding and fractures on ultimate recovery cannot be discussed.

It is important to note that diffusion does not penetrate large distances in a macroscopic/field scale since the depth of penetration is proportional to the square root of time. However if a field has fractures continuously located a couple of meters apart from each other, diffusion could have a significant effect on oil recovery. In a field's lifetime of around 20 years, CO_2 could diffuse several meters in this time (depending on parameters such as: permeability, temperature, pressure, concentration gradient, water shielding) (Skjæveland and Kleppe, 1992, Alavian and Whitson, 2010, Ghedan, 2009).

5.2.3 **Water impact on fractured cores**

This section discusses effect of water during CO_2 injection on fractured cores, and compares two cores at S_{wi} (L23 and L26) and two fully oil saturated cores (L21 and L22). In fractured cores where the oil production is mainly diffusion driven, water seems to predominately affect oil recovery after 0.5 pore volumes. Key numbers are tabulated in Table 5-7.

Figure 5-13 and Figure 5-14 shows average oil saturation and recovery factor as function of pore volumes of CO_2 injected. Figure 5-15 displays recovery factor as function the square root of pore volumes of CO_2 injected, and shows that the fractured cores have close to linear shape. This indicates that diffusion is the dominating recovery mechanism, explained by Fick's second law of diffusion.

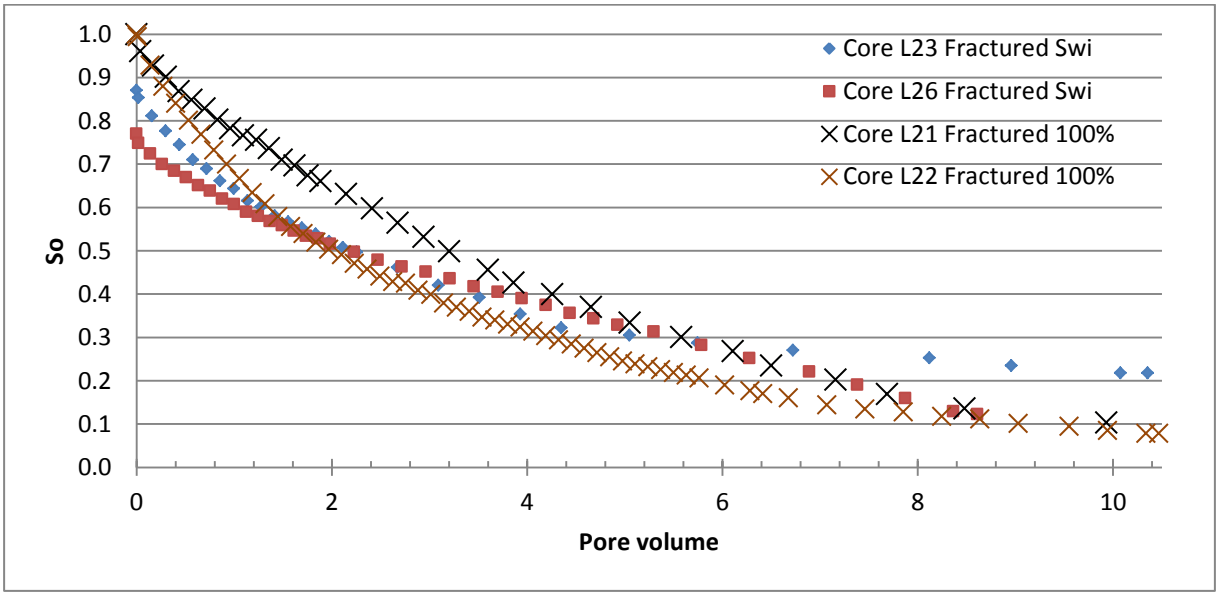

Figure 5-13 - Average oil saturation as a function of time during CO2 injection in water-wet, fractured limestone core plugs either fully saturated with oil or at irreducible water saturation.

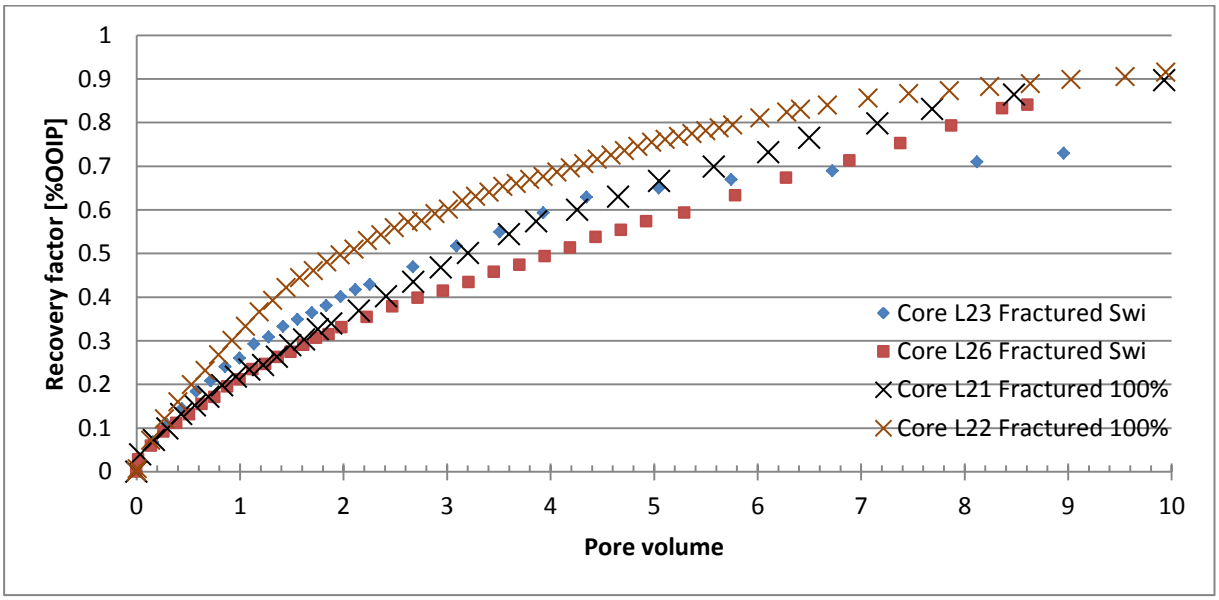

Figure 5-14 – Recovery factor as a function of time during CO2 injection in water-wet, fractured limestone core plugs either fully saturated with oil or at irreducible water saturation.

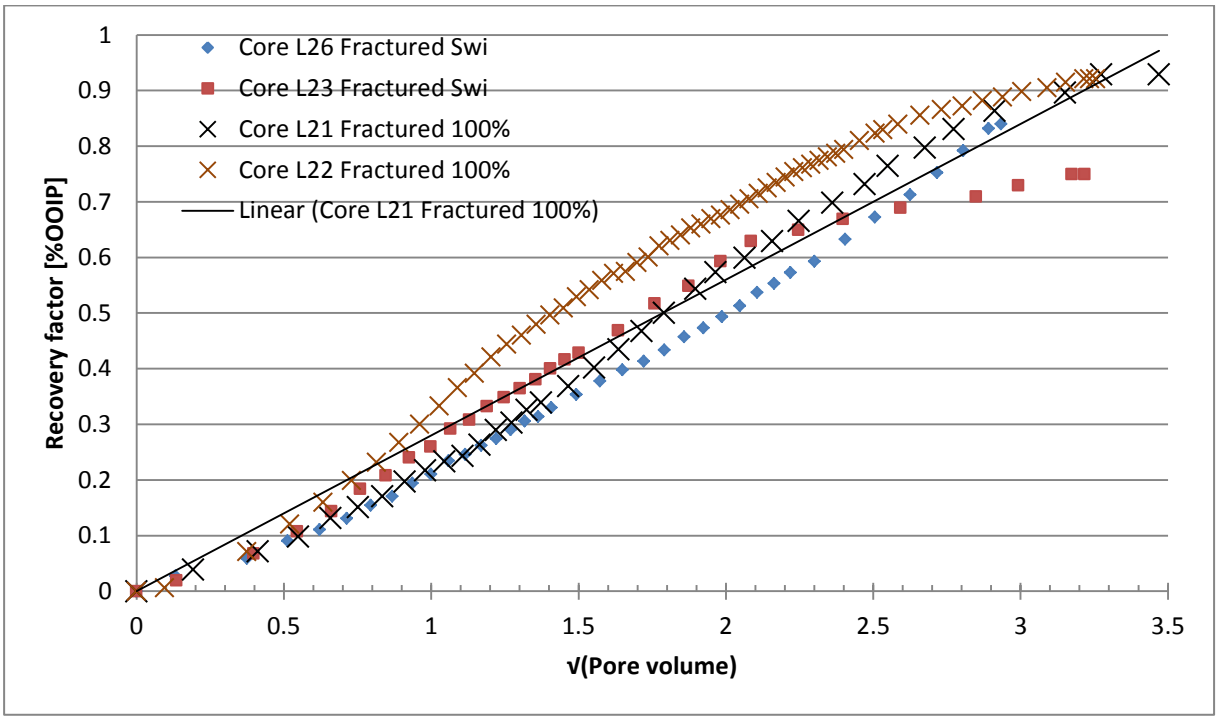

Figure 5-15 – Recovery factor as a function of the square root of time during CO2 injection fractured limestone core plugs at S_{wi} or fully oil saturated.

Table 5-7 - Comparing effect of water on oil recovery for CO2 injection on fractured cores.

	RF @ 1 PV	RF @ 2 PV	RF,total	PV @ RF,total
L23 - Swi	0.26	0.40	0.75	10
L26 - Swi	0.21	0.33	0.84	7.7
Swi - average	0.24	0.37	0.79	8.85
L21 – 100% oil	0.22	0.34	0.93	12
L22 – 100% oil	0.33	0.50	0.92	10.6
100% oil - average	0.28	0.42	0.93	11.30

As shown in Table 5-7, Figure 5-13 and Figure 5-14 the cores fully saturated with oil have a higher average oil recovery after approximately 0.5 pore volumes, and they have a higher total oil recovery then the cores with irreducible water saturation. The higher total oil recovery for fully oil saturated cores is expected because water shields the oil from the CO_2 in a water-wet porous medium (Zekri et al., 2007, Shyeh-Yung, 1991, Grogan, 1987). For the whole cores discussed in chapter 5.1.1, the water did not seem to affect the oil recovery rate before most of the oil was recovered, when the oil recovery process went from viscous driven to diffusion driven. For the fractured cores the fully saturated cores have a higher average oil recovery after approximately 0.5 pore volumes. This may be because water shielding seems to affect the diffusion rate, and since diffusion is the dominating recovery mechanism for fractured cores, water shielding affects oil recovery earlier than for whole cores. The fully oil saturated cores have a higher total recovery. However none of the curves seems to have flattened out and the cores would likely recover more oil. If the experiments had been run for longer and the curves had been allowed to flatten out the fully oil saturated cores would likely reach a higher ultimate recovery, as observed in chapter 5.1.1 for the fully oil saturated whole cores.

5.3 Increased CO_2 utilization in fractures

This chapter compares continuous CO_2 injection with Huff 'n' Puff on fractured cores. Continuous injection performed on two cores (L23 and L26) and Huff 'n' Puff on core L25. The Huff 'n' Puff experiment shows increased CO_2 utilization compared to continuous CO_2 injection.

Oil companies usually want to produce the oil as quickly as possible because of net present value, but the cost of what is injected might surpass what is earned in increased oil recovery (Zekri et al., 2000, Jahangiri and Zhang, 2011). Oil fields located onshore have a lower day rate than offshore installations, and can therefore be more economically viable to use Huff 'n' Puff techniques where the CO_2 is shut in, in order to diffuse, swell the oil, and reduce the oil viscosity (Zhang et al., 2006, Gozalpour et al., 2005). If the cost of injecting CO_2 is the dominating economic factor, then the Huff 'n' Puff technique might be used to increase the CO_2 utilization factor i.e. how much oil is produced per barrel of CO_2 (Schechter et al., 1998). Huff 'n' Puff is discussed in chapter 2.1. Huff 'n' Puff is a technique where injection and production is performed at the same well. For example injecting CO_2 into a well, letting the CO_2 diffuse and mobilize oil for a period of time, then producing the mobilized oil through the same well (Haskin and Alston, 1989). There is an increasing interest in Huff 'n' Puff because it is easy to apply, minor risk are involved, and small capital outlay is required (Zhang et al., 2006). Because increasing the CO_2 utilization factor is an important economic aspect, Huff 'n' Puff experiments have been performed in this thesis on a core with a fracture, where CO_2 has been injected cyclically for one hour at 4 ml/h, then shut-in for 2 hours as described in chapter 4.5.2. Huff 'n' Puff in this thesis is defined as CO_2 injected upstream, the CO_2 is then shut in to diffuse from the fracture to the matrix, this leads to oil filling the fracture and the oil is then produced downstream (thus not from the same well, as it is referred to in field context).

Key numbers are tabulated in Table 5-8. Figure 5-16 and Figure 5-17 show average oil saturation and recovery factor as a function of pore volumes injected. H&P is the Huff 'n' Puff experiment.

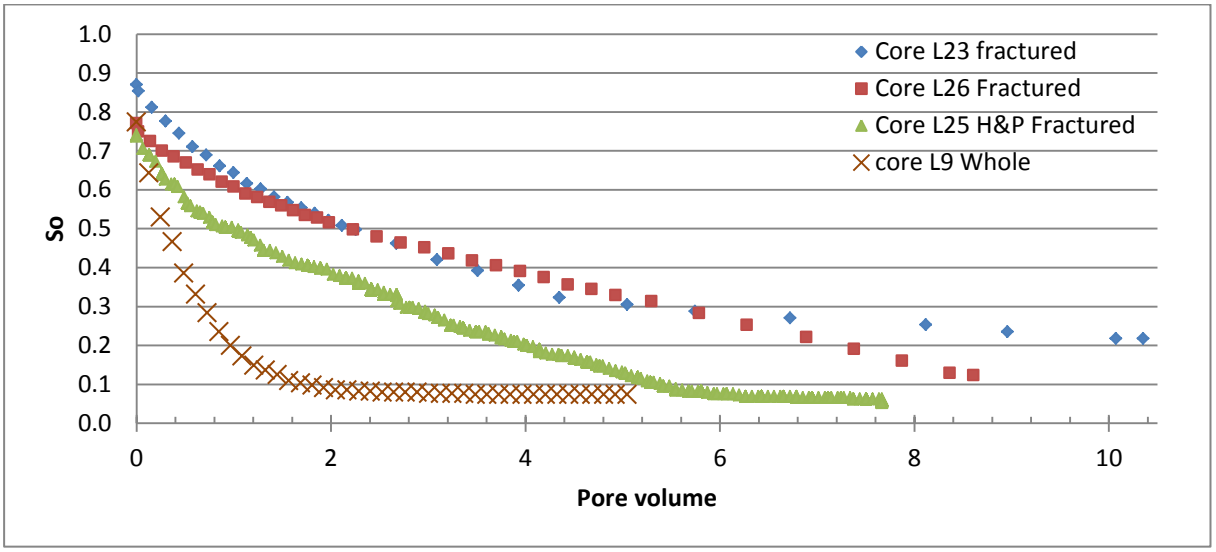

Figure 5-16 - Average oil saturation as a function of time during CO_2 injection in water-wet, whole and fractured limestone core plugs at irreducible water saturation.

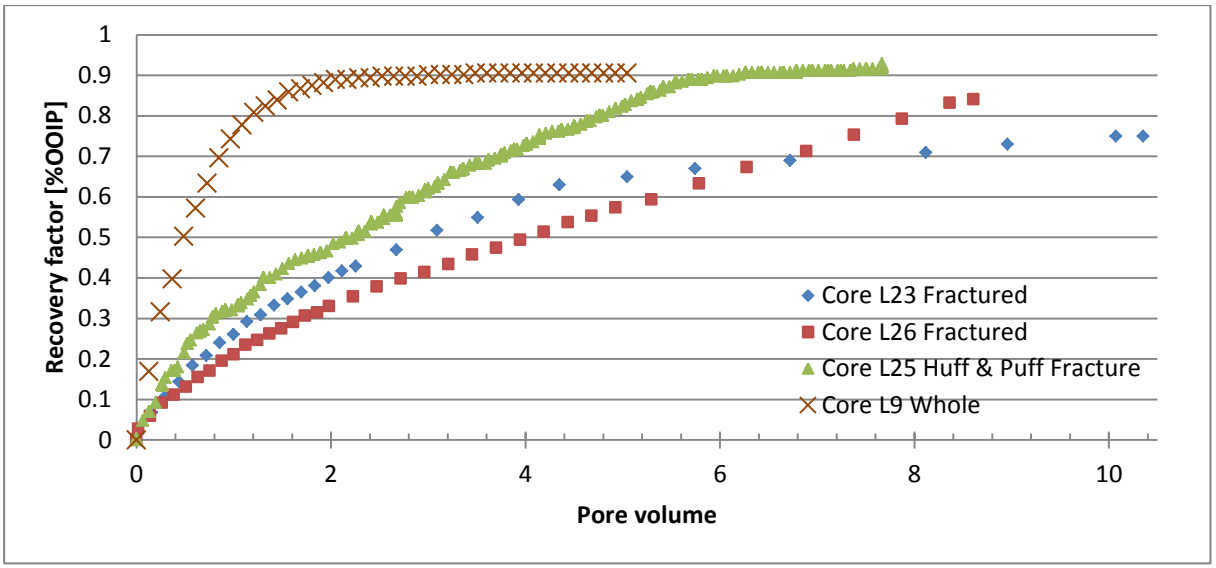

Figure 5-17 – Recovery factor as a function of time during CO_2 injection in water-wet, whole and fractured limestone core plugs at irreducible water saturation.

Table 5-8 - Oil recovery for continuous CO_2 injection compared to Huff 'n' Puff on fractured core.

Core	RF @ 1 PV	RF @ 2 PV	RF,total	PV @ RF,total
L9 - Whole	0.74	0.89	0.91	3.5
L23 - Fractured	0.26	0.40	0.75	10
L25 - H&P Fractured	0.33	0.48	0.93	8.6
L26 - Fractured	0.21	0.33	0.84	7.7

In the table below a CO_2 utilization factor is defined. Utilization factor is usually a factor used in the oil industry to describe how much CO_2 is injected in million cubic feet per barrel of oil produced (Schechter et al., 1998). In this case it shows the total oil produced [ml] per pore volume CO_2 injected. This gives an indication of how effectively the CO_2 is utilized (more oil produced per pore volumes i.e. more effective CO_2 utilization).

Table 5-9 – CO2 utilization values

	CO2 utilization [ml/pv]
Core L23	1.8
Core L26	2.4
Continuous CO2 injection	2.1
Core L25 H&P	2.8
Utilization Continuous vs. H&P [%]	29.3

The oil recovery per pore volume for the Huff 'n' Puff experiment is significantly increased compared to continuous CO_2 injection. For example after 1 pore volume L25 has produced 33% OOIP, compared to 23.5% OOIP in average for cores L23 and L26, as can be seen from Table 5-8, Figure 5-16 and Figure 5-17. After six pore volumes injected core plug L25 had produced 90% OOIP in comparison core L23 and core L26 had recovered in average 70% OOIP. This is a 28.6 % higher oil recovery for Huff 'n' Puff compared to continuous injection. The Huff 'n' Puff experiment had a CO_2

utilization factor of 2.8 ml/pv, whereas continuous CO_2 injection had an average of 2.1 ml/pv. This is an increased utilization of 29.3%.

The reason for the increased utilization of CO_2 during Huff 'n' Puff injection is that, when the core is shut in, the CO_2 gets more time to diffuse from the fracture into the matrix (oil going the opposite way from the matrix into the fracture). When CO_2 is injected after the shut in period, the CO_2 will displace the oil that has been diffused into the fracture. After the CO_2 has been injected for an hour, the fracture is fully saturated with CO_2, and the cycle is ready to start again. Since the diffusion rate is a function of the concentration gradient, the higher the concentration of CO_2 is in the fracture, the greater the rate of diffusion is (Darvish, 2007).

The CO_2 utilization could be increased if the incubation period (period without injection) was left for longer, because a higher production could be seen after the core was shut-in overnight. In an oil field the incubation period would be a trade-off between the drawbacks and benefits of injecting less CO_2. As mentioned in a fields lifetime CO_2 can diffuse several meters (Skjæveland and Kleppe, 1992). Diffusion and CO_2 behavior in fractures is more readily discussed in chapter 1.8 and 2.1.3.

It is important to note that even though the Huff 'n' Puff experiment had a higher amount of oil produced per pore volume compared to continuous injection, the experiment lasted for 15 days, while the continuous CO_2 injection experiments lasted for 3.5 days, which means that in a field case the day rate would have to be low compared to the price of CO_2 for Huff 'n' Puff to be economical.

Table 5-8, Figure 5-16 and Figure 5-17 show that oil production per pore volume injected is less effective for the Huff 'n' Puff core compared to continuous CO_2 injection in a whole core. However, Huff 'n' Puff is more effective than continuous CO_2 injection in a fractured core, which means that the negative effects that fractures have on oil production can be mitigated by giving the system more time for diffusion to work. Huff 'n' Puff is one way of mitigating the effects of fractures, another way is continuous injection at a lower rate, which would also give diffusion more time to work. The experiment gives an indication of how diffusion will work in a fractured field flooded with CO_2 at very low rates and could become an effective recovery mechanism if fractures are spaced close together.

Huff 'n' Puff would not lead to increased CO_2 utilization on whole cores, because injection and production is performed at either end of the core. The highest CO_2 concentration would then be located at the inlet of the core. Since diffusion is controlled by the concentration gradient, oil would diffuse in the direction of the inlet, and away from the outlet (Darvish, 2007).

5.4 Foam as mobility control

CO_2 has a high mobility and this causes fingering, early breakthrough and lower oil recovery. In chapter 5.1.3 the dramatic effect that fractures have on CO_2 oil recovery rate was discussed. Foam can create a viscous pressure drop, forcing the CO_2 into the matrix, leading to viscous displacement of the matrix and also reduces CO_2 mobility. Therefore CO_2-foam injection has been performed to study the effects on CO_2 EOR. CO_2-foam injection on whole and fractured cores will be discussed. (Farajzadeh et al., 2010)

5.4.1 Foam generation

The creation of foam can be confirmed in the water-wet cores. Comparing the differential pressures from Figure 5-18, the water-wet core L33 to the oil-wet core L14, the L33 core has 50 times higher differential pressure than oil-wet cores. This high differential pressure must be due to creation of foam, because core L33 actually has higher permeability than core L14, which without foam present would lead to a lower differential pressure at the same injection rate. Differential pressures was in the same range for the fractured cores compared as for the whole cores injected with CO_2-foam, see Figure 5-19, which should be significantly lower if no foam was created, as the permeability for the fractured core is 40 times larger. This establishes the creation of foam in both the whole and fractured water-wet CO_2-foam experiments. The oil-wet whole core (L14) has either no foam creation, or very weak foam creation. No foam creation for the oil-wet core is expected because in an oil-wet pore the oil will have a preference to occupy the space along the pore walls. This means that lamellae will find it difficult staying attached to the pore walls. Being detached from the pore walls will cause the lamella to collapse (Rossen, 1996).

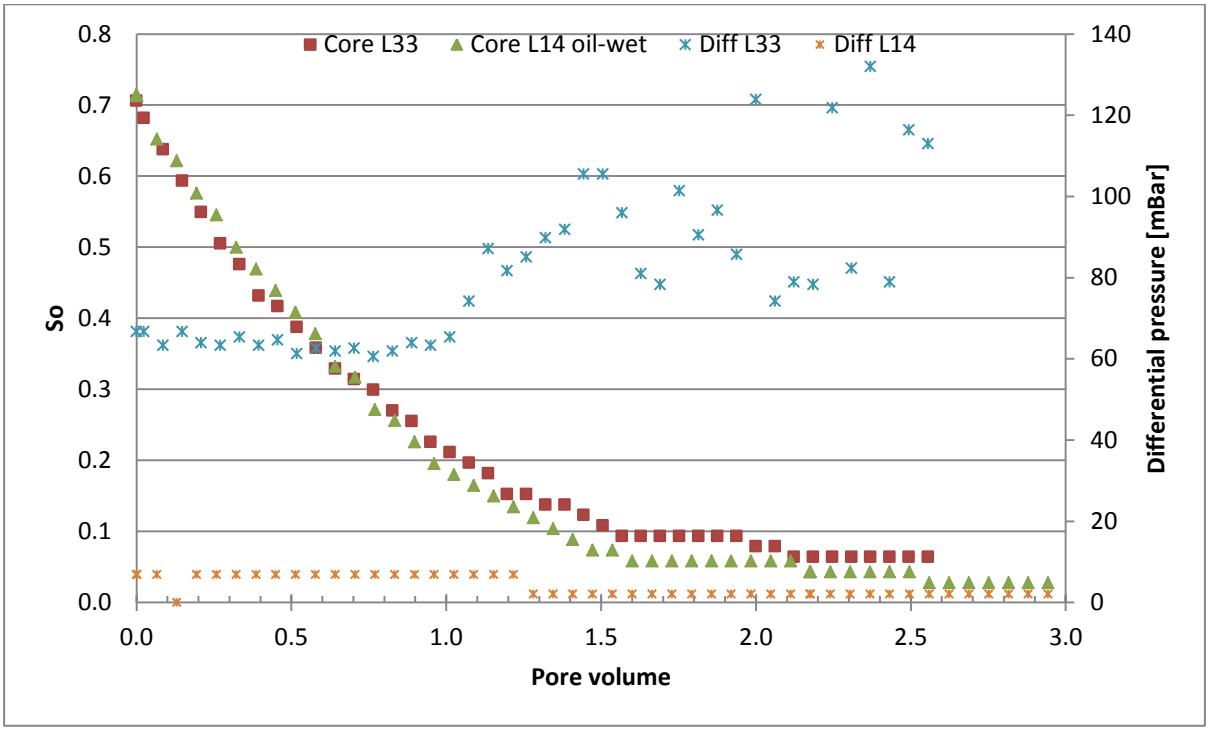

Figure 5-18 - Average oil saturation and differential pressure as a function of time during CO_2-foam injection in two water-wet and one moderately wet, un-fractured limestone core plugs at irreducible water saturation.

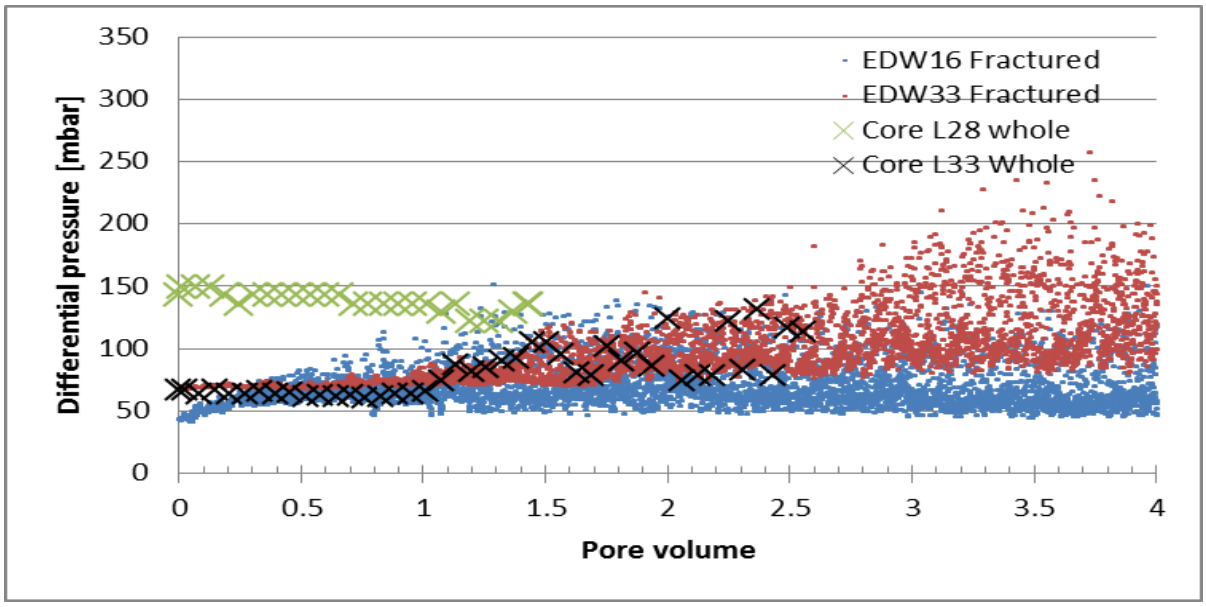

Figure 5-19 – Differential pressure as a function of time during CO2-foam injection in water-wet, either whole or fractured limestone core plugs at irreducible water saturation. EDW# are experiments from (Christophersen, 2012, Skibenes, 2012)

5.4.2 CO_2-foam injection in whole cores

This chapter compares oil recovery during pure CO_2 injection to CO_2-foam injection on whole cores. Three cores injected with pure CO_2 (L6, L9 and L10) and one cores injected with CO_2-foam (L33). The main observation was that the oil recovery for CO_2-foam injection was similar to CO_2 injection, although ultimate recovery was reached earlier, which may be due to stable foam being created when low oil saturations were reached. Key numbers are tabulated in Table 5-10.

Figure 5-20 and Figure 5-21 show average oil saturation and recovery factor as a function of pore volumes injected during CO_2 injection and CO_2-foam injection in whole cores. The curves show that the oil recovery curves have the same shape and that the experiments reached the same ultimate recovery for the CO_2-foam injection and the pure CO_2 injection tests. However ultimate recovery was reached earlier by core L33.

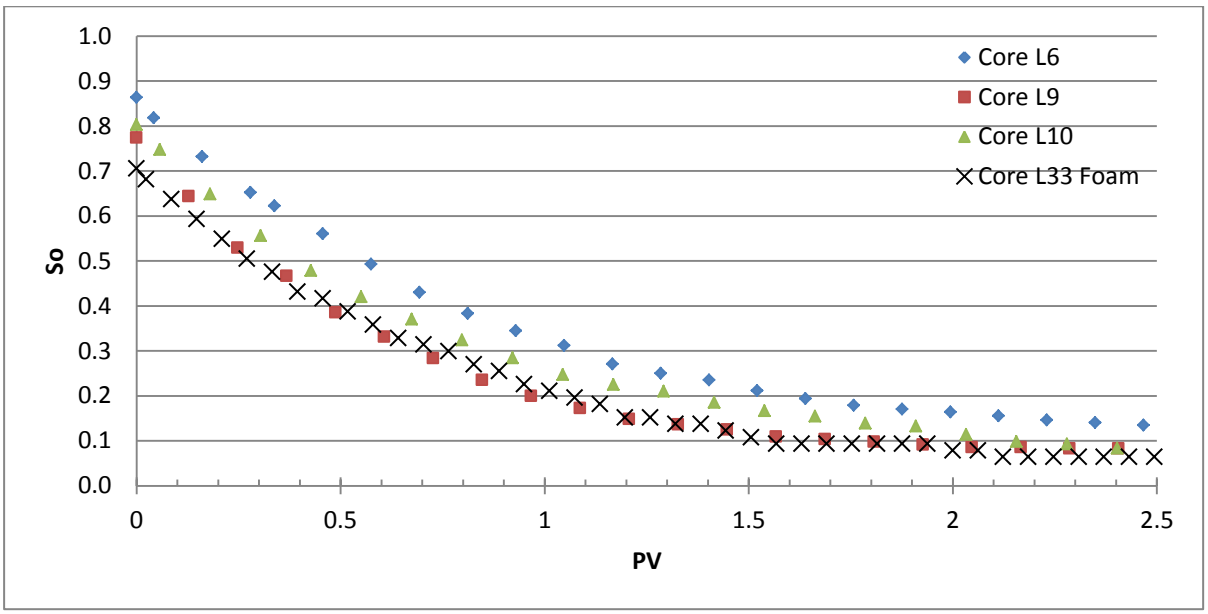

Figure 5-20 - Average oil saturation as a function of time during CO2 injection and CO_2-foam injection in water-wet, un-fractured limestone core plugs at irreducible water saturation.

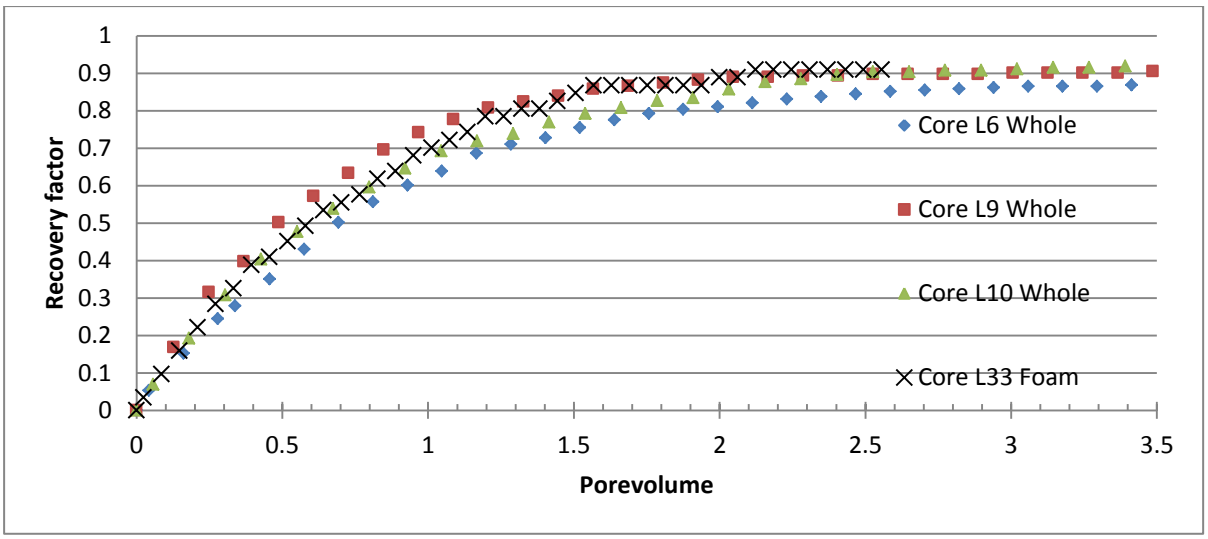

Figure 5-21 – Recovery factor as a function of time during CO2 injection and CO2-foam injection in water-wet, un-fractured limestone core plugs at irreducible water saturation.

Table 5-10 - Comparing oil recovery factor of OOIP for CO_2 injection to CO_2-foam injection.

	RF @ 1 PV	RF @ 2 PV	RF,total	PV @ RF,total
L6 – CO_2	0.64	0.81	0.87	4.3
L9 – CO_2	0.74	0.89	0.91	3.5
L10 – CO_2	0.69	0.86	0.92	3.6
L33 - Foam	0.70	0.89	0.91	2.1

Foam injection does, not increase the rate of recovery or the final recovery compared to pure CO_2 injection (see Table 5-10 and Figure 5-21). The only positive effect is that the final recovery for CO_2-foam injection compared to pure CO_2 is reached with less pore volumes of CO_2 injected. This may occur because as the oil saturation decreases, foam is less affected by the destructive effects of oil, and thus does not become effective before almost all of the oil is produced. The destructive properties of oil might cause the foam at the front to become unstable, which causes the displacement to be similar to that of pure CO_2-injection. (Farajzadeh et al., 2009, Schramm, 1993, Lau, 1988)

The fact that there was not a large effect on enhanced oil recovery may be due to the destructive effects of oil on foam. The minor effect on enhanced oil recovery may be due to less heterogeneity in whole cores compared to fractured cores, because foam has the ability to even out heterogeneities. If there is only a small degree of heterogeneity the foam will not significantly increase recovery of the already effective miscible displacement of pure CO_2 injection (Farajzadeh et al., 2010, Skjæveland and Kleppe, 1992).

In a reservoir the positive effects of foam will be more dominating, and the foam gives the CO_2 better macroscopic displacement. In lab scale, however, CO_2 injection is already a very effective recovery method, giving ultimate recovery in the range of 90%, because it is miscible with the oil (at high enough pressure), which leads to good microscopic efficiency. Negative effects of the highly mobile CO_2, such as fingering, channeling and gravity segregation, do not have time to become effective on such a small scale as a core plug. The effectiveness of CO_2 injection is also caused by the relatively small diffusion length, and this will significantly increase the efficiency in lab scale (Skjæveland and Kleppe, 1992). In a larger scale like a reservoir, where the negative effects such as fingering, channeling and gravity segregation do take place the foam might reduce the CO_2 mobility (reducing fingering and channeling) and delay segregation. In an oil-field the CO_2-foam at the front will follow the high permeable layers (path of least resistance). The CO_2-foam at the front will then create a viscous pressure drop, forcing the CO_2-foam coming from behind (chase fluid) to be diverted to the layers or regions that has not already been flooded (which are oil filled). This is an effect that is less significant in core flooding. (Farajzadeh et al., 2010, Kovscek et al., 1993, Alvarez et al., 1999).

5.4.3 CO_2-foam injection in fractured cores

This section compares oil recovery during pure CO_2 injection to CO_2-foam injection on fractured cores. Two cores are injected with CO_2 (L23 and L26) and two cores are injected with CO_2-foam (EDW16 and EDW33). An accelerated oil recovery was observed for CO_2-foam compared to pure CO_2. Foam creates a higher differential pressure and adds viscous displacement in addition to diffusion in fractured cores. Key numbers are tabulated in Table 5-11.

Figure 5-22 and Figure 5-23 show average oil saturation and recovery factor as a function of pore volumes injected during CO_2 and CO_2-foam in fractured cores. Table 5-11 shows recovery factor at different pore volumes injected. Figure 5-24 show recovery factor as a function of the square root of pore volumes injected.

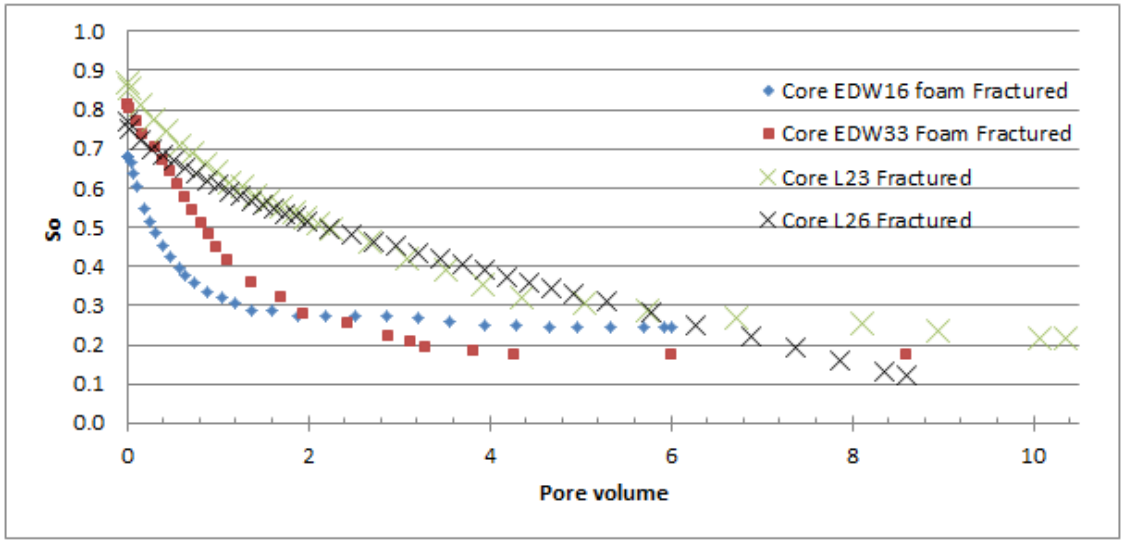

Figure 5-22 - Average oil saturation as a function of time during CO2 injection and CO_2-foam injection in water-wet, fractured limestone core plugs at irreducible water saturation. EDW# are experiments from (Christophersen, 2012, Skibenes, 2012)

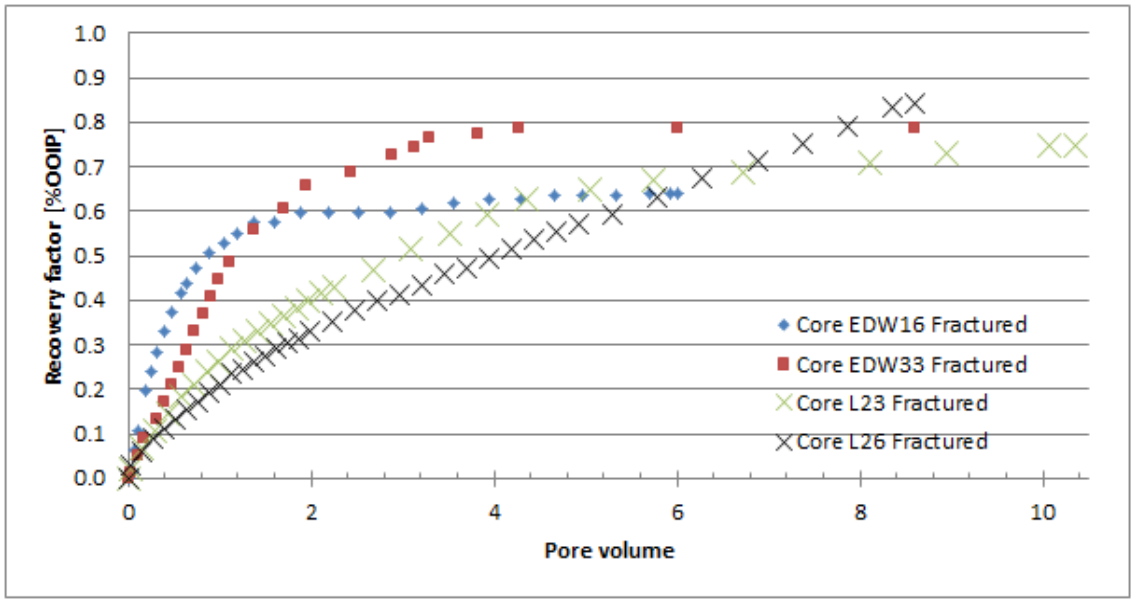

Figure 5-23 - Recovery factor as a function of time during CO2 injection and CO2-foam injection in water-wet, fractured limestone core plugs at irreducible water saturation. EDW# are experiments from (Christophersen, 2012, Skibenes, 2012)

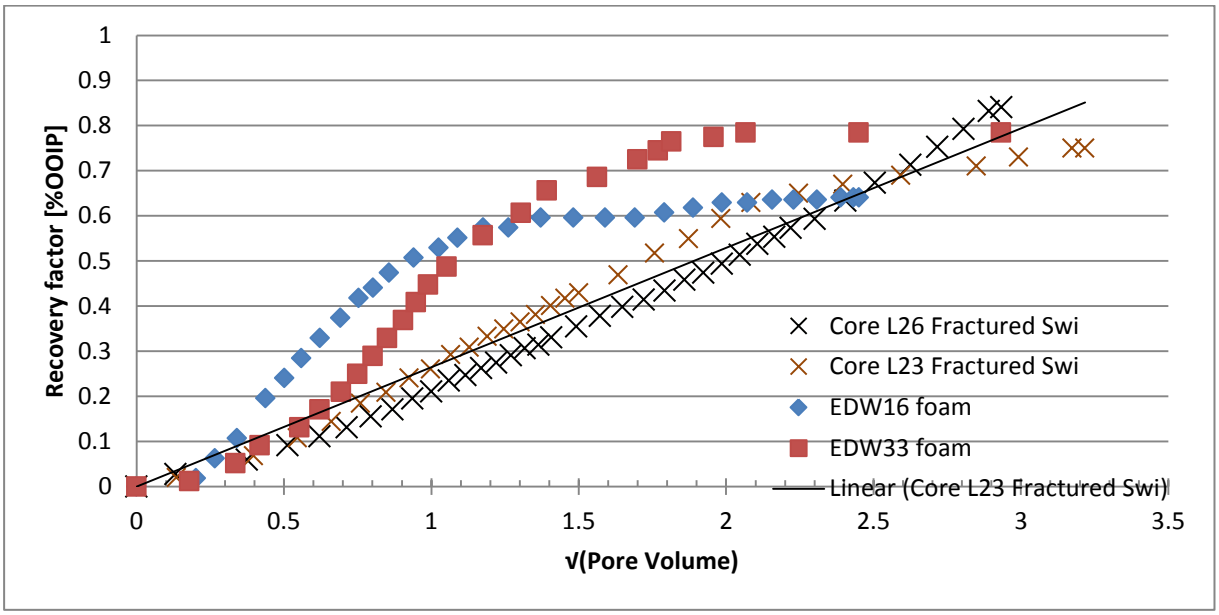

Figure 5-24 - Recovery factor as a function of the square root of time during CO2-injection and CO2-foam injection in water-wet, whole limestone core plugs at irreducible water saturation. EDW# are experiments from (Christophersen, 2012, Skibenes, 2012)

Table 5-11 - Comparing oil recovery factor for CO2 injection to CO2-foam injection on fractured cores.

	RF @ 1 PV	RF @ 2 PV	RF,total	PV @ RF,total
L23 – CO_2	0.26	0.40	0.75	10
L26 – CO_2	0.21	0.33	0.84	7.7
EDW16 - Foam	0.53	0.63	0.64	4.9
EDW33 -Foam	0.49	0.66	0.78	4.5

As shown in Figure 5-23 and Table 5-11 an accelerated oil recovery can be observed for the fractured cores injected with CO_2-foam, compared to the oil recovery the fractured cores injected with pure CO_2. The foams accelerated recovery is especially effective up to approximately two pore volumes. At 2 pore volumes the foam experiments have recovered on average 82% more oil (36.5% OOIP for pure CO_2 compared to OOIP 64.5% for CO_2-foam). On average ultimate recovery is reached approximately twice as rapidly.

The high recovery rate is caused by the greater viscous pressure drop across the fracture observed for CO_2-foam, forcing the CO_2 into the fracture leading to viscous displacement and increasing the dispersion rate (mechanical dispersion and diffusion), detailed in chapter 2.2.5 and 1.8.

As shown in Figure 5-24 oil recovery plotted as a function of the square root of time can indicate if recovery is diffusion driven or not. The two pure CO_2 floods have closer to linear curvature, which indicates that the oil recovery is dominantly diffusion driven. The two cores injected with CO_2-foam deviates from the linear line, which indicates that the oil recovery is not just diffusion driven, but also viscous driven. Hence, foam significantly increases recovery rates in fractures by introducing additional recovery mechanisms. Since the oil in the fracture is instantly produced, the surfactant is able to create stable foam in the fracture, without the degrading effect of oil. The stable foam creates a viscous pressure drop that forces the CO_2 to disperse into the matrix, thus displacing and swelling the oil (Farajzadeh et al., 2010, Farajzadeh et al., 2009).

The accelerated oil recovery is a very important aspect in the oil industry, because the net present value (NPV) makes the oil more worth today than in the future (assuming constant oil prices)(Jahangiri and Zhang, 2011). Also increasing the recovery rate can mean that the field can be produced faster, in fewer days/years, which leads to a reduction in expenses.

The higher ultimate recovery observed for the CO_2 cores, compared to the CO_2-foam cores, is explained by the higher irreducible water saturation for CO_2-foam cores, leading to increased water shielding and making CO_2 unable to contact all the oil in the core (Zekri et al., 2007, Shyeh-Yung, 1991, Grogan, 1987).

A benefit of foam is that it increases the macroscopic efficiency, which might be even more dominating in a larger scale than on cores as discussed in more detail in chapter 5.4.2 (Skjæveland and Kleppe, 1992).

In an oil reservoir injecting several pore volumes of CO_2 is not realistic, which is why increased recovery early in the production is important. A small amount of surfactant is needed to create foam, which makes this a potentially inexpensive investment (Farajzadeh et al., 2010). Only two liquid CO_2-foam experiments were performed for fractured, water-wet cores by Christophersen and Skibenes (Christophersen, 2012, Skibenes, 2012). These experiments are not identical, although they show the same trend. More experiments should be done to get a better picture of the effects of foam.

Experimental visualization of CO_2-foam in a fracture

Vertical CO_2-foam injection in Core EDW39 was visualized using an industrial CT located at Penn State University, State College, PA. Surfactant was injected for the first 0.5 pore volumes, because the lines upstream of the core contained surfactant and not CO_2-foam.

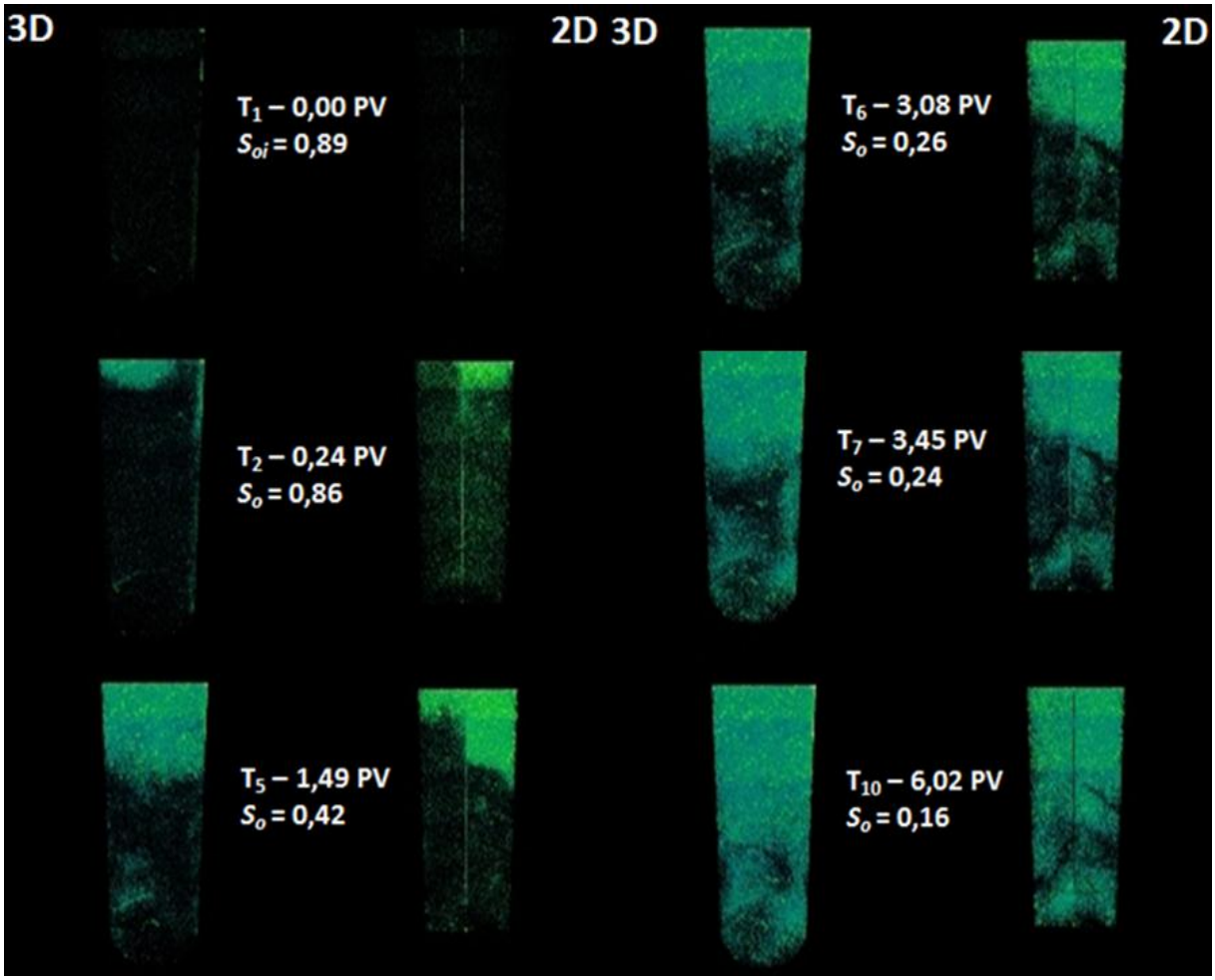

Figure 5-25- CT images on the neutrally wet core EDW39. Vertical CO2-foam injection from the top to the bottom. The pictures on the left shows 3D and on the right shows 2D images perpendicular to the fracture plane. Read pictures in numerical order of the pore volume. Modified from (Christophersen, 2012)

Figure 5-25 shows for the first 0.5 pore volume injected surfactant displacing oil like a typical waterflood (since surfactant moves into the matrix, the core might be more water-wet than oil-wet, resulting in imbibition). After 0.5 pore volume injected CO_2-foam is dispersed into the matrix, and a viscous displacement of the oil can be seen from the images. A majority of the CO_2 moves through the fracture, because the CO_2 has not finished displacing the matrix after more than 3 pore volumes of CO_2-foam injected. However a viscous displacement front can be seen moving down the matrix. At the experimental pressure of 80 bars and a temperature for 20 C, CO_2 has a higher density than n-Decane. The core is vertically mounted and with the high density of CO_2 this leads to gravity unstable displacement. This may be why CO_2 appears to be moving down the right hand side of the 2D images (note especially the CT image at 1.49 PV). The CT images show how foam causes viscous displacement to occur in the matrix with the presence of fractures.

5.4.4 Effect of wettability CO_2-foam injection

Whole Cores

This section discusses the effect of wettability during CO2-foam injection on whole cores, and compares one water-wet core (L33) and one moderately oil-wet core (L14). Final oil recovery for the oil-wet core was higher than for the water-wet core after CO_2-foam injection.

Figure 5-26 and Figure 5-27 show average oil saturation and differential pressure, and recovery factor as a function of pore volumes injected during CO_2-foam injection in a water-wet core and an oil-wet core. Key numbers are tabulated in Table 5-12.

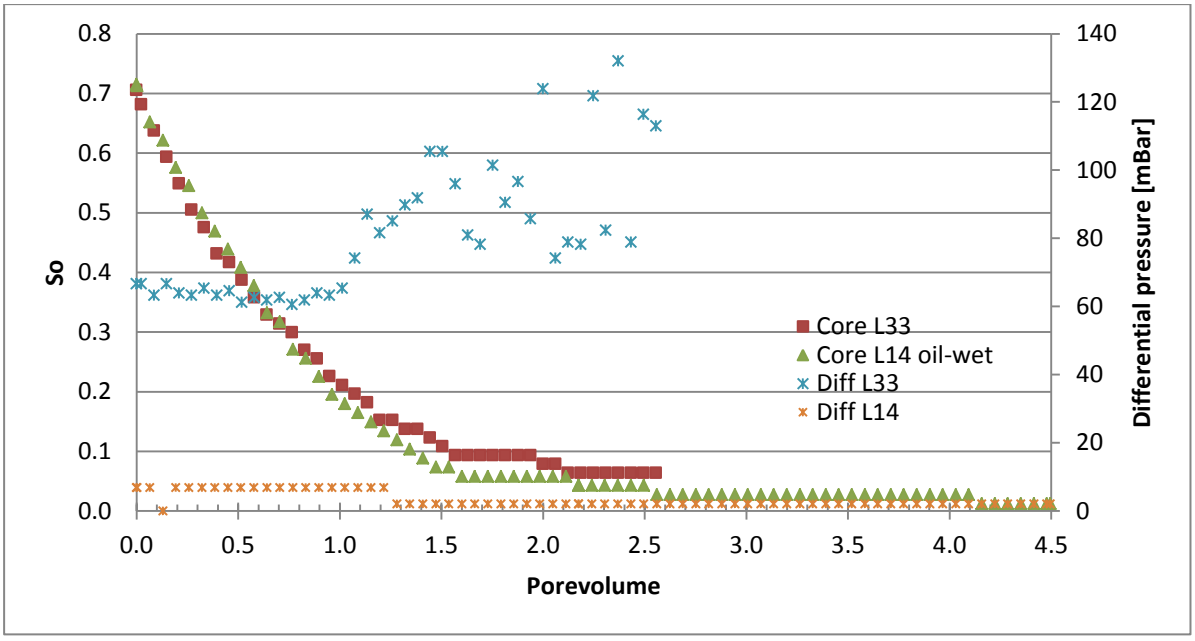

Figure 5-26 - Average oil saturation and differential pressure as a function of time during CO2-foam injection in either water-wet or oil-wet, whole limestone core plugs at irreducible water saturation.

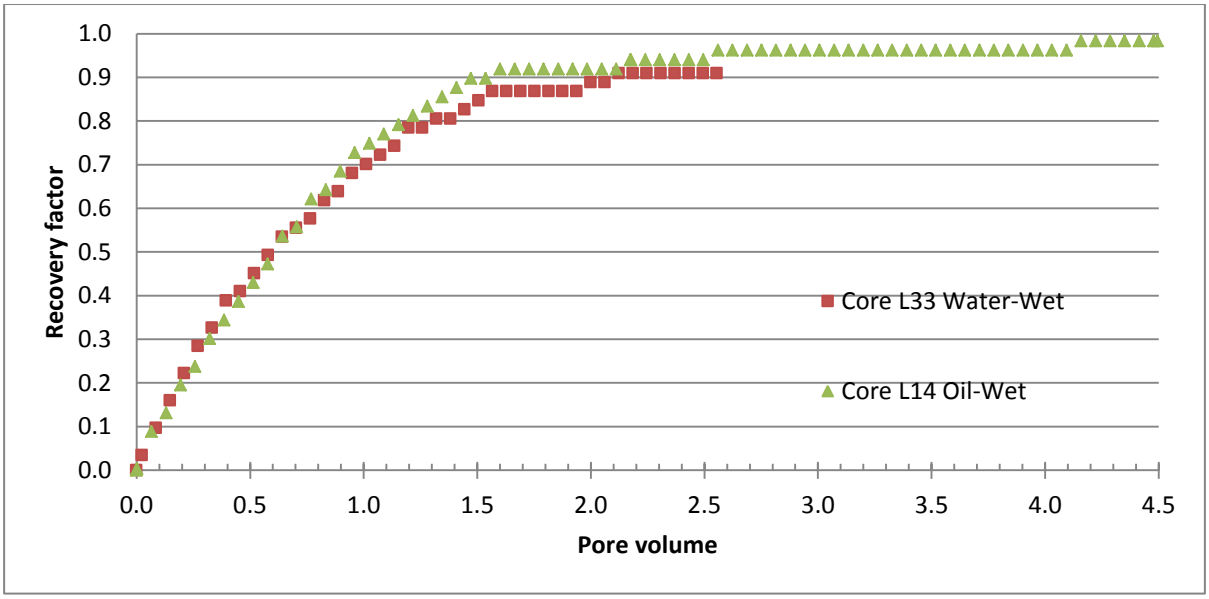

Figure 5-27 – Oil recovery factor as a function of time during CO2-foam injection in either water-wet or oil-wet, whole limestone core plugs at irreducible water saturation.

Table 5-12 - Comparing effect of wettability on oil recovery for CO_2-foam injection on whole cores. Core L33 is Water-wet. Core L14 is moderately oil-wet.

	RF @ 1 PV	RF @ 2 PV	RF,total	PV @ RF,total
L33	0.70	0.89	0.91	2.1
L14	0.75	0.92	0.98	4.1

In this chapter the wettability effect on oil recovery for CO_2-foam injection will be discussed. Core L33 is water-wet. Core L14 is moderately oil-wet. Both cores have approximately the same irreducible water saturation at 0.71. From Table 5-12, Figure 5-26 and Figure 5-27 it can be shown that Core L33 initially has a higher oil recovery for the first 0.7 pore volumes. After 0.7 pore volumes L14 has a higher oil recovery and ends up with a higher ultimate recovery. This initially higher recovery rate is likely caused by foam being created in Core L33, and not in core L14. This can be seen from the differential pressure in Figure 5-26, where the differential pressure is 50 times larger for core L33 compared to core L14. In an oil-wet pore the oil will have a preference to occupy the space along the pore walls. This means that lamellae will find it difficult staying attached to the pore walls(Rossen, 1996). The foam might cause the water-wet core to get a slightly more effective viscous displacement (Farajzadeh et al., 2010).

After 0.7 pore volumes core L14 has a higher recovery. The higher recovery after 0.7 pore volumes is probably caused by the water wet cores experiencing greater water blocking effects (Zekri et al., 2007, Shyeh-Yung, 1991, Lin and Huang, 1990). Water shielding becomes more significant later in the oil recovery process. In chapter 5.1.1 and 5.2.3 water blocking did not significantly affect the oil recovery before most of the easily recoverable oil had been recovered. The oil-wet core experiences a higher ultimate recovery, just as for the other oil-wet cores in this thesis, see chapter 5.1.3, this behavior was expected(Lin and Huang, 1990).

However the oil recoveries of the two cores, are relatively similar, and more experiments should be done to verify the conclusions drawn.

Fractured cores

This section discusses the effect of wettability during CO2-foam injection on fractured cores, and compares one water-wet core (EDW33) and two moderately oil-wet cores (EDW6 and EDW32). CO_2-foam is created in the oil-wet fractured cores. CO_2-foam reaches a higher final recovery for moderately oil-wet cores compared to water-wet core. Key numbers are tabulated in Table 5-13.

Figure 5-28 and Figure 5-29 show average oil saturation and recovery factor as a function of pore volumes injected during CO_2-foam injection in two fractured, water-wet cores and two fractured, oil-wet cores. Figure 5-30 shows the differential pressure for two fractured, water-wet cores and two fractured, oil-wet cores.

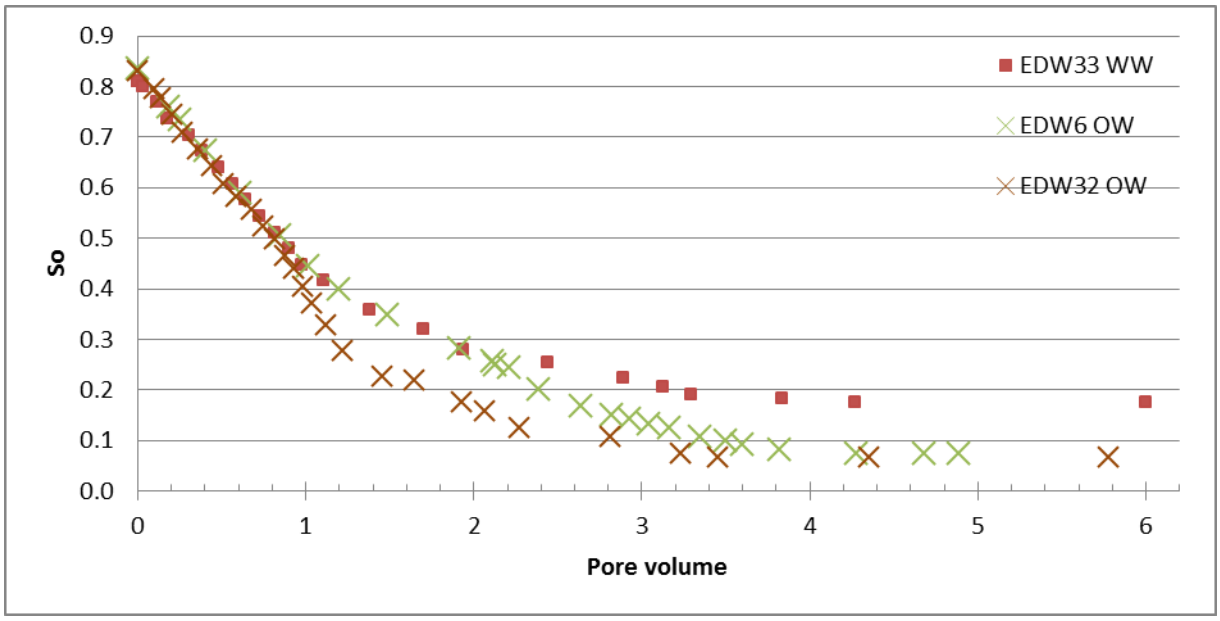

Figure 5-28 - Average oil saturation as a function of time during CO2-foam injection in either water-wet or oil-wet, fractured limestone core plugs at irreducible water saturation. EDW# are experiments from (Christophersen, 2012, Skibenes, 2012)

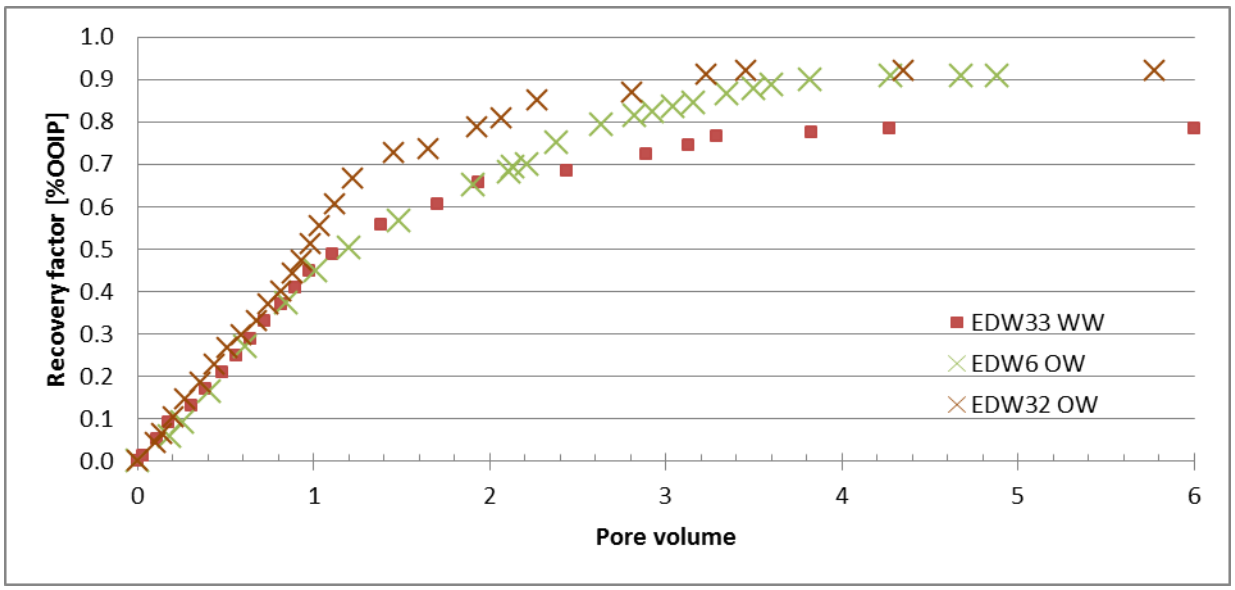

Figure 5-29 – Oil recovery factor as a function of time during CO2-foam injection in either water-wet or oil-wet, fractured limestone core plugs at irreducible water saturation. EDW# are experiments from (Christophersen, 2012, Skibenes, 2012)

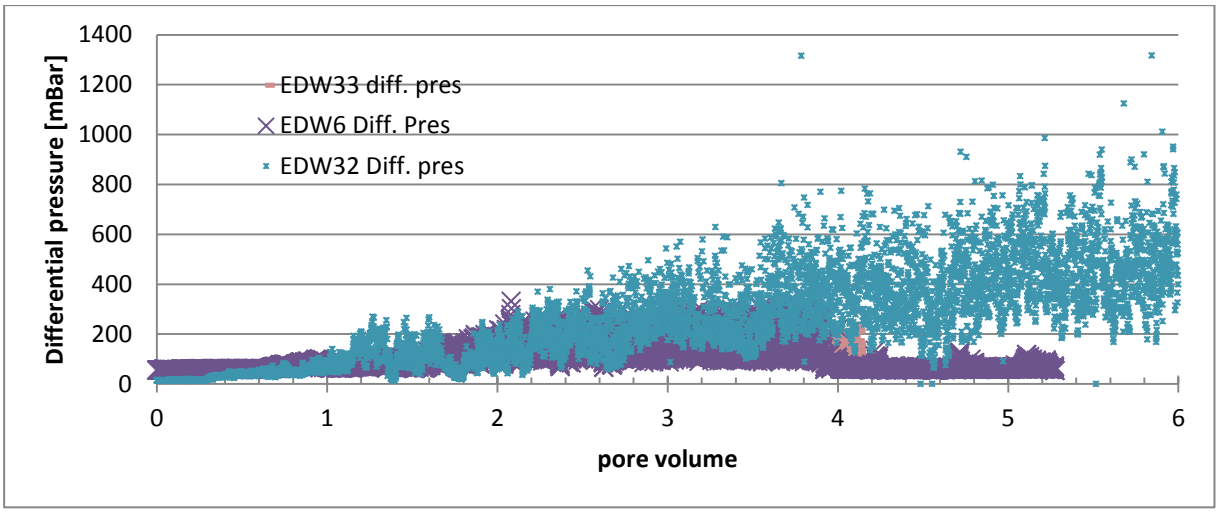

Figure 5-30 – Differential pressure as a function of time during CO2-foam injection in either water-wet or oil-wet, fractured limestone core plugs at irreducible water saturation. EDW# are experiments from (Christophersen, 2012, Skibenes, 2012)

Table 5-13 - Effect of wettability on oil recovery for CO2-foam injection in fractured cores. EDW# are experiments from (Christophersen, 2012, Skibenes, 2012)

	RF @ 0.5 pv	RF @ 1 PV	RF @ 2 PV	RF,total	PV @ RF,total
EDW33 WW	0.21	0.49	0.66	0.78	4.5
EDW6 OW	0.20	0.45	0.68	0.91	4.2
EDW32 OW	0.27	0.55	0.81	0.92	3.45

As shown for Table 5-13, Figure 5-28 and Figure 5-29 oil recovery is not affected for the water-wet core EDW33 compared to the oil-wet cores for the first pore volume. The similar oil recovery may be caused by the fact that as CO_2-foam flows through the fracture, the surfactant alters the wettability of the fracture to more water-wet conditions. In an oil-wet pore the oil will have a preference to occupy the space along the pore walls. This means that lamellae will find it difficult staying attached to the pore walls(Rossen, 1996). Some researchers claim to have created weak foams in oil-wet medium, but this is probably caused by the surfactants ability to change the wettability of the rock (Sanchez, 1992). The altered wettability in the fracture causes the foam to become stable in the fracture, and creating a viscous pressure drop forcing CO_2 to disperse into the matrix (Farajzadeh et al., 2010, Rossen, 1996). The creation of foam is further confirmed when looking at Figure 5-30. The differential pressure is in the same range for all the cores, indicating that the foam is just as strong in the water-wet fractured cores as in the oil-wet fractured cores. This behavior is different for the whole cores in Figure 5-26, where no foam was created, and the differential pressure for the oil-wet core was approximately 50 times smaller. After approximately one pore volume the oil-wet cores oil recovery becomes on average more effective than for the water-wet cores. The oil-wet cores become more effective because of of less water-shielding in moderately wet and oil-wet porous media (Lin and Huang, 1990, Zekri et al., 2007, Shyeh-Yung, 1991). The oil-wet cores reaches a higher ultimate recovery (Lin and Huang, 1990).

5.4.5 CO_2 vs. CO_2-foam in fractured cores

In this section 4 experiments will be compared: One Huff 'n' Puff experiment, one fracture core with continuous CO_2 injection, one whole core with continuous CO_2 injection and one fractured core with CO_2-foam injection. The cores chosen have been the most comparable and successfully performed experiments of the different categories.

CO_2-foam injection mitigate the heterogeneity effect that fractures have on a porous medium, and may cause the CO_2 to be dispersed into matrix of the fractured cores, thereby displacing oil with viscous force, in addition to the diffusion.

Figure 5-31 and Figure 5-32 show average oil saturation and recovery factor as a function of pore volumes injected during CO_2 injection and CO_2-foam injection in whole and fractured cores. Table 5-14 compares recovery factor for pore volumes injected.

Table 5-14 - Comparing oil recovery factor of OOIP for CO_2 injection to CO_2-foam injection.

	Rf @ 1 pv	Rf @ 2 pv	Rf,total	PV @ Rf,total
L9 - whole	0.74	0.89	0.91	3.5
L23 - Fractured	0.26	0.40	0.75	10
EDW33 - Fractured Foam	0.49	0.66	0.78	4.5
L25 - H&P Fractured	0.33	0.48	0.93	8.6

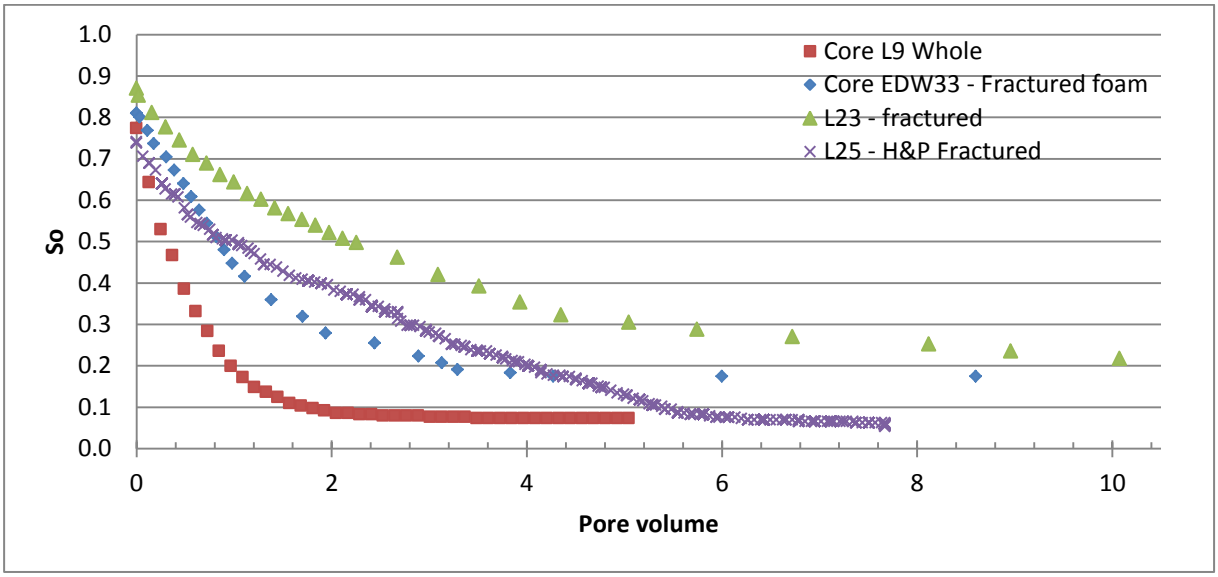

Figure 5-31 - Average oil saturation as a function of time during CO2 injection and CO_2-foam injection in water-wet, whole and fractured limestone core plugs at irreducible water saturation.

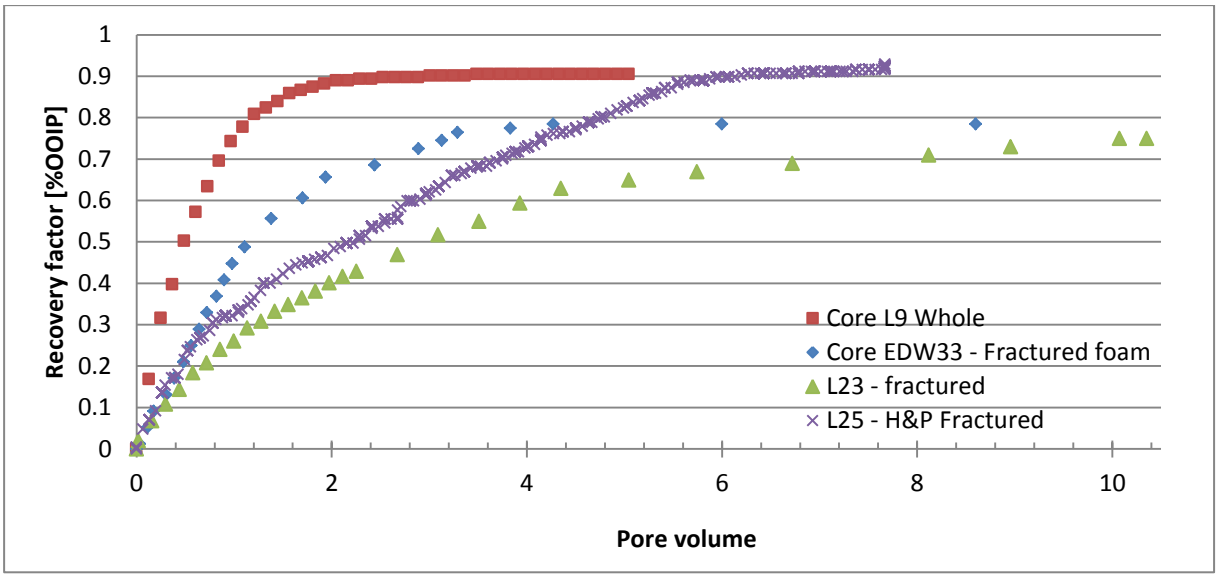

Figure 5-32 – Recovery factor as a function of time during CO2 injection and CO2-foam injection in water-wet, whole and fractured limestone core plugs at irreducible water saturation.

Table 5-14, Figure 5-31 and Figure 5-32 shows that both the Huff 'n' Puff and CO_2-foam experiment perform better than the fractured core. After 1 and 2 pore volume the foam experiment is the most effective. This shows that foam is a good candidate to mitigate the negative effects of fractures in cores. The viscous forces created by the foam, gives the curve of core EDW33 a similar shape to the whole core. Fractured reservoirs have good potential for CO_2-foam injection, since foam mitigates the negative effects of fractures. On large scale fractures can give a positive effect in regard to diffusion because the depth of penetration of diffusion is proportional to the square root of time, so fractures space closely together could lead to potential good recovery because the distances from the concentration source (the fracture), to the oil can become quite small. Fractured reservoirs also have in general low oil recovery, which increases the potential of miscible CO_2-foam injection. (Hirasaki and Zhang, 2004, Roehl, 1985, Skjæveland and Kleppe, 1992, Farajzadeh et al., 2010)

5.5 Numerical simulations of CO_2 EOR in fractured carbonate

Simulation results compared to experimental results
How the numerical simulations were made and run, is described in chapter 4.4.

Figure 5-33 shows a numerical simulation of a limestone core compared with experimental CT image visualization from Baird (2013). The numerical simulation is a simulation based on experimental data from CO_2 injection into the fractured limestone core L23. The CT images are from a CO_2 injection in a chalk core plug, with the same spacer and end pieces used as the experiment performed on core L23. The images represent the left side of a core split down the middle, with a fracture located on the right side. End pieces are located on the top and bottom of the core.

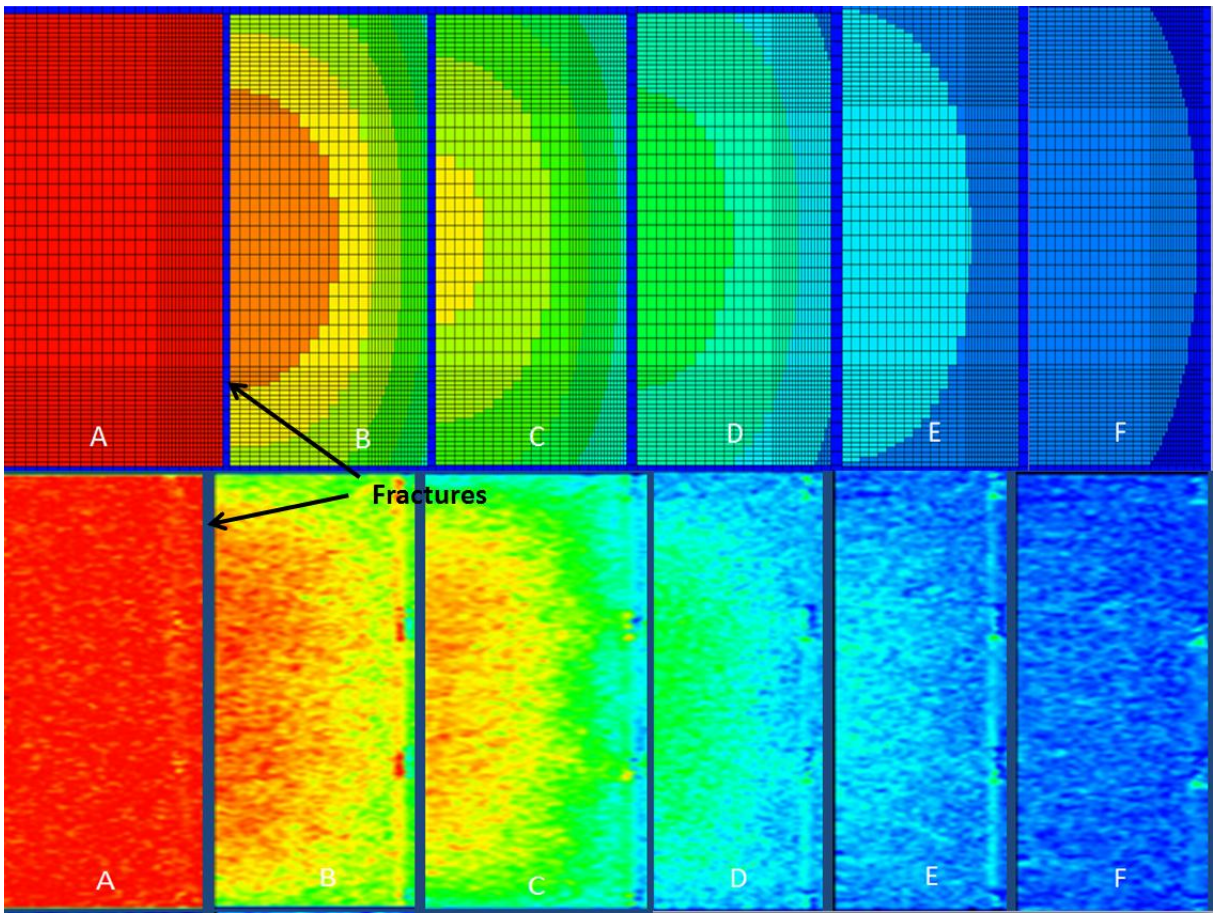

Figure 5-33 – comparing simulations from CMG Results 3D (pictures on the top) to experimental CT visualization (pictures on the bottom) on CO_2 injection in a chalk core (Baird, 2013). Warm colors represent high oil saturation while cold colors represent low oil saturation. Each image has a fracture located on the right side, with end pieces located on the top and bottom. Letters show which images that are comparable.

The numerical simulation is a homogenous simulation, meaning that the heterogeneity of limestone was not taken into account. Since chalk is a homogenous rock type and CO_2 displacement occurs for both the simulation and the CT visualization, the images can be compared to see if the simulation has similar behavior as the experiment performed on chalk. The only different parameter is the permeability, and thus CO_2 injection in chalk will take longer time penetrating into the matrix. Therefore the times cannot be compared.

The color curvature of the simulation images shows that the diffusion contribution from the end pieces and the fracture has been taken into account, and it shows a similar diffusion process compared to the experimental visualization. Since CO_2 is miscible with n-Decane, the CO_2 will diffuse from the end pieces and the fracture into the matrix to restore equilibrium (oil going the opposite direction from the matrix to the fracture and end pieces). According to Fick's second law of diffusion, if the boundary conditions with a constant concentration at the boundary, in this case the fracture, then the depth of penetration is proportional to the square root of time. This means that the further into the matrix CO_2 diffuses, the slower diffusion occurs, therefore the oil far away from the concentration sources (fracture and end pieces) will be the last to be recovered by diffusion.

The pictures show a good overlap from simulations and the experimental data. The good overlap is an indication that the simulations can be further used to examine the effect of different parameters (such as water saturation, wettability, permeability, fracture permeability).

Figure 5-34 shows two of the diffusion coefficients that were run to find a diffusion coefficient that would be a good approximation to our experimental results (several more were run, but only two were included to give a clear picture of the effect of different diffusion coefficients). The diffusion coefficient of 1×10^{-4} cm^2/s gave good approximation to our experimental data. The good overlap of the simulation and experimental data in Figure 5-34 is another indication that this simulation is a good base for future simulations. The effect of oil swelling is included in the diffusion coefficient found through the numerical simulations. Baird calculated a diffusion coefficient of 1.8×10^{-5} cm^2/s, which is approximately 5 times lower than ours. A lower diffusion coefficient is expected in chalk, since the permeability of chalk is approximately 10 times lower. The diffusion coefficient found by Baird includes the effect of oil swelling. (Baird, 2013, Bijeljic and Blunt, 2006).

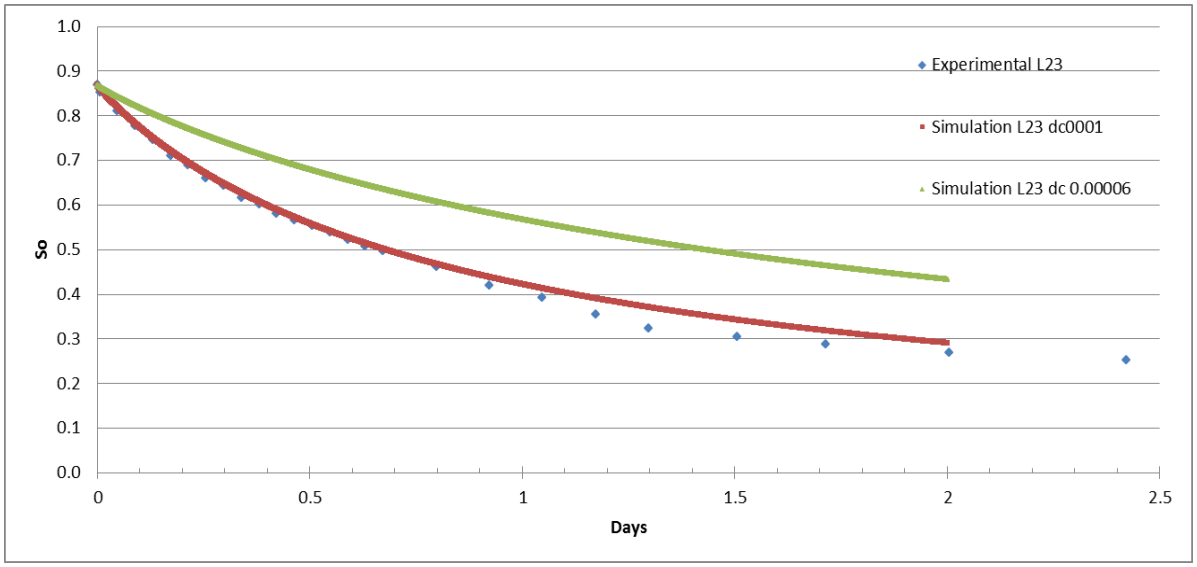

Figure 5-34 - Oil saturation as a function of time. dc0001 signifies simulations run with diffusion coefficient of 1×10^{-4} cm^2/s

The numerical simulations performed showed a good overlap of the experimental data indicating the simulations should be used further to increase the understanding and for a better depth of analysis and reduce time usage compared to advanced, time-consuming experimental work.

Oil-wet simulations

The numerical simulation is a simulation based on experimental data from CO_2 injection into the fractured limestone core L26. Figure 5-35 shows oil saturation as a function of time for experimental data, and simulated data run with oil-wet and water-wet rock type.

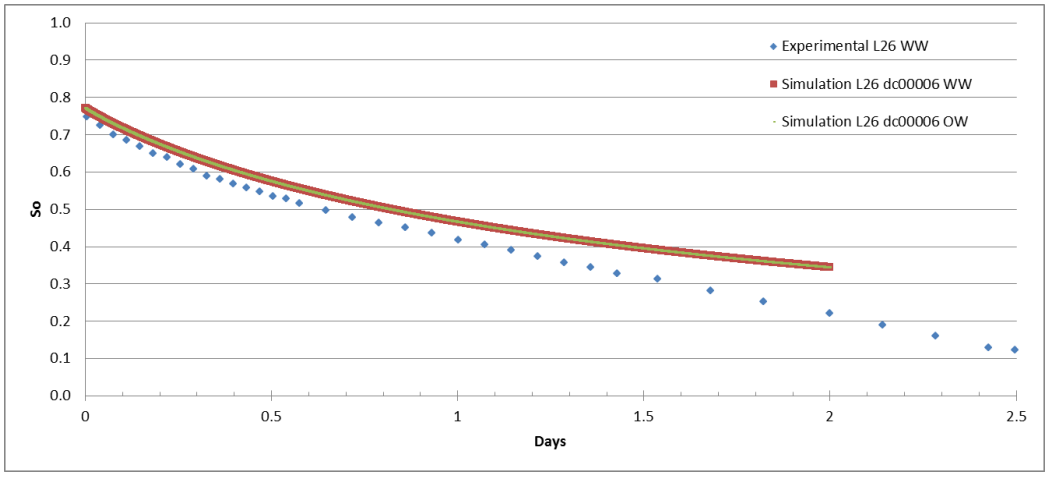

Figure 5-35 – Oil saturation as a function of time. dc00006 signifies simulations run with diffusion coefficient of 6×10^{-5} cm^2/s

As shown in Figure 5-35, when running the simulations with keywords `ROCKFLUID RPT 1 OILWET`, this should change the rock type to oil-wet and it changes the capillary curve, and relative permeability curve for the matrix. However the production profile was identical (Oil recovery should be different with an oil-wet rock type), which indicates more work should be done to simulate oil-wet rock behavior.

Tertiary CO_2 injection simulations

The numerical simulation is a simulation based on experimental data from CO_2 injection into the fractured limestone core L23. Figure 5-36 shows oil saturation as a function of time for the experimental data and the simulated data for secondary and tertiary oil recovery.

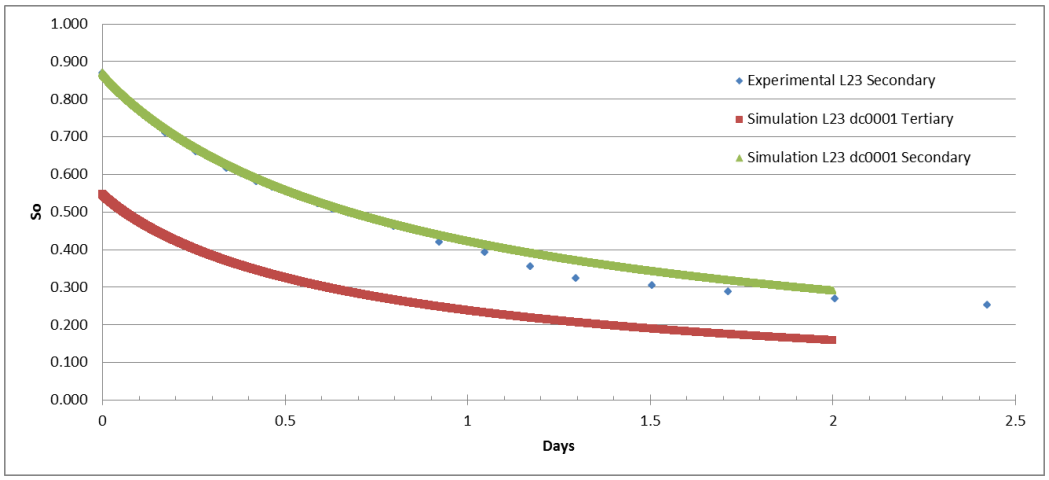

Figure 5-36 - Oil saturation as a function of time. dc00006 signifies simulations run with diffusion coefficient of 6×10^{-5} cm^2/s

Tertiary recovery has not been performed experimentally on a fractured system. This should be done to further validate the numerical model to compare the tertiary CO_2 injection simulation to experimental data.

6. Conclusions

Based on the experimental work and numerical simulations performed, the following conclusions have been drawn:

CO_2 injection for EOR in general reaches a recovery of approximately 90% OOIP both in fractured and whole cores.

The presence of fractures dramatically reduces the rate of oil recovery. Oil recovery during CO_2-injection in fractured cores is mainly driven by diffusion, with negligible viscous displacement.

The presence of water either as initial irreducible water saturation, or after a waterflood reduces the total oil recovery. Water also lowers the rate of diffusional oil recovery in fractured reservoirs.

The injection of CO_2-foam accelerates oil recovery compared to pure CO_2 injection in fractured cores. Foam creates a higher differential pressure and adds viscous displacement in addition to diffusion in fractured cores.

The recovery rates in pore volumes injected for the Huff 'n' Puff injection is significantly increased compared to continuous CO2 injection.

Moderately oil-wet cores demonstrate a higher total oil recovery than water-wet cores for both CO_2 and CO_2-foam injection.

Moderately-oil wet cores prevent the creation of foam in whole cores. In Moderately-oil wet fractured cores, however, foam creation does occur, likely due to the surfactants ability to alter the wettability of the fracture.

During CO_2-foam injection, differential pressure is higher near the end of production, indicating that oil has a detrimental effect on foam.

The numerical simulations performed showed a good overlap of the experimental data indicating the simulations should be used further to increase the understanding and for a better depth of analysis and reduce time usage compared to advanced, time-consuming experimental work.

The results from this thesis shows the potential for CCUS in fractured carbonate reservoirs, even though the oil recovery rate is reduced with fractures, the total oil recovery is still high and diffusion can be an effective recovery mechanism.

6.1 Future work

All the experiments performed in this thesis have been done with liquid CO_2. They should be also done for supercritical CO_2 (higher temperature), since most reservoirs are under supercritical conditions. However Haugen(experiments on chalk), Christophersen(experiments on limestone) and Skibenes(experiments on limestone) concluded that the recovery behavior on core scale were almost indistinguishable between liquid CO_2 and supercritical CO_2 (Haugen, 2012, Christophersen, 2012, Skibenes, 2012).

Tertiary CO_2 injection should be performed with fractures, and tertiary CO_2 injection should also be performed with more effective water injection to see how higher water saturation affects the CO_2 recovery.

The simulation that has been built should be used further in collaboration with experimental results, to quickly analyze results and create statistics. This can be an effective way to increase the depth of CO_2 analysis.

More work should be done to simulate oil-wet rock behavior.

All of the experiments should be repeated to get a good reproducibility, and to confirm the results of this thesis.

The experiments should be performed with more imaging techniques such as MRI and CT, to get a better understanding of the effects of CO_2 injection.

The experiments should be performed on larger scale, such as block experiments too see the effects of upscaling.

The confining pressure should be controlled by a pump, to avoid problems of CO_2 flowing around the core.

More wettability experiments should be performed, to get a better overview on the wettability effects on CO_2 injection.

7. Nomenclature

EOR	Enhanced oil recovery
MMP	Minimum miscibility pressure
CO_2	Carbon dioxide
MRI	Magnetic resonance imaging
CT	Computed tomography
SWW	Strongly water-wet
OW	Moderately oil-wet
V_p	Pore volume
V_b	Bulk volume
V_m	Matrix volume
Φ	Porosity
ρ	Density
So	Oil saturation
S_{wi}	Irreducible water saturation
$S_{or,w}$	Residual oil after waterflood
$S_{or.\ CO2}$	Residual water after CO_2-flood
RF	Recovery factor
PV	Pore volume
Q	Fluid flow rate
μ	Fluid viscosity
Δp	Pressure drop across the unit length
L	Sample length
A	Cross section area
K	Absolute permeability
K_r	Relative permeability
K_e	Effective Permeability
λ	Mobility of a fluid
M	Mobility ratio
K_{matrix}	Matrix permeability
K_{frac}	Fracture permeability
I_{A-H}	Amott-Harvey index
I_w	Amott water index
I_o	Amott oil index
σ	Interfacial tension
P_c	Capillary pressure
R	Pore radius
θ	Wetting angle between two fluid
N_{vc}	Capillary number
D_o	diffusion coefficient in the absence of a porous media
D	Effective diffusion coefficient
C	Concentration of one component
x	Traveled distance
t	time
F	Formation electrical resistivity
Pe	Peclet number

8. References

ABDALLAH, W. B., J.S., CARNEGIE, A., EDWARDS, J., HEROLD, B., FORDHAM, E. G., A.

HABASHY, T., SELEZNEV, N., SIGNER, C., HUSSAIN, H., MONTARON, B. & ZIAUDDIN, M. 2007. Fundamentals of Wettability. *Oilfield Review,* 19.

ADEPOJU, O. O., LAKE, L. W. & JOHNS, R. T. 2013. Investigation of Anisotropic mixing in miscible displacements. *SPE Reservoir Evaluation & Engineering,* 16**,** pp. 85-96.

AL-BASRY, A. H., AL-HAJERI, S. K., SAADAWI, H. N. H., ARYANI, F. M. A., OBEIDI, A. A., NEGAHBAN, S. & BIN-DHAAER, G. S. 2011. Lessons Learned from the First Miscible CO2-EOR Pilot Project in Heterogeneous Carbonate Oil Reservoir in Abu Dhabi. *SPE Middle East Oil and Gas Show and Conference*

Manama, Bahrain: Society of Petroleum Engineers.

ALAVIAN, S. A. & WHITSON, C. H. 2010. CO2 EOR Potential in Naturally Fractured Haft Kel Field, Iran. *SPE Reservoir Evaluation & Engineering*

13**,** pp. 720-729.

ALVAREZ, J. M., RIVAS, H. J. & ROSSEN, W. R. 1999. Unified Model for Steady-State Foam Behavior at High and Low Foam Qualities. *SPE Annual Technical Conference and Exhibition.* Houston, Texas: Society of Petroleum Engineers.

ANDERSON, W. 1986. Wettability Literature Survey- Part 2: Wettability Measurement. *Journal of Petroleum Technology,* 38**,** 1246-1262.

BAIRD, S. 2013. *CO2 EOR by Diffusion in Fractured Chalk.* Master, University of Bergen.

BIJELJIC, B. & BLUNT, M. J. 2006. A physically based description of dispersion in porous media. *SPE Annual Technical Conference and Exhibition.* San Antonio, Texas, USA: Society of Petroleum Engineers.

BIRD, R. B., STEWART, W. E. & LIGHTFOOT, E. N. 1960. *Transport Phenomena*

CAMPBELL, B. T. & JR., F. M. O. 1985. flow visualization for CO2/crude-oil displacements. *Society of Petroleum Engineers Journal,* 25**,** 665-678.

CHANG, S.-H. & GRIGG, R. B. 1998. Effects of Foam Quality on Flow Rate on CO2-Foam Behavior at Reservoir Conditions. *SPE/DOE Improved Oil Recovery Symposium.* Tulsa, Oklahoma: Society of Petroleum Engineers.

CHRISTOPHERSEN, A. 2012. Økt oljeutvinning ved injeksjon av CO2-skum i en oppsprukket karbonatbergart ved forskjellige fuktforhold.

CRAIG, F. F. 1971. Reservoir Engineering Aspects of waterflooding. *Society of Petroleum Engineers Inc.,* 3.

CUSSLER, E. L. 1997. *Diffusion: Mass Transfer in Fluid Systems*.

DARVISH, G. R. 2007. *Physical effects controlling mass transfer in matrix fracture system during CO2 injection into chalk fractured reservoirs.*, NTNU.

DO, H. D. & PINCZEWSKI, W. V. 1991. Diffusion Controlled Swelling of Reservoir Oil by Direct Contact with Injection Gas. *Chemical Engineering Science,* 46**,** 1259-1270.

DONG, M., HUANG, S. & SRIVASTAVA, R. 1999. Effect of Solution Gas in Oil on CO2 Minimum Miscibility Pressure. *Annual Technical Meeting.* Calgary, Alberta: Petroleum Society of Canada.

ENICK, R. M., OLSEN, D. K., AMMER, J. R. & SCHULLER, W. 2012. mobility and conformance control for CO2 EOR via Thickeners, Foams and Gels - A literature review of 40 years of research and pilot tests. *SPE Improved Oil Recovery Symposium.* Tulsa, Oklahoma, USA: Society of Petroleum Engineers.

FARAJZADEH, R., ANDRIANOV, A., KRASTEV, R., HIRASAKI, G. & ROSSEN, W. R. 2012. Foam-Oil Interaction in Porous Media: Implications for Foam Assisted Enhanced Oil Recovery. *SPE EOR Conference at Oil and Gas West Asia.* Muscat, Oman: Society of Petroleum Engineers.

FARAJZADEH, R., ANDRIANOV, A. & ZITHA, P. L. J. 2009. Foam Assisted Enhanced Oil Recovery at Miscible and Immiscible Conditions. *Kuwait International Petroleum Conference and Exhibition.* Kuwait City, Kuwait: Society of Petroleum Engineers.

FARAJZADEH, R., WASSING, L. B. M. & BOERRIGTER, P. M. 2010. Foam Assisted Gas Oil Gravity Drainage in Naturally-Fractured Reservoirs. *SPE Annual Technical Conference and Exhibition.* Florence, Italy: Society of Petroleum Engineers.

FERNØ, M. A. 2013. *RE: Personal communication.*

FERNØ, M. A., TORSVIK, M., HAUGLAND, S. & GRAUE, A. 2010. Dynamic Laboratory Wettability Alteration. *Energy & Fuels,* 24**,** 3950-3958.

FRIEDMANN, F., SMITH, M. E., GUICE, W. R., GUMP, J. M. & NELSON, D. G. 1994. Steam-Foam Mechanistic Field Trial in the Midway-Sunset Field. *SPE Reservoir Engineering,* 9**,** 297-304.

GHEDAN, S. G. 2009. Global Laboratory Experience of CO2-EOR Flooding. *SPE/EAGE Reservoir Characterization and Simulation Conference.* Abu Dhabi, UAE: Society of Petroleum Engineers.

GOZALPOUR, F., REN, S. R. & TOHIDI, B. 2005. CO2 EOR and Storage in Oil Reservoirs. *Oil & Gas Science and Technology - Rev. IFP,* 60**,** 537-546.

GROGAN, A. T. P., W.V. 1987. The Role of Molecular Diffusion Processes in Tertiary CO2 Flooding. *Journal of Petroleum Technology,* 39**,** 591-602.

HASKIN, H. K. & ALSTON, R. B. 1989. An evaluation of co2 huff n puff tests in Texas. *Journal of Petroleum Technology,* 41**,** 177-184.

HAUGEN, M. 2012. *CO2 Injection In Fractured Chalk For Enhaned Oil Recovery.* Master, University of Bergen.

HIRASAKI, G. & ZHANG, D. L. 2004. Surface Chemistry of Oil Recovery From Fractured. Oil-wet, Carbonate Formations. *SPE Journal,* 9**,** 151-162.

HIRASAKI, G. J. 2012. *RE: Personal communications.*

HITE, J. R., BLANTON, M. L., KUHLMAN, M. I. & FAIR, W. B. 2012. Managing Risk in EOR Projects. *SPE Latin America and Caribbean Petroleum Engineering Conference.* Mexico City, Mexico: Society of Petroleum Engineers.

HOLTER, Ø., INGEBRETSEN, F. & PARR, H. 2010. *Fysikk og Energiressurser,* University of Oslo.

HUH, D. G. H. L. L. 1989. Comparison of Steady- and Unsteady-State Flow of Gas and Foaming Solution in Porous Media. 220-240.

JAHANGIRI, H. R. & ZHANG, D. 2011. Optimization of the Net Present Value of Carbon Dioxide Sequestration and Enhanced Oil Recovery. *Offshore Technology Conference.* Houston, Texas, USA.

KARIMAIE, H., LINDEBERG, E. G. B., TORSAETER, O. & DARVISH, G. R. 2007. Experimental Investigation of Secondary and Tertiary Gas Injection in Fractured Carbonate Rock. *EUROPEC/EAGE Conference and Exhibition.* London, U.K.: Society of Petroleum Engineers.

KLINKENBERG, L. J. 1941. The Permeability of Porous Media to Liquids and Gases. American Petroleum Institute.

KOVSCEK, A. R., PATZEK, T. W. & RADKE, C. J. 1993. Fundamentals of Foam Transport in Porous Media. *SPE Annual Technical Conference and Exhibition.* Houston, Texas: 1993 Copyright 1993, Society of Petroleum Engineers, Inc.

LAKE, L. W. 1989. *Enhanced Oil Recovery*, Prentice Hall Incorporated.

LAU, H. C. O. B. S. M. 1988. Effects of Spreading and Nonspreading Oils on Foam Propagation Through Porous Media. *SPE Reservoir Engineering,* 3**,** 893-896.

LIEN, J. R. 2006. *RE: Reservoarteknikk I.*

LIN, E. C. & HUANG, E. T. S. 1990. The Effect of Rock Wettability on Water Blocking During Miscible Displacement. *SPE Reservoir Engineering,* 5**,** 205-212.

MALIK, Q. M. I., M.R. 2000. Potential of Greenhouse Gas Storage and Utilization Through Enhanced Oil Recovery in Canada. World Petroleum Congress.

MATHIASSEN, O. M. 2003. *CO2 as Injection Gas for Enhanced Oil Recovery and Estimation of the Potential on the Norwegian Continental Shelf.* NTNU – Norwegian University of Science and Technology.

MORROW, N. R. & BUCKLEY, J. 2006. Wettability and Oil Recovery by Imbibition and Viscous Displacement from Fractured and Heterogeneous Carbonates. *Chemical & Petroleum Engineering*

MORSI, K., LESLIE, J. & MACDONALD, D. 2004. CO2 Recovery and utilization for EOR. *Abu Dhabi International Conference and Exhibition.* Abu Dhabi, United Arab Emirates: Society of Petroleum Engineers.

MÛLLER, T. & LAKE, L. 1991. Theoretical study of water blocking in miscible flooding. *SPE Reservoir Engineering,* 6**,** 445-451.

NETL, N. E. T. L.-. 2010. Carbon Dioxide Enhanced Oil Recovery - Untapped Domestic Energy Supply and Long Term Carbon Storage Solution. *The Energy Lab*.

NIST. 2013. *http://webbook.nist.gov/ - National Institute of Standards and Technology* [Online].

NOAA, N. O. A. A. A.-. 2013. *Greenhouse Gases - http://www.ncdc.noaa.gov/oa/climate/gases.html* [Online]. [Accessed (accessed 26.02.2013).

NYBØ, R. 2012. *RE: Personal communications.*

OSTERLOH, W. T. & JANTE JR, M. J. 1992. Effects of Gas and Liquid Velocity on Steady-State Foam Flow at High Temperature. *SPE/DOE Enhanced Oil Recovery Symposium.* Tulsa, Oklahoma: 1992 Copyright 1992, Society of Petroleum Engineers Inc.

PERKINS, T. K. J., O.C. 1963. A Review of Diffusion and Dispersion in Porous Media

PICHA, M. S. 2007. Enhanced Oil Recovery by Hot CO2 Flooding. *SPE Middle East Oil and Gas Show and Conference.* Kingdom of Bahrain: Society of Petroleum Engineers.

ROEHL, P. O. C., P.W. 1985. *Carbonate Petroleum Reservoirs*.

ROOF, J. G. 1970. Snap-Off of oil droplets in water-wet pores.

ROSSEN, W. R. 1996. Foams - Theory, Measurements and Application, Chapter 11: Foams in Enhanced Oil Recovery.

SANCHEZ, J. M. H., A.D. 1992. Foam Flow Through an Oil-Wet Porous Medium: A Laboratory Study. *SPE Reservoir Engineering,* 7**,** 91-97.

SCHECHTER, D. S., GRIGG, R., GUO, B. & SCHNEIDER, B. 1998. Wellman Unit CO2 flood: reservoir pressure reduction and flooding the water/oil transition zone. *SPE Annual Technical Conference and Exhibition.* New Orleans, Louisiana: Society of Petroleum Engineers.

SCHRAMM, L. L. T., A. T.

NOVOSAD, J.J. 1993. Microvisual and Coreflood Studies of Foam Interactions With a Light Crude Oil. *SPE Reservoir Engineering,* 8**,** 201-206.

SHYEH-YUNG, J.-G. J. 1991. Mechanisms of Miscible Oil Recovery: Effects of Pressure on Miscible and Near-Miscible Displacement of Oil by Carbon Dioxide. *SPE Annual Technical Conference and Exhibition.* Dallas, Texas: 1991 Copyright 1991, Society of Petroleum Engineers Inc.

SIGMUND, P. M. 1976. Prediction of Molecular Diffusion At Reservoir Conditions. Part II - Estimating the Effects Of Molecular Diffusion and Convective Mixing In Multicomponents Systems. *Journal of Canadian Petroleum Technology,* 15**,** 53-64.

SKARRESTAD, M. & SKAUGE, A. 2011. *RE: Fluid Properties and Recovery Methods.*

SKAUGE, A., AARRA, M. G., SURGUCHEV, L., MARTINSEN, H. A. & RASMUSSEN, L. 2002. Foam-Assisted WAG: Experience from the Snorre Field. *SPE/DOE Improved Oil Recovery Symposium.* Tulsa, Oklahoma: Copyright 2002, Society of Petroleum Engineers Inc.

SKIBENES, A. T. 2012. *Injeksjon av CO2-skum for økt oljeutvinning i oppsprukket karbonatbergart under ulike fuktforhold.* Master, University of Bergen.

SKJÆVELAND, S. M. & KLEPPE, J. 1992. SPOR - Recent Advances in Improved Oil Recovery Methods For North Sea Sandstone Reservoirs. *Norwegian Petroleum Directorate,* Chapter 9**,** 207-250.

SVENNINGSEN, S. 2011. *An experimental study of CO2 injection for enhanced oil recovery in chalk and limestone.* Master, University of Bergen.

SWEATMAN, R. E., CROOKSHANK, S. & EDMAN, S. 2011. outlook and technologies for offshore CO2 EOR/CCS projects. *Offshore Technology Conference.* Houston, Texas, USA.

TRIVEDI, J. J. & BABADAGLI, T. 2006. Efficiency of Miscible Displacement in Fractured Porous Media. *SPE Western Regional/AAPG Pacific Section/GSA Cordilleran Section Joint Meeting.* Anchorage, Alaska, USA: Society of Petroleum Engineers.

TRIVEDI, J. J. & BADADAGLI, T. 2008. Experimental Analysis of CO2-Sequestration Efficiency During Oil Recovery in Naturally Fractured Reservoirs. *SPE Eastern Regional/AAPG Eastern Section Joint Meeting.* Pittsburgh, Pennsylvania, USA: Society of Petroleum Engineers.

VIKINGSTAD, A. K., SKAUGE, A., HØILAND, H. & AARRA, M. 2005. *Foam-oil Interactions Analysed by Static Foam Tests.* University of Bergen.

WALSH, M. P., NEGAHBAN, S. & GUPTA, S. P. 1989. an analysis of water shielding in water-wet porous media. *SPE Annual Technical Conference and Exhibition.* San Antonio, Texas: 1989 Copyright 1989, Society of Petroleum Engineers, Inc.

WILKE, C. R. C., P. 1955. Correlation of Diffusion Coefficients in Dilute Solutions. *AIChE Journal,* 1.

WYLIE, P. L. & MOHANTY, K. K. 1999. Effect of Wettability on Oil Recovery by Near-Miscible Gas Injection. *SPE/DOE Improved Oil Recovery Symposium.* Tulsa, Oklahoma: 1998 Copyright 1998, Society of Petroleum Engineers, Inc.

XING, D., WEI, B., MCLENDON, W. J., ENICK, R. M., MCNULTY, S., TRICKETT, K., MOHAMED, A., CUMMINGS, S., EASTOE, J., ROGERS, S., CRANDALL, D., TENNANT, B., MCLENDON, T., ROMANOV, V. & SOONG, Y. 2012. CO2-Soluble, Nonionic, Water-soluble surfactants that stabilixe CO2-in-Brine-Foams. *SPE Journal,* 17**,** pp. 1172-1185.

ZEKRI, A. Y., JERBI, K. K. & EL-HONI, M. 2000. Economic Evaluation of Enhanced Oil Recovery. *International Oil and Gas Conference and Exhibition in China.* Beijing, China: Copyright 2000, Society of Petroleum Engineers Inc.

ZEKRI, A. Y., SHEDID, S. A. & ALMEHAIDEB, R. A. 2007. Possible alteration of tight limestone rocks properties and effect of water shielding on the performance of supercritical CO2 flooding for carbonate formation. *SPE Middle East Oil and Gas Show and Conference.* Kingdom of Bahrain: Society of Petroleum Engineers.

ZHANG, Y. P., SAYEGH, S. G., HUANG, S. & DONG, M. 2006. Laboratory Investigation of Enhanced Light-Oil Recovery by CO2/Flue Gas Huff-n-Puff Process. *Canadian International Petroleum Conference.* Calgary, Alberta: Petroleum Society of Canada.

ZOLOTUKHIN, A. B. U., J. 2000. *introduction to petroleum reservoir engineering*.

Appendix A - Estimation of uncertainties in the experimental work

In experimental work there are always uncertainties in relation to the results. The accuracy of the instruments used in the experiments is very high. Therefore the biggest contribution to the uncertainty will be related to the execution of the experiments and the readings. Preparing the cores prior to the experiments and while performing the experiments, many instruments are used. All of these measurements have a related uncertainty. All these uncertainties will contribute to the total experimental uncertainty. In addition to being thorough in minimizing the uncertainties by being accurate and having good laboratory routines, the total uncertainty will be reduced by performing several experiments that show good reproducibility.

The uncertainty for a value R, is given by the variables *x,y,z,..,i*, with each corresponding uncertainty given as $\delta_x, \delta_y, \delta_z, \ldots, \delta_i$, and can be calculated with the given formula:

$$\delta_R = \sqrt{\left(\frac{\partial R}{\partial x}\delta_{\bar{x}}\right)^2 + \left(\frac{\partial R}{\partial y}\delta_{\bar{y}}\right)^2 + \left(\frac{\partial R}{\partial z}\delta_{\bar{z}}\right)^2 + - \cdots + \left(\frac{\partial R}{\partial i}\delta_{\bar{\imath}}\right)^2} \tag{0.1}$$

*x,y,z,..,i,*are variables without correlation and $\bar{x}, \bar{y}, \bar{z}, \ldots, \bar{\imath}$ are arithmetic averages of the measured variables, and can be calculated with the given formula:

$$\bar{x} = \frac{x_1 + x_2 + \cdots + x_N}{N} = \frac{1}{N}\sum_{i=1}^{N} x_i \tag{0.2}$$

If the value R is given as a product of variables, for example x^a, y^b, z^c then the formula can be written:

$$\frac{\delta_{\bar{R}}}{R} = \sqrt{\left(a\frac{\partial_{\bar{x}}}{\bar{x}}\right)^2 + \left(b\frac{\partial_{\bar{y}}}{\bar{y}}\right)^2 + \left(c\frac{\partial_{\bar{z}}}{\bar{z}}\right)^2} \tag{0.3}$$

Uncertainties regarding core analysis:

- Uncertainties regarding slide caliper
- Uncertainties regarding weight
- The assumption that the geometry of the core plug is perfect

Porosity

The bulk volume can be calculated with the help of the given formula $V_b = \pi r^2 L$. Length and diameter was measured with a slide caliper with an accuracy of ± 0.01mm. The uncertainty can be calculated with the help of formula (0.3).

The pore volume can be found as described in chapter 3.4. The weight accuracy is given as ± 0.001g, and the accuracy in the density of Ekofisk brine is negligible.

Permeability

Permeability was measured as described in chapter 3.5. Accuracy for length and area measurements is the same as for the porosity measurements. Pump rate uncertainty equals ±5%, viscosity uncertainty is negligible and pressure measurements has an uncertainty of 2% of full scale (20 bars). The uncertainty can then be calculated with formula (0.3).

Flooding uncertainties

When performing coreflooding, there are uncertainties regarding reading of the produced liquid volume and uncertainties regarding pore volume. We found the saturation uncertainty to be in the range of approximately ±2%. The estimated dead volume uncertainty is estimated to be approximately ± 1 ml. The reading of produced volume is estimated to be 0.5 ml for the measuring cylinder, and 0.25 ml for the uncertainty from the production images taken by the webcam. The uncertainty in the diaphragm used in the differential pressure measurements for the foam experiments is 10.2 mBar.

Figure 0-1 Shows oil saturation as a function of pore volumes injected for whole core L9 including uncertainties. Because of the pump injection rate has an uncertainty of 5 %, this uncertainty will increase with time, however the oil saturation uncertainty will is constant.

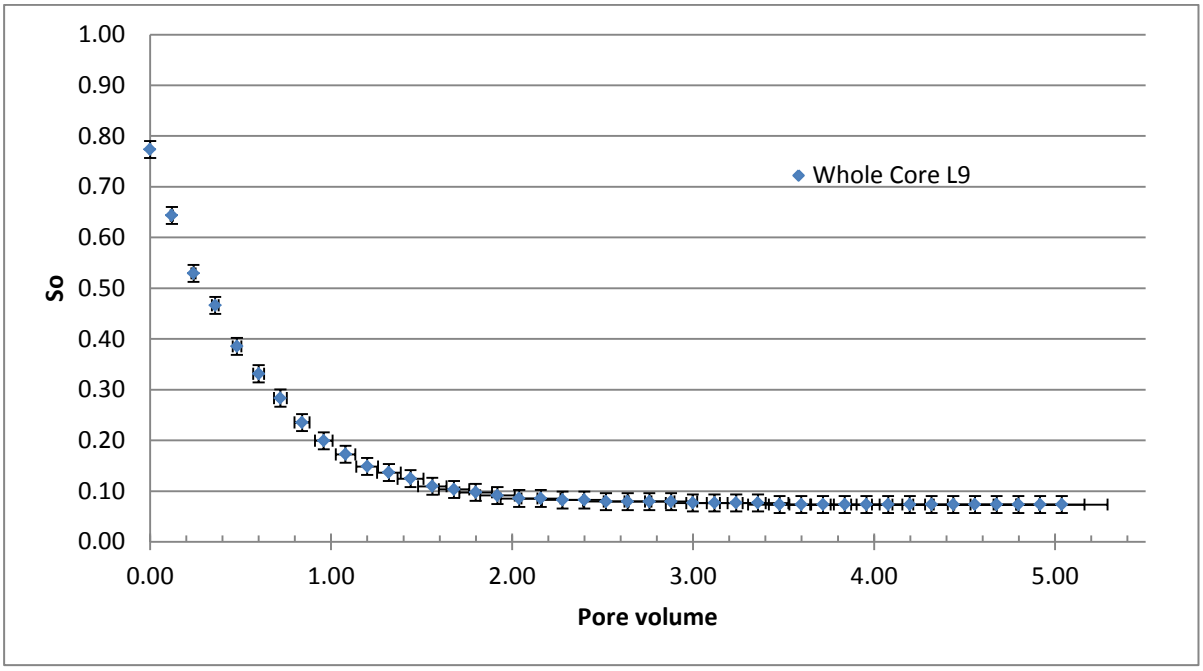

Figure 0-1 – Oil saturation as a function of time including uncertainties for a whole limestone core with irreducible water saturation.

Appendix B – Simulation data file

```
RESULTS SIMULATOR GEM 201210

INUNIT SI
WSRF WELL 1
WSRF GRID TIME
OUTSRF GRID SO SG SW PRES *X 'NC10' *X 'CO2'
OUTSRF RES NONE
WPRN GRID 0
OUTPRN GRID NONE
OUTPRN RES NONE
** WPRN ITER MATRIX

**$  Distance units: m
RESULTS XOFFSET          0.0000
RESULTS YOFFSET          0.0000
RESULTS ROTATION         0.0000  **$  (DEGREES)
RESULTS AXES-DIRECTIONS 1.0 -1.0 1.0
**$ ************************************************************************
**$ Definition of fundamental cartesian grid
**$ ************************************************************************
GRID VARI 34 21 1
KDIR DOWN
DI IVAR
 0.1 32*0.002229 0.1
DJ JVAR
 20*0.00249 0.05
DK ALL
 714*0.01031067

**$ Property: NULL Blocks  Max: 1  Min: 1
**$  0 = null block, 1 = active block
NULL CON           1

**$ Property: Porosity  Max: 0.254  Min: 0.254
POR ALL
0.999 32*0.223  0.999
0.999 32*0.223  0.999
0.999 32*0.223  0.999
0.999 32*0.223  0.999
0.999 32*0.223  0.999
0.999 32*0.223  0.999
0.999 32*0.223  0.999
0.999 32*0.223  0.999
0.999 32*0.223  0.999
0.999 32*0.223  0.999
0.999 32*0.223  0.999
0.999 32*0.223  0.999
0.999 32*0.223  0.999
0.999 32*0.223  0.999
0.999 32*0.223  0.999
0.999 32*0.223  0.999
0.999 32*0.223  0.999
0.999 32*0.223  0.999
0.999 32*0.223  0.999
34*0.999

**$ Property: Permeability I (md)   Max: 58.639  Min: 58.639
PERMI ALL
500000   32*58.639    500000
500000   32*58.639    500000
500000   32*58.639    500000
500000   32*58.639    500000
500000   32*58.639    500000
500000   32*58.639    500000
500000   32*58.639    500000
500000   32*58.639    500000
500000   32*58.639    500000
500000   32*58.639    500000
500000   32*58.639    500000
500000   32*58.639    500000
500000   32*58.639    500000
```

500000 32*58.639 500000
500000 32*58.639 500000
500000 32*58.639 500000
500000 32*58.639 500000
500000 32*58.639 500000
500000 32*58.639 500000
500000 32*58.639 500000
34*500000

**$ Property: Permeability J (md) Max: 58.639 Min: 58.639
PERMJ ALL
500000 32*58.639 500000
500000 32*58.639 500000
500000 32*58.639 500000
500000 32*58.639 500000
500000 32*58.639 500000
500000 32*58.639 500000
500000 32*58.639 500000
500000 32*58.639 500000
500000 32*58.639 500000
500000 32*58.639 500000
500000 32*58.639 500000
500000 32*58.639 500000
500000 32*58.639 500000
500000 32*58.639 500000
500000 32*58.639 500000
500000 32*58.639 500000
500000 32*58.639 500000
500000 32*58.639 500000
500000 32*58.639 500000
500000 32*58.639 500000
34*500000
**$ Property: Permeability K (md) Max: 58.639 Min: 58.639
PERMK ALL
500000 32*58.639 500000
500000 32*58.639 500000
500000 32*58.639 500000
500000 32*58.639 500000
500000 32*58.639 500000
500000 32*58.639 500000
500000 32*58.639 500000
500000 32*58.639 500000
500000 32*58.639 500000
500000 32*58.639 500000
500000 32*58.639 500000
500000 32*58.639 500000
500000 32*58.639 500000
500000 32*58.639 500000
500000 32*58.639 500000
500000 32*58.639 500000
500000 32*58.639 500000
500000 32*58.639 500000
500000 32*58.639 500000
500000 32*58.639 500000
500000 32*58.639 500000
34*500000

**$ Property: Pinchout Array Max: 1 Min: 1
**$ 0 = pinched block, 1 = active block
PINCHOUTARRAY CON 1
SECTORARRAY 'FRACTURE1' ALL
1 33*0 1 33*0 1 33*0 1 33*0 1 33*0 1 33*0 1 33*0 1 33*0 1 33*0 1 33*0 1 33*0 1
33*0 1 33*0 1 33*0 1 33*0 1 33*0 1 33*0 1 33*0 1 33*0 1 33*0 1 33*0 1 33*0 1 33*0
SECTORARRAY 'FRACTURE2' ALL
33*0 1 33*0 1 33*0 1 33*0 1 33*0 1 33*0 1 33*0 1 33*0 1 33*0 1 33*0 1 33*0 1 33*0
1 33*0 1 33*0 1 33*0 1 33*0 1 33*0 1 33*0 1 33*0 1 33*0 1 33*0 1 33*0 1 33*0 1*1
SECTORARRAY 'FRACTURE3' ALL
681*0 32*1 1*0
SECTORARRAY 'MATRIX' ALL
0 32*1 2*0 32*1 2*0 32*1 2*0 32*1 2*0 32*1 2*0 32*1 2*0 32*1 2*0 32*1 2*0 32*1 2*0
32*1 2*0 32*1 2*0 32*1 2*0 32*1 2*0 32*1 2*0 32*1 2*0 32*1 2*0 32*1 2*0 32*1 2*0
32*1 2*0 32*1 2*0 32*1 2*0 32*1 2*0 32*1 35*0

**DEPTH 1 34 1 1000

DEPTH-TOP ALL

```
714*1000
**$ Model and number of components

MODEL PR
**=-=-=Component Selection/Properties
**REM
NC 2 2
COMPNAME 'CO2' 'NC10'
HCFLAG
0 1
VISCOR HZYT
MIXVC 1
VISCOEFF 0.1023 0.023364 0.058533 -0.040758 0.0093324
PVC3 1.2
MW
44.01 142.286
AC
0.225 0.49
PCRIT
72.8 20.8
VCRIT
0.094 0.603
TCRIT
304.2 617.6
PCHOR
78 433.5
SG
0.818 0.734
TB
-78.45 174.15
OMEGA
0.457236 0.457236
OMEGB
0.0777961 0.0777961
VSHIFT
0 0
HEATING_VALUES
0 6473.36
VISVC
0.094 0.603
BIN
0.11

TRES 20
VISW 1.09

**DIFCOR-OIL        *WILKE
*DIFFC-OIL          0.0001 0



ROCKFLUID
RPT 1
**$       Sw       krw      krow       Pcow
SWT
          0        0       1.0         0
        1.0       1.0         0         0
**$       Sl       krg      krog
SLT
          0        1         0
          1        0         1
RPT 2
**$       Sw       krw      krow          Pcow
SWT
       0.13        0         1   21.75568367
       0.15   0.0014    0.9846   17.40454694
       0.18   0.0036    0.9539   12.32822075
       0.23   0.0074    0.8881   7.977084013
        0.3   0.0127    0.7655   4.786250408
       0.33    0.015    0.7021   3.843504115
      0.391   0.0196     0.553   2.921730302
      0.469   0.0581    0.3229   2.707813916
      0.564   0.1312    0.1444   2.444918235
      0.632   0.2036    0.0408   2.270423148
      0.674   0.2574    0.0058   2.152362305
```

```
      0.702    0.2974    0.0003   2.069748722
       0.71    0.3095    0.0002   2.047354871
      0.718    0.3218    0.0001   2.026454911
      0.722    0.3281         0  -2.175568367
**$       Sl       krg      krog
SLT
         0.13         1          0
         1        0          1


RTYPE ALL
1*1  32*2   1*1
1*1  32*2   1*1
1*1  32*2   1*1
1*1  32*2   1*1
1*1  32*2   1*1
1*1  32*2   1*1
1*1  32*2   1*1
1*1  32*2   1*1
1*1  32*2   1*1
1*1  32*2   1*1
1*1  32*2   1*1
1*1  32*2   1*1
1*1  32*2   1*1
1*1  32*2   1*1
1*1  32*2   1*1
1*1  32*2   1*1
1*1  32*2   1*1
1*1  32*2   1*1
1*1  32*2   1*1
1*1  32*2   1*1
1*1  32*2   1*1
34*1
INITIAL
USER_INPUT

**VERTICAL BLOCK_CENTER WATER_OIL
**REFPRES
**9200
**REFDEPTH
**1000
**DWOC
**5000
**REFPRES
**9200
**REFDEPTH
**1000
**DWOC
**5000

*PRES     *KVAR  9200.0
*SW       *IJK                          1 1:21 1    0
                                                                  34 1:21 1    0
                                                                  2:33 21 1    0
                                                                  2:33 1:20 1  0.13
ZGLOBALC 'NC10' ALL
 0 32*1 2*0 32*1 2*0 32*1 2*0 32*1 2*0 32*1 2*0 32*1 2*0 32*1 2*0 32*1 2*0 32*1
 2*0 32*1 2*0 32*1 2*0 32*1 2*0 32*1 2*0 32*1 2*0 32*1 2*0 32*1 2*0 32*1 2*0
 32*1 2*0 32*1 2*0 32*1 2*0 32*1 2*0 32*1 2*0 32*1 35*0
ZGLOBALC 'CO2' ALL
 1 32*0 2*1 32*0 2*1 32*0 2*1 32*0 2*1 32*0 2*1 32*0 2*1 32*0 2*1 32*0 2*1 32*0
 2*1 32*0 2*1 32*0 2*1 32*0 2*1 32*0 2*1 32*0 2*1 32*0 2*1 32*0 2*1 32*0 2*1
 32*0 2*1 32*0 2*1 32*0 2*1 32*0 2*1 32*0 2*1 32*0 35*1

NUMERICAL
MAXSTEPS 150000
DTMAX 0.001
DTMIN 0.00001
NORM PRESS 200
NORM SATUR 0.6
NORM GMOLAR 0.3
NORM AQUEOUS 0.6
NORM TEMP 10
MAXCHANGE GMOLAR 0.9
CONVERGE HC 0.02
NCHECK-CEQ 3
```

```
NEWTONCYC 100
ITERMAX 200
ITERMIN 100
RUN

DATE 2013 4 11
DTWELL 0.0001


REFINE 1 3 1
RANGE 9:26 15:20 1

REFINE 3 3 1
RANGE 2:8 15:20 1
RANGE 27:33 15:20 1

REFINE 3 1 1
RANGE 2:8 1:14 1
RANGE 27:33 1:14 1

DATE 2013 4 11.0014
DATE 2013 4 11.08333
DATE 2013 4 11.12500
DATE 2013 4 11.16667
DATE 2013 4 11.20833
DTWELL 0.0001
DATE 2013 4 11.25000
DATE 2013 4 11.29167
DATE 2013 4 11.33333
DATE 2013 4 11.37500
DATE 2013 4 11.41667
DATE 2013 4 11.45833
DATE 2013 4 11.50000
DATE 2013 4 11.54167
DATE 2013 4 11.58333
DATE 2013 4 11.62500
DATE 2013 4 11.66667
DATE 2013 4 11.70833
DATE 2013 4 11.75000
DATE 2013 4 11.79167
DATE 2013 4 11.83333
DATE 2013 4 11.87500
DATE 2013 4 11.91667
DATE 2013 4 11.95833
DATE 2013 4 12.00000
DATE 2013 4 12.04167
DATE 2013 4 12.08333
DATE 2013 4 12.12500
DATE 2013 4 12.16667
DATE 2013 4 12.20833
DATE 2013 4 12.25000
DATE 2013 4 12.29167
DATE 2013 4 12.33333
DATE 2013 4 12.37500
DATE 2013 4 12.41667
DATE 2013 4 12.45833
DATE 2013 4 12.50000
DATE 2013 4 12.54167
DATE 2013 4 12.58333
DATE 2013 4 12.62500
DATE 2013 4 12.66667
DATE 2013 4 12.70833
DATE 2013 4 12.75000
DATE 2013 4 12.79167
DATE 2013 4 12.83333
DATE 2013 4 12.87500
DATE 2013 4 12.91667
DATE 2013 4 12.95833
DATE 2013 4 13.00000

RESULTS SPEC 'Permeability I'
RESULTS SPEC SPECNOTCALCVAL -99999
RESULTS SPEC REGION 'All Layers (Whole Grid)'
RESULTS SPEC REGIONTYPE 'REGION_WHOLEGRID'
RESULTS SPEC LAYERNUMB 0
```

```
RESULTS SPEC PORTYPE 1
RESULTS SPEC CON 51.045
RESULTS SPEC SPECKEEPMOD 'YES'
RESULTS SPEC STOP


RESULTS SPEC 'Permeability J'
RESULTS SPEC SPECNOTCALCVAL -99999
RESULTS SPEC REGION 'All Layers (Whole Grid)'
RESULTS SPEC REGIONTYPE 'REGION_WHOLEGRID'
RESULTS SPEC LAYERNUMB 0
RESULTS SPEC PORTYPE 1
RESULTS SPEC CON 51.045
RESULTS SPEC SPECKEEPMOD 'YES'
RESULTS SPEC STOP


RESULTS SPEC 'Permeability K'
RESULTS SPEC SPECNOTCALCVAL -99999
RESULTS SPEC REGION 'All Layers (Whole Grid)'
RESULTS SPEC REGIONTYPE 'REGION_WHOLEGRID'
RESULTS SPEC LAYERNUMB 0
RESULTS SPEC PORTYPE 1
RESULTS SPEC CON 51.045
RESULTS SPEC SPECKEEPMOD 'YES'
RESULTS SPEC STOP


RESULTS SPEC 'Porosity'
RESULTS SPEC SPECNOTCALCVAL -99999
RESULTS SPEC REGION 'All Layers (Whole Grid)'
RESULTS SPEC REGIONTYPE 'REGION_WHOLEGRID'
RESULTS SPEC LAYERNUMB 0
RESULTS SPEC PORTYPE 1
RESULTS SPEC CON 0.254
RESULTS SPEC SPECKEEPMOD 'YES'
RESULTS SPEC STOP


RESULTS SPEC 'Pressure'
RESULTS SPEC SPECNOTCALCVAL -99999
RESULTS SPEC REGION 'All Layers (Whole Grid)'
RESULTS SPEC REGIONTYPE 'REGION_WHOLEGRID'
RESULTS SPEC LAYERNUMB 0
RESULTS SPEC PORTYPE 1
RESULTS SPEC CON 9230
RESULTS SPEC SPECKEEPMOD 'YES'
RESULTS SPEC STOP


RESULTS SPEC 'Rock Density'
RESULTS SPEC SPECNOTCALCVAL -99999
RESULTS SPEC REGION 'All Layers (Whole Grid)'
RESULTS SPEC REGIONTYPE 'REGION_WHOLEGRID'
RESULTS SPEC LAYERNUMB 0
RESULTS SPEC PORTYPE 1
RESULTS SPEC CON 2012
RESULTS SPEC SPECKEEPMOD 'YES'
RESULTS SPEC STOP


RESULTS SPEC 'Water Saturation'
RESULTS SPEC SPECNOTCALCVAL -99999
RESULTS SPEC REGION 'All Layers (Whole Grid)'
RESULTS SPEC REGIONTYPE 'REGION_WHOLEGRID'
RESULTS SPEC LAYERNUMB 0
RESULTS SPEC PORTYPE 1
RESULTS SPEC CON 0
RESULTS SPEC SPECKEEPMOD 'YES'
RESULTS SPEC STOP


RESULTS SPEC 'Initial Water Saturation'
RESULTS SPEC SPECNOTCALCVAL -99999
RESULTS SPEC REGION 'All Layers (Whole Grid)'
```

```
RESULTS SPEC REGIONTYPE 'REGION_WHOLEGRID'
RESULTS SPEC LAYERNUMB 0
RESULTS SPEC PORTYPE 1
RESULTS SPEC CON 0
RESULTS SPEC SPECKEEPMOD 'YES'
RESULTS SPEC STOP


RESULTS SPEC 'Block Temperature'
RESULTS SPEC SPECNOTCALCVAL -99999
RESULTS SPEC REGION 'All Layers (Whole Grid)'
RESULTS SPEC REGIONTYPE 'REGION_WHOLEGRID'
RESULTS SPEC LAYERNUMB 0
RESULTS SPEC PORTYPE 1
RESULTS SPEC CON 20
RESULTS SPEC SPECKEEPMOD 'YES'
RESULTS SPEC STOP


RESULTS SPEC 'Global Composition$C' 'CO2'
RESULTS SPEC SPECNOTCALCVAL -99999
RESULTS SPEC REGION 'All Layers (Whole Grid)'
RESULTS SPEC REGIONTYPE 'REGION_WHOLEGRID'
RESULTS SPEC LAYERNUMB 0
RESULTS SPEC PORTYPE 1
RESULTS SPEC CON 1
RESULTS SPEC SPECKEEPMOD 'YES'
RESULTS SPEC STOP


RESULTS SPEC 'Global Composition$C' 'NC10'
RESULTS SPEC SPECNOTCALCVAL -99999
RESULTS SPEC REGION 'All Layers (Whole Grid)'
RESULTS SPEC REGIONTYPE 'REGION_WHOLEGRID'
RESULTS SPEC LAYERNUMB 0
RESULTS SPEC PORTYPE 1
RESULTS SPEC CON 2
RESULTS SPEC SPECKEEPMOD 'YES'
RESULTS SPEC STOP


RESULTS SPEC 'Grid Thickness'
RESULTS SPEC SPECNOTCALCVAL -99999
RESULTS SPEC REGION 'All Layers (Whole Grid)'
RESULTS SPEC REGIONTYPE 'REGION_WHOLEGRID'
RESULTS SPEC LAYERNUMB 0
RESULTS SPEC PORTYPE 1
RESULTS SPEC CON 0.0103107
RESULTS SPEC SPECKEEPMOD 'YES'
RESULTS SPEC STOP
```